

DTIC FILE COPY

2

AD-A202 241

STUDY OF THE CONTINUOUS/DIFFUSE AURORA USING PARTICLE OBSERVATIONS FROM THE DYNAMICS EXPLORER SATELLITES

Final Technical Report
AFOSR Contract F49620-85-C-0029
SwRI Contract 15-8482

for
DIRECTORATE FOR CHEMICAL AND ATMOSPHERIC SCIENCES
AIR FORCE OFFICE OF SCIENTIFIC RESEARCH
BOLLING AFB, D.C. 20332

by
J. R. Sharber
J. D. Winningham

DTIC
SELECTED
DEC 09 1988
S H D

October 1988



SOUTHWEST RESEARCH INSTITUTE
Instrumentation and Space Research Division
6220 Culebra Road, San Antonio, Texas 78284
(512) 684-5111 • FAX (512) 647-4325

88 12 1988

Approved for public release,
distribution unlimited

UNCLASSIFIED

SECURITY CLASSIFICATION OF THIS PAGE

REPORT DOCUMENTATION PAGE

Form Approved
OMB No. 0704-0188

1a. REPORT SECURITY CLASSIFICATION Unclassified			1b. RESTRICTIVE MARKINGS			
2a. SECURITY CLASSIFICATION AUTHORITY			3. DISTRIBUTION / AVAILABILITY OF REPORT Approved for public release; Distribution Unlimited			
2b. DECLASSIFICATION / DOWNGRADING SCHEDULE						
4. PERFORMING ORGANIZATION REPORT NUMBER(S) 15-8482-3			5. MONITORING ORGANIZATION REPORT NUMBER(S) AFOSR-TR-88-1202			
6a. NAME OF PERFORMING ORGANIZATION Southwest Research Institute		6b. OFFICE SYMBOL (if applicable) 15	7a. NAME OF MONITORING ORGANIZATION AFOSR/NC			
6c. ADDRESS (City, State, and ZIP Code) 6220 Culebra Road P.O. Drawer 28510 San Antonio, TX 78284			7b. ADDRESS (City, State, and ZIP Code) Bldg 410 Bolling AFB DC 20332-6448			
8a. NAME OF FUNDING / SPONSORING ORGANIZATION AFOSR		8b. OFFICE SYMBOL (if applicable) NC	9. PROCUREMENT INSTRUMENT IDENTIFICATION NUMBER F49620-85-C-0029			
8c. ADDRESS (City, State, and ZIP Code) Bldg. 410 Bolling AFB, DC 20332-6448			10. SOURCE OF FUNDING NUMBERS			
			PROGRAM ELEMENT NO. 61102F	PROJECT NO. 2310	TASK NO. A2	WORK UNIT ACCESSION NO.
11. TITLE (Include Security Classification) STUDY OF THE CONTINUOUS/DIFFUSE AURORA USING PARTICLE OBSERVATIONS FROM THE DYNAMICS EXPLORER SATELLITES						
12. PERSONAL AUTHOR(S) J. R. Sharber, J. D. Winningham						
13a. TYPE OF REPORT Final Technical		13b. TIME COVERED FROM 01/01/85 TO 10/17/88	14. DATE OF REPORT (Year, Month, Day) 17 October 1988		15. PAGE COUNT 67	
16. SUPPLEMENTARY NOTATION						
17. COSATI CODES			18. SUBJECT TERMS (Continue on reverse if necessary and identify by block number) <i>are void</i>			
FIELD	GROUP	SUB-GROUP				
19. ABSTRACT (Continue on reverse if necessary and identify by block number) This is the second annual technical report of Contract F49620-85-C-0029 which began in January 1985 and supports an investigation of the continuous/diffuse (C/D) aurora and related auroral studies using as the primary data observations from instruments on the Dynamics Explorer satellites. These satellites carried particle detection instrumentation referred to as the High Altitude Plasma Instrument (HAPI) on the DE-1 and the Low Altitude Plasma Instrument (LAPI) on DE-2, and together provided high resolution spectral and angular measurements of electron and positive ions at altitudes between 500 km and 4 ^{sub} R_E above the auroral region. The objectives of the research are: (1) to provide a thorough description of the particle populations which produce the quiet and activated continuous/diffuse aurora, (2) to attempt to determine what mechanisms act within the plasma sheet and on supra-auroral field lines to precipitate the continuous/diffuse auroral particles, (3) to attempt to find a simple and effective way to model the effects of this aurora and (4), added during the first year of the contract, applying the Dynamics Explorer database to selective investigations of						
20. DISTRIBUTION / AVAILABILITY OF ABSTRACT <input checked="" type="checkbox"/> UNCLASSIFIED/UNLIMITED <input type="checkbox"/> SAME AS RPT <input type="checkbox"/> DTIC USERS			21. ABSTRACT SECURITY CLASSIFICATION Unclassified			
22a. NAME OF RESPONSIBLE INDIVIDUAL Lt Col James G. Stobie			22b. TELEPHONE (Include Area Code) 202-767-4963		22c. OFFICE SYMBOL AFOSR/NC	

19a. ABSTRACT (continued)

of the high-latitude auroral regions.

Research has included a description of quiet and disturbed diffuse auroral particles, a study of particles and waves in the diffuse aurora, an attempt to determine the mechanisms of the precipitation, and studies of polar arcs, ionization, and convection in the high-latitude regions.

The research has resulted in 11 journal or monograph publications and 11 presentations at scientific meetings.

TABLE OF CONTENTS

	<u>Page</u>
Abstract	
I. Introduction	1
II. Objectives of the Research	1
III. The Diffuse Aurora	2
A. Background	2
B. Dynamics Explorer Observations of the Diffuse Aurora	3
1. General	3
2. Quiet and Disturbed Diffuse Aurora	5
C. Waves and the Diffuse Aurora	12
D. The Diffuse Auroral Equatorward Edge, Trough, and Plasmopause	15
E. Mechanisms of Diffuse Auroral Production	16
IV. Related Studies	18
A. Arcs, Convection, and Ionization in the Polar Cap	18
B. Particle Calibration of the DE-1 Scanning Auroral Imager	18
V. Publications	18
VI. Professional Personnel	21
VII. Interactions (Coupling Activities)	21
VIII. Inventions or Patent Disclosures	22
IX. Accomplishments	22
X. References	23
Appendix A: E- and F- Region Study of the Evening Sector Auroral Oval	
Appendix B: Plasma Waves Associated with Diffuse Auroral Electrons at Mid-Altitudes	
Appendix C: Further Boundary Conditions on the Low-Energy Electrons in the Plasmopause Regions	



	✓

Distribution/		
Availability Codes		
Avail and/or		
Dist Special		
A-1		

I. INTRODUCTION

This is the final report of a three-year study of the continuous/diffuse aurora and related auroral studies using as the primary data source the particle observations of the Dynamics Explorer satellite. These two satellites were launched at 90° inclination in the same local time plane in August 1981. Initially DE-1 had an apogee at 1000 km altitude and a period of 6h 50m; DE-2 had an apogee at 1000 km altitude and a period of 90 minutes. The plasma instruments, the High Altitude Plasma Instrument (HAPI) on DE-1 and the Low Altitude Plasma Instrument (LAPI) on DE-2 each produced high-resolution differential spectral and angular measurements of electrons and ions over the auroral regions. In addition to the particle experiments, the satellites carried instrumentation to measure plasma concentrations, temperatures and flows, electric and magnetic field components, magnetic field perturbations, and plasma wave intensities. In our research, we have taken advantage of the comprehensive nature of the plasma diagnostic instrumentation as well as selected magnetic conjunctions of the two satellites, i.e. times when DE-1 and DE-2 made simultaneous crossings of the same magnetic field line.

II. OBJECTIVES OF THE RESEARCH

The objectives as stated in the original proposal were:

- (1) to provide a thorough description of the particle populations which produce the quiet and activated continuous/diffuse aurora,
- (2) to attempt to determine what mechanisms act within the plasma sheet and on supra-auroral field lines to precipitate the continuous/diffuse auroral particles, and
- (3) to attempt to find a simple and effective way to model the effects of this aurora on the ionosphere.

In addition to these stated objectives of the original proposal, during the first year of the contract the principal investigator added a fourth scientific objective, that of applying the Dynamics Explorer database to selective investigations of the high-latitude auroral regions. These investigations had the goal of determining the relationships between the particles, fields, and plasmas of the polar regions. They made full use of the DE complement of observations taken with simultaneous AFGL aircraft and ground-based observations and were coordinated closely with personnel of AFGL. As we will show, these studies have been highly successful.

As will be shown in this report, the first two objectives of the original proposal and the added fourth objective have been successfully met. The modeling objective, which has had to rely on the results of the other objectives has only partially been accomplished at this time. This is a very important research goal not only from the standpoint of auroral/magnetospheric/ionospheric science, but because of its importance to the general problem of predictability of the state of the ionosphere. We therefore will include this as an objective of our proposal for the next three year increment of funding.

III. THE DIFFUSE AURORA

A. Background

The first measurements of the diffuse aurora showing its optical and morphological characteristics (Whalen et al., 1971) were based on AFGL instrumental aircraft flights into the auroral regions that took place in 1968. Lui et al. (1973) reported on the diffuse aurora in terms of images from ISIS-2. The Whalen et al. paper and several subsequent papers have referred to the diffuse aurora as the "continuous aurora" because of its continuous temporal-- and to a large extent spatial--signature. Globally, it is a rather uniform, nearly circularly band of auroral optical emissions centered a few degrees toward midnight from the magnetic pole having an annular width of $\sim 2\text{-}5^\circ$ of latitude. It was later shown that in the evening-midnight sector its latitude of peak precipitation generally lies equatorward of the oval of discrete auroras and is essentially always present (Weber et al., 1977; Whalen et al., 1977; Winningham et al., 1975; Sharber, 1981; Whalen, 1983).

It has been widely believed for some time (Kennel, 1969) that the diffuse aurora involves the scattering by waves or turbulence of plasma sheet particles into the loss cone to produce the optical emissions observed at auroral latitudes (eg., see review by Ashour-Abdalla and Kennel, 1978, and references therein, Swift, 1981; Fontaine and Blanc, 1983; Robinson and Vondrak, 1985). The particles undergo little acceleration before reaching the auroral ionosphere. Based on a report on OGO-5 observations by Kennel et al. (1970) showing strong wave emissions in the 1-10 mV/m range, Lyons (1974) developed a theory of diffuse auroral precipitation resulting from diffusion of electrons into the loss cone by electron cyclotron harmonic (ECH) waves. Lyons computed a bounce-averaged diffusion coefficient and showed that the observed ECH waves would generally cause strong pitch angle diffusion of plasma sheet electrons of energies in the few hundred eV to few keV range. A later treatment of the problem by Belmont et al. (1983) that removed the bounce-averaging condition found that wave amplitudes required for strong diffusion of electrons were ~ 2.6 times greater than those computed by Lyons. The same paper showed that ECH waves observed by GEOS-2 were far less intense than the OGO-5 report had suggested. For example, only 9% of the time did the waves exceed 2 mV/m, the amplitude required to put 1 keV electrons on strong diffusion. It thus appeared that the ECH waves, once thought to play a major role in diffuse aurora production, were not observed with sufficient intensity frequently enough to produce the required strong diffusion.

Since publication of the Belmont et al. (1983) paper, there has developed increasing support for this finding. A study by Fairfield and Viñas (1984) using ISEE data illustrated the importance of single-particle motion in determining the latitudes of diffuse auroral precipitation. Fontaine et al. (1986), using data from EISCAT, GEOS-2, and ARCAD-3, found that the electron cyclotron waves observed at GEOS-2 were seldom intense enough to cause strong pitch angle diffusion of electrons of energies > 2 keV, even though above the aurora electrons had energies up to ~ 26 keV. It was concluded that these ECH waves could not be the unique cause of the diffuse aurora. More recent studies using observations from SCATHA and AMPTE-IRM (Roeder and Koons, 1988) and P78-1 and SCATHA (Shumaker et al., 1988) have reached the same conclusion.

It is clear that key questions regarding diffuse auroral particle precipitation still remain. The most significant of these is the question of the precipitation mechanism; i.e., if the particles are scattered by waves or wave turbulence, what types of waves are involved? It is now clear that electron cyclotron harmonic waves are not the answer. We are now required to go back to the process of describing the particle, wave, and plasma environment in the diffuse auroral regions with the goal of coming up with an alternate mechanism. The DE satellite observations provide an excellent opportunity to do this.

B. Dynamics Explorer Observations of the Diffuse Aurora

In this section we make use of our own published observations where possible as well as new observations from ongoing studies.

1. General

Winningham et al. (1975) identified the CPS and BPS in terms of precipitating particle signatures. They were defined as low-altitude regions (≤ 1500 km) which map respectively to the central plasma sheet (CPS) and the adjacent boundary regions above and below the central plasma sheet referred to as the plasma sheet boundary layers. They can usually be identified by structure on an energy-time spectrogram of particle data, i.e., by the energy spectra and angular characteristics. The (low-altitude) CPS is now synonymous with "diffuse auroral region."

The diffuse auroral region as well as the BPS are shown particularly well by the spectrogram portion of Figure 1 taken from a paper written in support of this contract (Senior et al., 1987) and included in this report as Appendix A). The diffuse auroral region extends from 0534:55 UT to 0535:45 UT (70.2° to 67.2° invariant latitude.) In this region the electrons have a broad quasi-Maxwellian spectrum peaking at 1-2 keV energy. The BPS extends poleward from ~70.2° IL to ~71.6° IL and is characterized by a more sharply peaked spectrum indicative of the strong parallel electric fields of this region. We note that similar peaking occurs at lower energies within the diffuse aurora latitudes as has been previously pointed out by Johnstone and Winningham (1982).

To place the diffuse aurora in the context of the Birkeland current system we note by the second panel of Figure 1 that the diffuse auroral region is embedded within a region of downward field-aligned current that extends equatorward of the electron precipitation boundary to 62.8° IL. We also note that the BPS region is associated with a relatively intense upward field-aligned current. These observations are consistent with other measurements made on ISIS-2, DE, TRIAD, and the ground based radars (Senior et al., 1987).

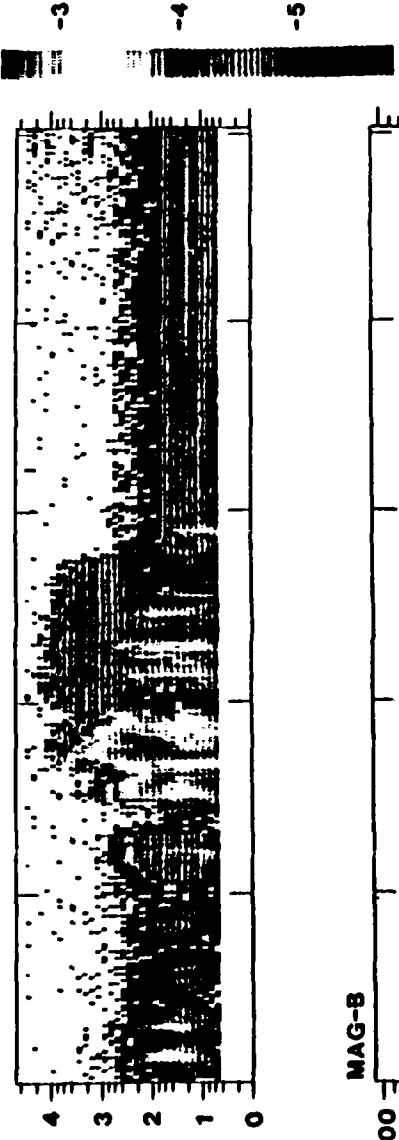
The last panel of Figure 1 adds the ionospheric density measured at DE-2 altitude (shown below the panel). This particular study was one involving observations from the Chatanika radar, DE-2, and NOAA-6. The plasma enhancement that appears on the poleward shoulder of the trough (~0535:50 UT) was observed both at DE-2 (at ~640 km altitude) and in scans of the Chatanika radar. For further details, the complete study (Senior et al. 1987) is included in this report as Appendix A.

DE-2

81315 (NOV. 11, 1981)

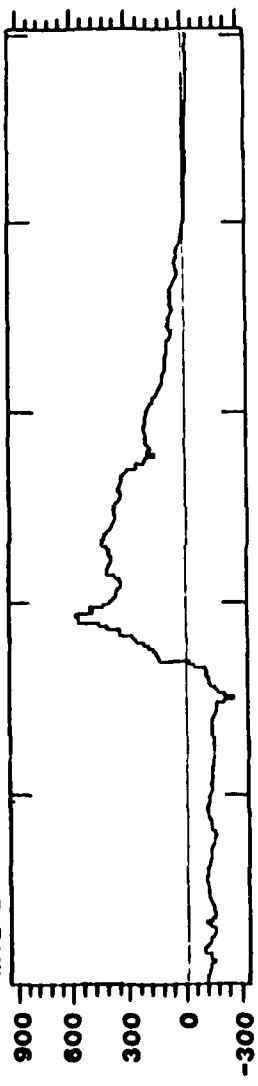
LOG ENERGY FLUX

LAPI - ENERGY FLUX (ergs/cm² s sr eV)



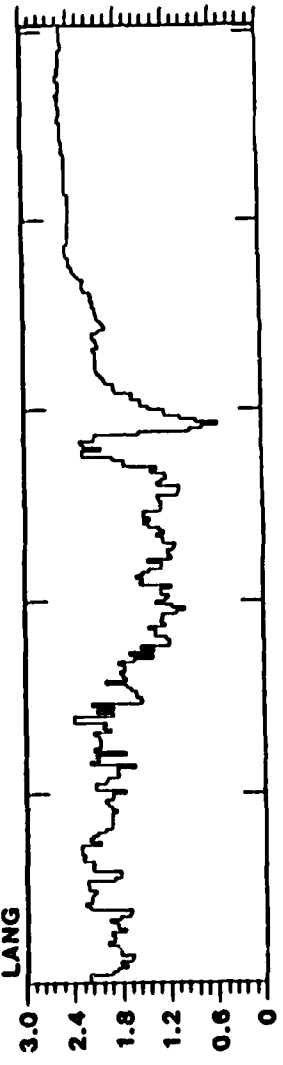
LOG ELECTRON ENERGY (eV)
P.A. = 8°

MAG-B



ΔB_{ϕ} (nT)

LANG



$N_i / 10^8$

UT (H:M)	05:34	05:35	05:36	05:37	05:38
IL(DEG)	73.3	69.9	66.4	62.8	59.2
ALT(KM)	672	653	631	612	589
MLT(HR)	17.31	17.69	18.03	18.26	18.47

Fig. 1 DE-2 pass over the auroral region on Day 315 (11 November), 1981. Electrons of 8° pitch angle are shown in the top panel. DE-2 magnetic field perturbations and ion density are shown in the second and third panels respectively. The diffuse aurora is seen between 70.2° and 67.2° IL and is embedded in a region of downward field aligned current.

One of the findings of the Senior et al. study was the measurement of ionization extending $1\ 1/2'$ to $2'$ equatorward of the equatorward boundary of electron precipitation. Using a modified Jasperse and Basu (1982) ionization and production code, a major portion of this ionization was attributed to precipitating ions as measured by LAPI on DE-2 and by the energetic particle detector on NOAA-6.

2. Quiet and Disturbed-Time Diffuse Auroras

It is well known that during quiet times the auroral oval moves poleward. The diffuse auroral region follows this pattern and generally becomes thinner as it moves to higher latitudes. The term "generally" is applied here since small quiet-time substorms can occur; and during such substorms, local bulges can appear in the precipitation belt. Our working definition of "quiet time" is low DST magnitude (relatively few particles in the ring current) and low AE magnitude (<100 nT) after several hours of similarly low AE.

One example of a quiet time pass is that of Day 264 (September 21) of 1981 shown in Figure 2. The diffuse auroral electrons of Figure 2(a) (top panel) are observed between $\sim 1437:25$ UT ($70.4'$ IL) and $1437:00$ UT ($\sim 68.4'$ IL) and thus precipitate into a region less than $2'$ of latitude. The second and third panels show energy flux, number flux and average electron energy. The downward electron energy flux is about 0.1 erg/cm² s sr at these latitudes. At latitudes poleward of $1437:25$ UT, the electrons are lower in energy but appear to differ from the "diffuse auroral" (CPS) electrons in that (a) their energies are lower and (b) some enhancements are seen on the background of the less structured precipitation. The Hall and Pederson conductivities are shown in the lower panel.

The electron spectra between $1437:15$ and $1438:15$ UT are shown in Figure 3. The spectral peak associated with this very quiet time diffuse aurora has a prominent near-Maxwellian component that increases in characteristic energy toward the latitude of peak precipitation. In the figure, this occurs in the third panel where the characteristic energy is ~ 600 eV. The figure also shows that the incident electron flux is isotropic within the $\sim 62'$ loss cone. Examination of similar plots at other pitch angles shows that isotropy occurs out to $>90'$. In some quieter cases this is not observed and the loss cone shows a depletion.

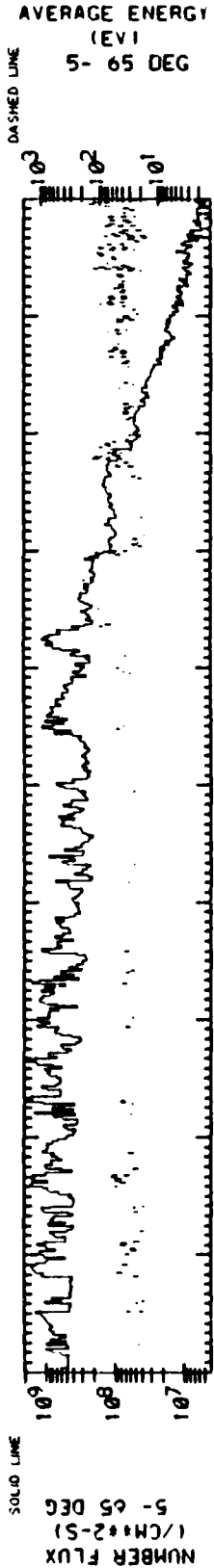
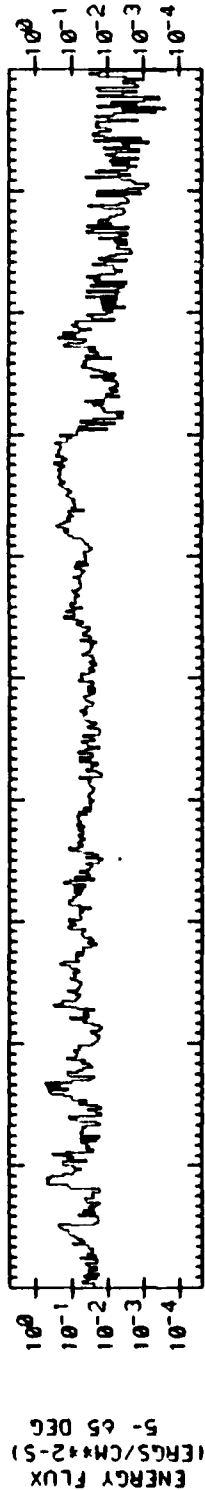
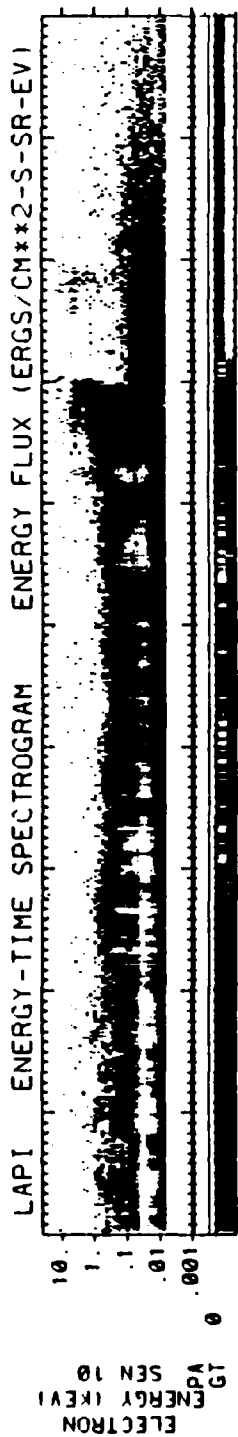
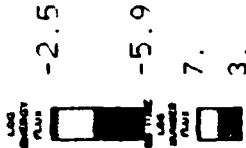
On the spectrogram, the structure becomes more prominent and the background precipitation diminishes toward high latitudes. This signature is characteristic of IMF north cases (in this case IMF B = $+5$ nT) as has been reported previously (Sharber and Winningham, 1986; Coley et al., 1987) and is consistent with the more recent study of the convection, optical, and precipitation patterns (Carlson et al., 1988) supported in part by this contract (see Sec. IV.A)..

The ions shown in Figure 2(b) show similarities to the less structured component of background electron precipitation. The most energetic region of ion precipitation occurs slightly equatorward of the peak of electron precipitation. However, it is clear that ions precipitate as far poleward as $\sim 81.4'$. This latitude is most likely the location of the polar cap boundary, i.e., the boundary between open and closed field lines. This illustrates the reduced size of the polar cap proper under these conditions and is in accord with optical observations and modeling (Toffoletto and Hill, 1988) of the quiet time polar regions. In this picture the quiet time BPS has expanded to include a broad range of latitudes extending into the region that at more active times is the polar cap (Winningham, 1975; Meng, 1981).

81 264

DE-2 DATA

SWRI



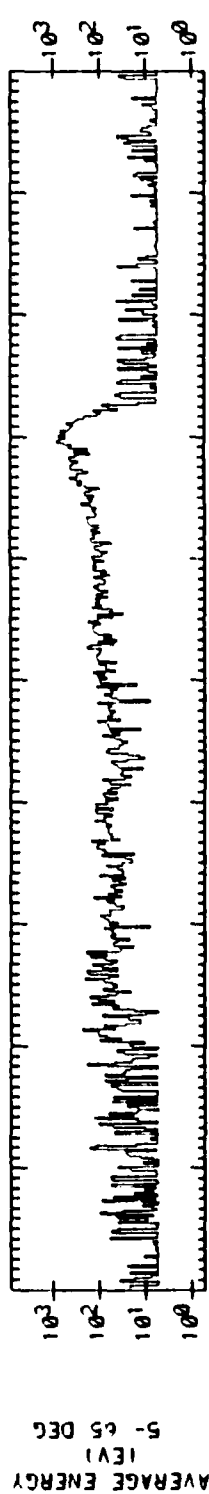
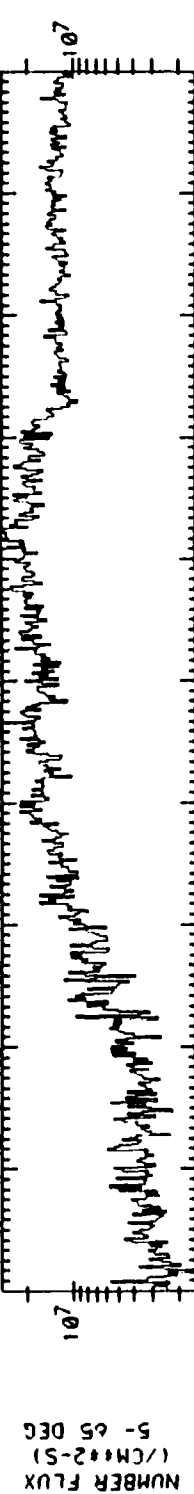
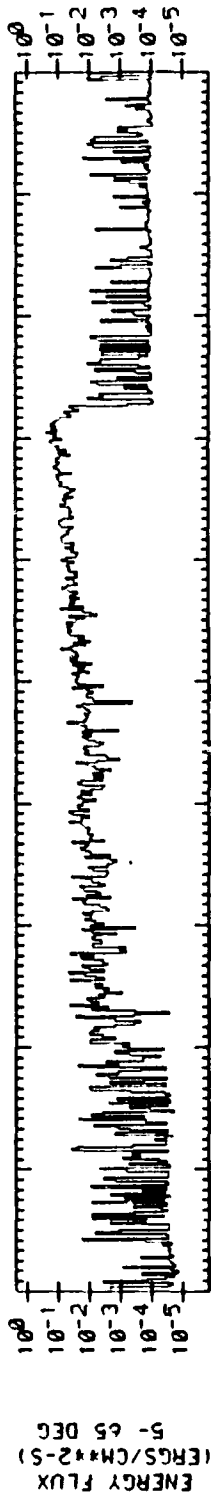
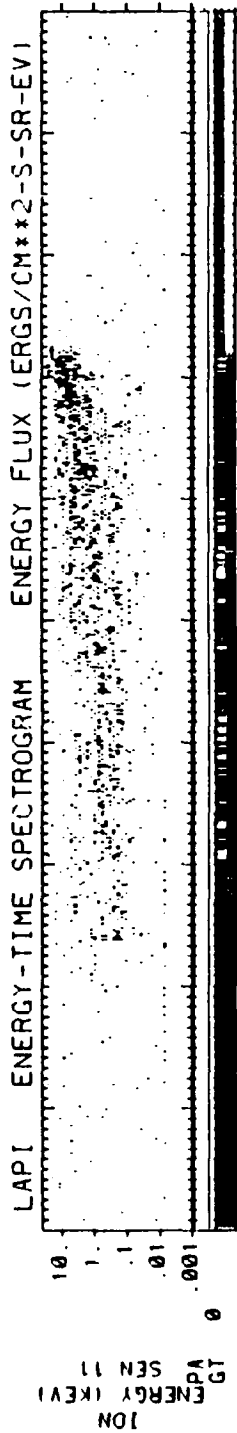
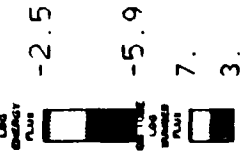
UT(H:M:S)	14:32:00	14:34:00	14:36:00	14:38:00	14:40:00
ILAT(D)	87.6	80.8	74.0	67.1	60.3
MLT(HR)	16.7	18.1	19.5	20.8	22.2
ALT(KM)	411	454	498	542	586
GLAT(D)	78.6	75.1	71.5	67.9	64.4
GLONG(D)	-56.2	-15.8	24.6	65.0	105.4

Fig. 2(a) LAPI electron spectrogram (0° pitch angle), plasma parameters, and conductivities for the quiet-time pass of Day 264 (September 21), 1961.

81264

DE-2 DATA

SWRI

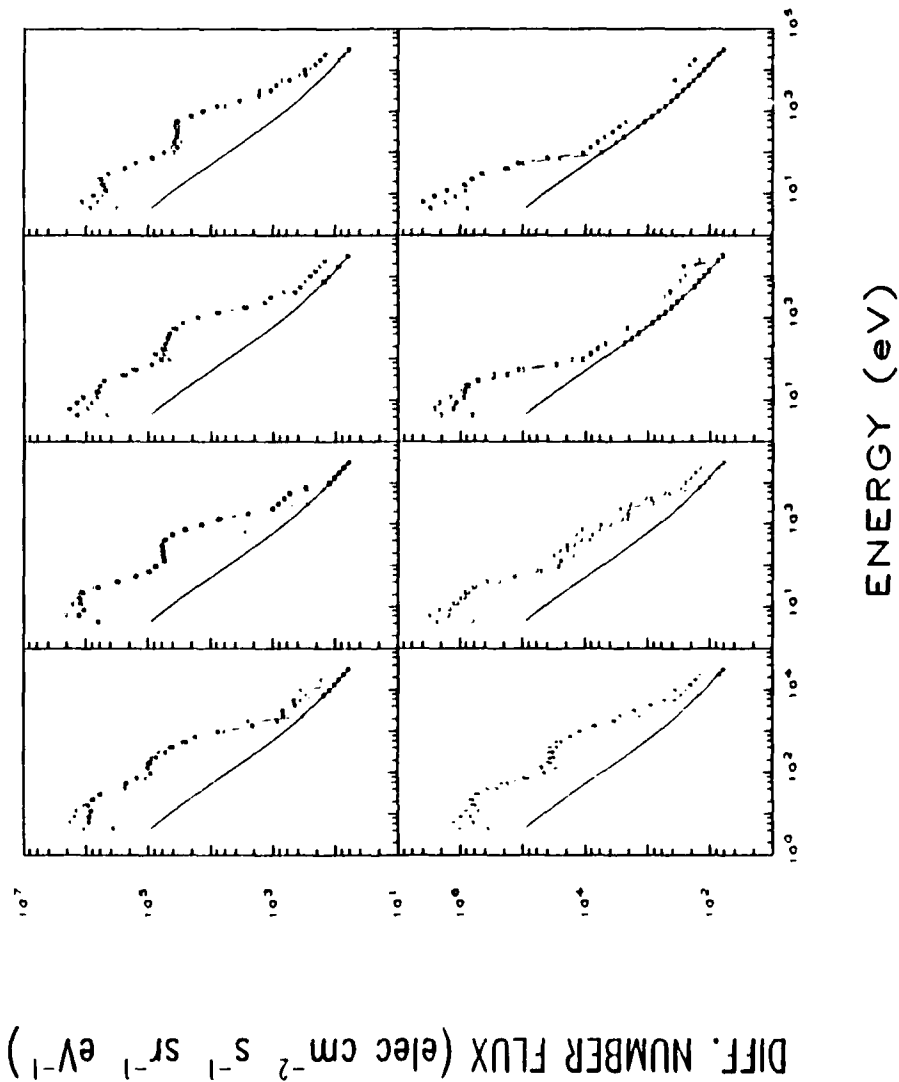


UT(H:M:S)	14:32:00	14:34:00	14:36:00	14:38:00	14:40:00
ILAT(D)	87.6	80.8	74.0	67.1	60.3
MLT(HR)	16.7	18.1	19.5	20.8	22.2
ALT(KM)	411	454	498	542	586
GLAT(D)	78.6	75.1	71.5	67.9	64.4
GLONG(D)	-56.2	-15.8	24.6	65.0	105.4

Fig. 2(b) LAPI ion spectrogram and plasma parameters for Day 264.

81264 DE-2
LAPI ELECTRONS

INVL 70.13 67.68
GLONG 120.93 120.76
MLT 22.48 22.51
GLAT 76.28 73.62
ALT 529 543



FLOW VEL. 0.00 km/s
SC POT. -1.50 V

HH:MM	NUMBER OF SWEEPS	SS:MSC	PA
14:37	6		
SYM/SEN	(DEG.)		
A	25:943	6.0	7.5
B	25:943	58.5	58.5
C	31:959	7.5	7.5
D	31:959	58.5	60.0
E	37:943	6.0	7.5
F	37:943	58.5	60.0
G	43:959	6.0	60.0
H	43:959	58.5	58.5
I	49:943	6.0	60.0
J	49:943	58.5	58.5
K	55:959	6.0	60.0
L	55:959	58.5	58.5
M	01:943	6.0	7.5
N	01:943	58.5	58.5
O	07:959	6.0	60.0
P	07:959	58.5	58.5

Fig. 3 Electron spectra of Day 264 between 1437:26 and 1438:08 UT. The quasi-Maxwellian spectra show near isotropy for this quiet-time pass.

Thus, although the diffuse aurora proper is narrower in latitude during quiet times, a region of lower energy particles often extends to high latitudes. When these particles are energetic and intense enough, they can produce an auroral-E layer at high latitudes. The pattern on the spectrogram of Figure 2 represents the particle signature of an optical emission pattern that has been seen in images of the polar cap during such times (S. Murphree, personal communication; and Plate 13 of Frank et al., 1986). In this pattern, UV and 630 nm emissions are seen covering as much as half of the area normally designated the polar cap. In the latter reference, the signature is associated with the occurrence of a theta aurora. It fills the dawn polar cap from the theta bar to the oval.

During disturbed times the diffuse aurora can become very broad, covering many degrees of latitude, as is shown by the spectrogram and plots of Figure 4. The format is the same as that of Figure 2 except that upcoming ions have been added. The figure shows HAPI particle data measured during the first hour of Day 285 (Oct. 12) 1981 during a three-hour interval characterized by $K_p = 4-$. A solar storm had just occurred with Dst reaching its most negative value during hour 20 of the previous day. The electron spectrogram shows that the poleward edge of auroral oval activity is low in latitude, $\sim 72^\circ$ IL. Only polar rain was detected poleward of this latitude. The BPS extends at least down to about 68.9° IL (~ 0032 UT). The diffuse auroral region extends from 68.9° IL equatorward to 57.9° IL covering almost 11° of latitude.

This pass exhibits several features common to diffuse auroral precipitation during disturbed times. One of these is in the presence of DC electric fields found quite far equatorward within diffuse auroral latitudes. In this pass such a field is indicated between 0042 and 0045 UT by the ion inverted V event (second of Figure 4(b) panel) shown by the upcoming ions. The energies of the ions in the pattern is a measure the potential drop below the satellite. Evidence of a small field aligned potential drop above the satellite (~ 100 eV at the peak) is also seen at the same latitudes in the electron spectrogram.

High resolution observation of electrons precipitating into the disturbed-time diffuse auroral regions as in Figure 4(a) shows vividly the structured, active nature of the electron populations. Much of the structure results from the presence of small DC and quasistatic electric fields. This structure in the electron data, filamentation of auroral forms, and resulting field-aligned currents and plasma waves are a subject of much interest and will be investigated further in the next funding increment.

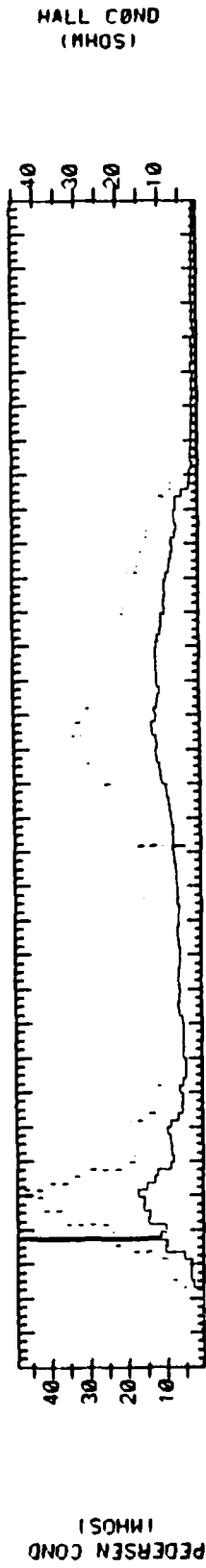
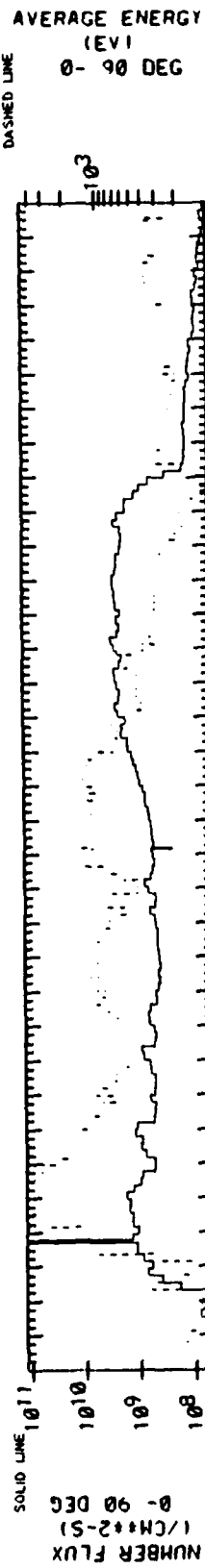
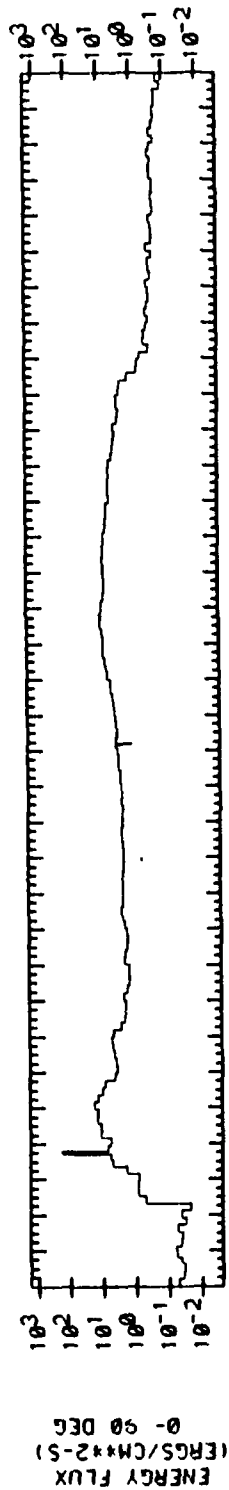
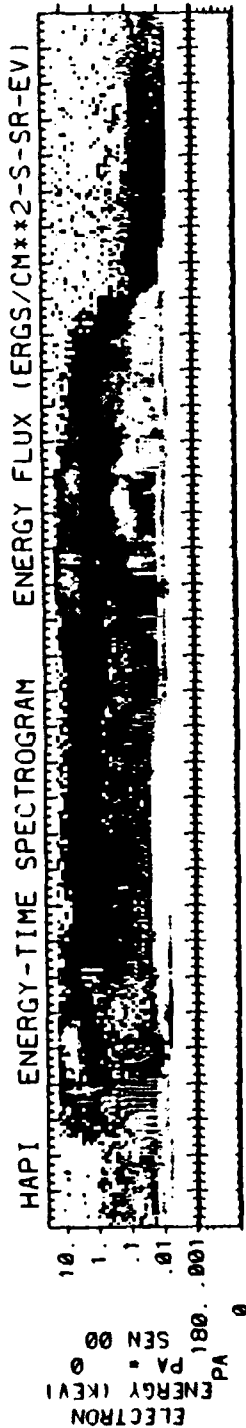
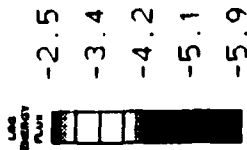
Another feature of the diffuse aurora present in disturbed time passes is the low-energy electron population at the equatorward edge of precipitation. We see in Figure 4(a) that this population may be detached from the high energy (\sim keV) electrons present in the spectrogram down to $\sim 60.5^\circ$ IL (0046 UT). Other passes show an even greater detachment of this population. The electron energies, i.e. ≤ 1 keV will produce 630 nm-rich emissions that will also contain significant amounts of 427.8 nm and 557.7 nm wavelengths. These events show certain similarities to type-A red auroras observed during the main phase of auroras (Robinson et al., 1985). They are not the "detached arcs" reported from the ISIS-2 observations in that such arcs were attributed to electrons in the 1 keV to >40 keV energy range (Wallis et al., 1979; Vondrak et al., 1983).

The association of this low-energy electron population with the equatorward edge of the disturbed-time diffuse aurora has emerged as a direct result of this investigation.

81285

DE-1 DATA

SWRI



UT(H:M:S)	00:30:00	00:40:00	00:50:00
ILAT(D)	70.3	62.9	55.5
MLT(HR)	22.0	21.9	21.7
ALT(KM)	11648	9410	7171
GLAT(D)	47.5	36.2	25.0
GLONG(D)	-46.5	-49.3	-52.1

Fig. 4(a) HAPI electron spectrogram (0° pitch angle), plasma parameters and conductivities for the disturbed-time pass of Day 285 (October 12), 1981.

81285

DE-1 DATA

SWRI

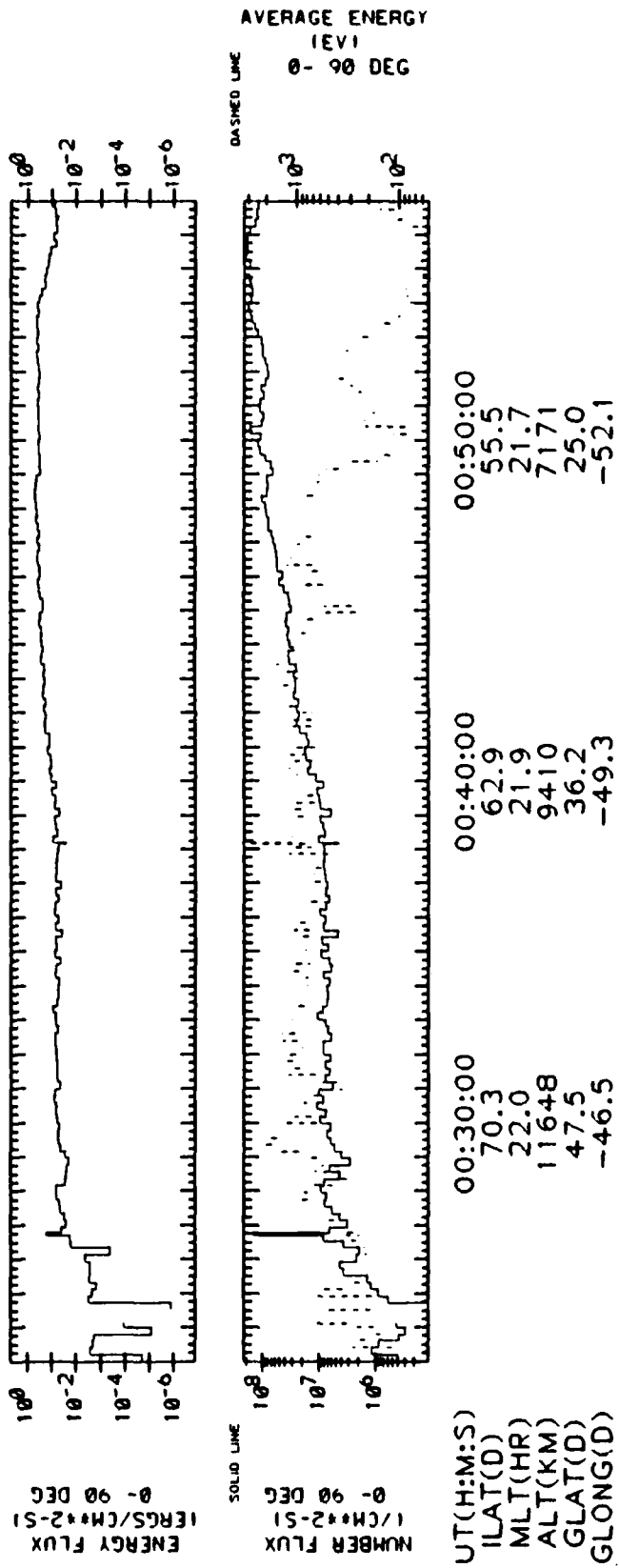
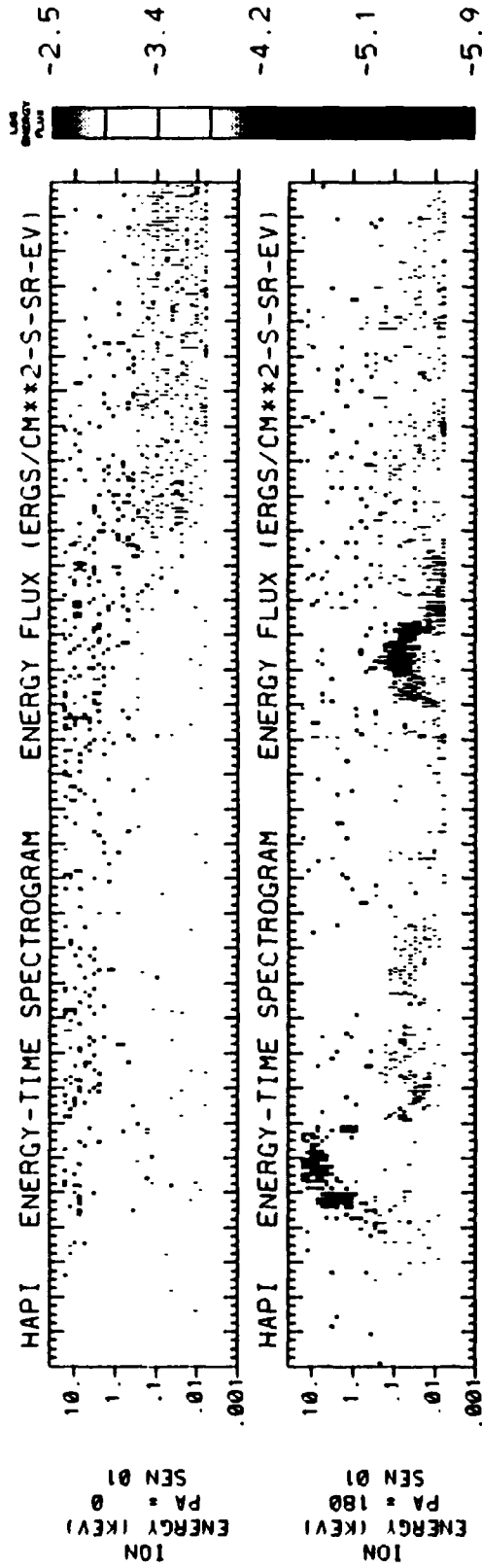


Fig. 4(b) HAPI spectrograms of precipitating (top panel) and returning (second panel) ions and plasma parameters (lower panels) for Day 285.

In fact they became evident as the DE particle data were surveyed to find SAR arc observations in the equatorward edge/trough/plasmapause study (section III.D). They occur during storm main and recovery phases. Further study of this population as it relates to convection, precipitation, and the sub-auroral electric fields will continue during the next phase of support.

A larger body of DE data that includes the observations of this section is now being analyzed in preparation for publication.

C. DE Observations of Waves in the Diffuse Auroral Regions

This study has involved a collaborative effort between researchers of SwRI and the University of Iowa where the Plasma Wave Instrument on DE-1 was built. The waves question is extremely important in that it has bearing on the precipitation mechanism. Our first step has been an effort to survey the simultaneous particle and wave data to determine what relationships, if any, exist between the particles producing the diffuse aurora and waves detected at the intermediate altitudes covered by DE-1 (i.e., $\sim 1 - 3.5 R_E$).

Using simultaneous observations from the High Altitude Plasma Instrument and the Plasma Wave Instrument on board the Dynamics Explorer-1 satellite, we have examined 28 auroral zone crossings equally divided among dayside and nightside cases covering a range of Kp values from 1- to 8. We find that in the diffuse auroral region (CPS), electrostatic emissions of frequencies up to a few kHz are associated with the low-energy, field-aligned electron beams.

An example spectrogram taken from a recently submitted publication (Sharber et al., 1988b; included in this report as Appendix B) is shown in Figure 5. The figure shows the HAPI electron data (top panel) and the PWI electric and magnetic field amplitude measurements (middle and lower panels) and identifies the diffuse auroral particles and the electrostatic emissions. Figure 6 shows both the 20-100 eV field-aligned beams and a single spin HAPI contour plot showing the beams between 0350:08 and 0350:14 UT. Of 18 cases (11 nightside; 7 dayside) examined at high resolution in the particle data, 15 (9 nightside; 7 dayside) exhibited the field-aligned beams with the electrostatic waves. In most cases the beams were upward-directed, but occasionally they traveled both up and down the field line. The three cases showing no beams occurred during intervals of $K_p \leq 2$. We interpret the electrostatic emissions as electron acoustic mode waves excited by the field-aligned beams. A stability analysis based on the plasma parameters of one of the passes supports this interpretation.

This study has been a very successful one and has produced two presentations at meetings and two publications (see Appendix B). The reader is referred to that paper for further details. As we state in that paper, in addition to the electrostatic waves shown in Figure 6, another wave signature, possibly a whistler mode wave similar to plasmaspheric hiss, has been identified. The emission is usually seen throughout the diffuse auroral region. Some passes show a break between the plasmaspheric hiss (which usually peaks near the equatorward edge of the diffuse aurora) and this similar but lower frequency emission. We have identified this signature in all 14 of the dayside passes and in 9 of the 14 nightside cases studied in the initial survey. An example is shown as Figure 3 of Appendix B.

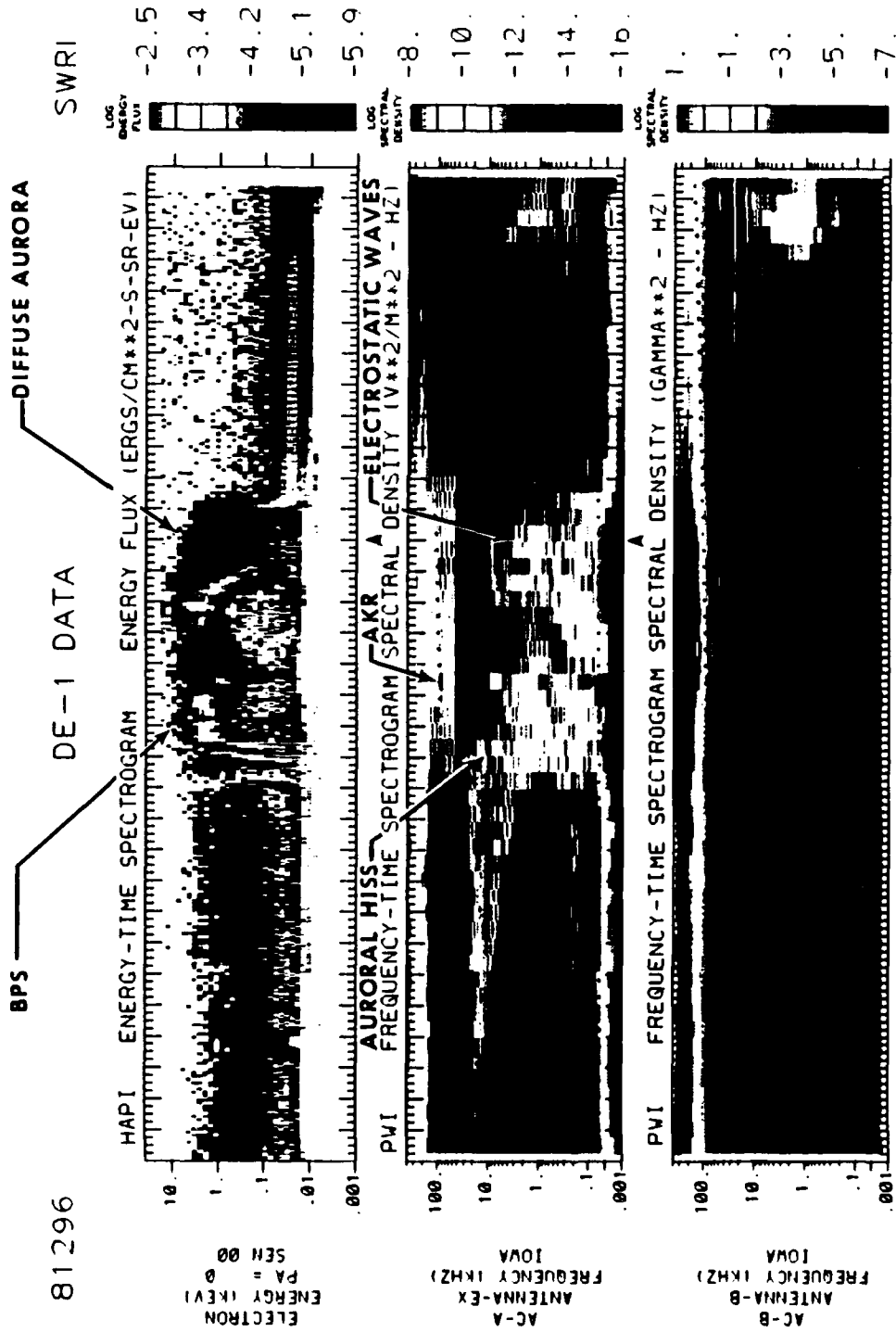


Fig. 5 Nightside example of simultaneous particle and wave measurements from DE-1 on Day 296 (Oct. 23) 1981. HAPI measurements of 0° pitch angle electrons are shown in the top panel. The second and third panels are frequency-time spectrograms of the PWI electric and magnetic field amplitude measurements. The electrostatic waves labeled (second panel) are associated with the beams near 0349 and 0350 UT.

D. The Diffuse Aurora Equatorward Edge, the Trough, and the Plasmapause

This investigation began with a study four occasions when DE-1 and DE-2 were in magnetic conjunction. Its purpose was to investigate the relationships between the diffuse auroral region, the midlatitude trough, and the plasmapause at high (DE-1) and low (DE-2) altitudes. The interrelationships between these regions, treated initially in this contract in the Senior et al. (1987) study (Appendix A), are continued in this study. They are important in determining the relationship between the particle precipitation and convective flow patterns. The study is comprehensive in that we were using data from particle, plasma electric and magnetic fields, and waves experiments on the DE satellites. The passes are all within the evening- midnight sector and take place during both quiet and disturbed times.

Our findings have shown that during both quiet and disturbed times, very little difference with respect to altitude was observed in the diffuse auroral region and equatorward boundary locations. In three of the four cases, the trough was collocated with the equatorward edge of diffuse auroral precipitation. In the fourth (and quietest) case, the trough spans latitudes of the entire diffuse auroral region. The plasmapause, identified directly by the RIMS (retarding ion mass spectrometer) ion measurements, lies on or equatorward of the equatorward trough wall. During the quiet times this wall is not steep and may span several degrees of latitude, an observation consistent with Green et al. (1986) and Rodger et al. (1986). A population of low-energy electrons similar to those observed previously over SAR arcs (stable auroral red arcs seen during magnetic storm times at plasmapause latitudes--Gurgiolo et al. (1982) and Slater et al. (1987) was measured by LAPI on DE-2 on each of the four cases under study. A determination of the characteristics of these electrons has become a separate study.

The study has resulted in an AGU meeting presentation and a publication now in preparation.

The SAR arc part of this investigation was considered especially important in that in some cases where SAR arcs were not observed, signatures in the low-energy electron measurements (Gurgiolo et al., 1982) were seen. As a result a case study was conducted, focusing on two time intervals in which the DE satellites passed over this equatorial boundary region. The crossings which took place on Days 291 and 305 occurred in late storm recovery phases. The findings of that study follow:

- The low-energy electrons are observed in the plasmapause region as determined by either direct measurement by RIMS and PWI on DE-1 or by the ionospheric electron temperature increase seen in the LANG data on DE-2.
- The electrons were detected in LAPI's lowest three energy channels (5.1 - 8.8 eV) and were observed most intensely over a latitude range of $\sim 12^\circ$ in one case (Day 291) and $\sim 1.5^\circ$ in the other (Day 305).
- The low-energy electrons observed in these cases differ from "SAR arc electrons" only in that their densities and temperatures are lower. Densities for both these cases are a few electrons cm^{-3} ; temperatures were low on the Day 291 case (6630° K) and higher for the Day 305 case (11,600° K).

- When conjugate photoelectrons were observed with sufficient intensity (Day 305), their fluxes were diminished where the low-energy electrons were observed. This decrease has been reported for SAR arcs as well (Gurgolo et al., 1982) and suggests scattering of the population on plasmapause field lines.
- In both examples, enhancements in electron fluxes between 1 and 15 keV are seen at latitudes where the low-energy electrons are observed.
- The low-energy electrons are associated with enhancements in the Geiger fluxes (Day 305) or structure in these fluxes (Day 291). Both situations occur on the poleward gradient of the outer belt trapped fluxes; although in the Day 291 case, the low-energy electrons extended equatorward to latitudes where very little gradient and structure were present. The Geiger tubes respond primarily to electrons of $E > 35$ keV and protons of $E > 500$ keV, but extension of the electron spectrum to high energies can account for the Geiger tube responses.
- In the Day 305 example, emissions in the frequency range ~ 100 - 1000 Hz are observed at the same latitudes as the precipitating low-energy electrons, enhancements in the LAPI keV electron fluxes and Geiger counters, and the reduction in conjugate photoelectron flux. These emissions are probably plasmaspheric hiss; their part in the energy transfer process is currently the subject of further investigation.

Our observations are consistent with the findings of Kozyra et al. (1987) in which it is demonstrated that Coulomb interactions are the primary mechanism of energy transfer from the magnetosphere to the ionosphere in the plasmapause region.

The study is comprehensive in the sense that several plasma and field instruments were used in addition to the HAPI and LAPI data. An earlier version of it was presented at the SPI Conference at MIT on Ionosphere-Magnetosphere-Solar Wind Coupling Processes. The study has been published in the conference proceedings (Sharber et al., 1988a). The publication is included in this report as Appendix C.

E. Mechanisms of Diffuse Auroral Precipitation

Kennel (1969) stated that one of the consequences of a turbulent magnetospheric plasma is pitch angle scattering of the inner plasma sheet population and subsequent scattering of the particles into the loss cone to produce auroral emissions in the upper atmosphere at the foot of the field line. The problem seemed a straightforward one and was applied specifically by Lyons (1974) who developed a theory of diffuse auroral precipitation resulting from diffusion of electrons into the loss cone by electron cyclotron harmonic (ECH) waves. Lyons's theory was successful as a theory, but required ECH waves of strength 1-10 mV/m to diffuse plasma sheet electrons of a few tenths to a few keV in energy. These wave amplitudes resulted from a "bounce-averaged" diffusion coefficient and were prefaced by an observation of ECH waves from OGO-5 (Kennel et al., 1970) showing such strengths. Since that time, many observations from other satellites have shown that the wave strengths are generally not high enough to produce the required strong pitch angle diffusion (Fontaine and Blanc, 1983; Fontaine et al., 1986; Roeder and Koons, 1988; Shumaker et al., 1988). Thus it is clear that to precipitate diffuse auroral electrons will require either that another wave be

identified (no other wave with sufficient strength appears to be present in the equatorial plasma sheet (Roeder and Koons, 1988)) or that another process, eg. the effects of particle motion in the convecting plasma sheet be given greater emphasis (Fairfield and Viñas, 1984).

One of the conclusions of the Roeder and Koons (1988) study is that "the only method of solving the diffuse auroral problem is more coordinated studies of the particles and the wave fields at several points along a geomagnetic field line."

Our waves study under this contract, very timely in this regard, was begun before the above statement was made. Our object was to survey the mid-altitude range ($\sim 1 R_E$ to $3.5 R_E$) DE-1 plasma and wave data to see what relationships, if any, exist between the simultaneously measured particles and waves. Our results (see Sec. III.C. and Appendix B) are the identification of two types of waves that can be associated with the diffuse aurora. One is an acoustic mode wave, driven by low energy (<100 eV) field-aligned electron beams. The other has been identified but not studied in detail yet. It is electromagnetic, probably a whistler mode wave similar to plasmaspheric hiss. The acoustic mode waves and electron beams were seen in 15 of 18 cases studied at high resolution. The three cases for which no beams were seen took place in intervals of $Kp < 2$. Acoustic mode waves are not unique to the diffuse aurora in that they have been observed previously in the cusp (Lin et al., 1985). The electromagnetic wave (Figure 3 of Appendix B) was observed in all 14 dayside passes and in 9 of the 14 nightside cases analyzed.

The electron acoustic waves would not be expected to precipitate keV electrons, but would instead interact more efficiently with electrons with energies comparable to the beam energies. The beams themselves can carry significant field-aligned currents and may at times be the current carriers of the Region 2 currents. In the waves study (Appendix B) we found that the beams in the diffuse auroral regions occur within a broad region of mostly downward (Region 2) current. A detailed study of the currents is now required, but if the finding is a general one, a direct coupling mechanism between the diffuse aurora the ionosphere will be established. The coupling would exhibit the kind of dependence on Kp as is shown by the Birkeland current system.

The whistler mode waves, although very strong, will resonate with electrons of only very high energies (hundreds of keV or greater) at DE-1 altitudes. Thus, they do not precipitate diffuse auroral electrons in the mid-altitude range.

Regarding the diffuse auroral ion precipitation, it seems that either the Speiser mechanism (Lyons and Speiser, 1982) or the effects of convective flow in the tail and near-earth regions (see Hardy et al., 1988 and references therein) will account for the precipitation at least for non-substorm times. In both cases, particularly the electron case, more work will be required before a complete explanation is reached. Our initial attempt to find the mechanism(s) at DE-1 altitudes must be followed by more wave and particle comparisons at other altitudes along the field lines between the few R_E altitudes of DE-1 and the equatorial regions. The investigation will be a major part of our proposal for continued AFOSR support.

IV. RELATED STUDIES

A. Arcs, Convection, and Ionization in the Polar Cap

Several studies have been conducted in this area. One of these, "Ionospheric Convection Signatures and Magnetic Field Topology" (Coley et al., 1987) investigates the relationships between auroral zone convective electric field patterns, precipitating electrons, and the open-closed nature of the magnetic field as determined by the Geiger fluxes (electron $E > 35$ keV, ion $E > 500$ keV) from DE-2. The paper has been published in JGR.

Another somewhat more comprehensive study has been conducted using particle and plasma flow observations from LAPI and IDM (ion drift meter) on DE-2, and polar cap arc observations made from the all-sky imaging photometer aboard the AFGL Airborne Ionospheric Observatory. These measurements were made during the January 1982 coordinated aircraft/satellite campaign to study the polar ionosphere. Its objective has been to determine the relationships between polar cap arcs, incident enhancements of several hundred eV electrons, and the convection electric field direction.

The study established the importance, during IMF north or very weak IMF south conditions, of extended (along the sun-earth direction) "finger-like" convection cells in the polar cap regions and the one-to-one correspondence of these elongated cells with electron precipitation and gradients in plasma (ion) drift velocity where the $\nabla \cdot \mathbf{E} < 0$ condition is met. The electron precipitation associated with the polar arc patterns are the same as those shown in the quiet-time, IMF north case of this report (see Figure 2, Sec. III.B.). The study demonstrates a coherent pattern of convection, particle precipitation, and current flows in the high-latitude polar regions. A paper, "Coherent Mesoscale Convection Patterns During Northward IMF," Carlson et al., 1988) has been accepted for publication in JGR.

B. Particle Calibration of the DE-1 Scanning Auroral Imager

Although the active observation period for the LAPI detector lasted from August, 1981 through February, 1983, the HAPI experiment on DE-1 ceased operation in late December, 1981. The DE-1 Scanning Auroral Imager (Frank et al., 1981) is still operating and can provide needed spectral and intensity information on the incoming particles if it has been calibrated against simultaneous particle observations. In this study two passes were selected in which a magnetic conjunction between DE-1 and -2 existed. LAPI (on DE-2) electron measurements of downcoming energy flux were compared with SAI measurements of auroral emissions at 577.7 and 630.0 nm. The DE data were then used as inputs to the auroral F-region ionosphere model of Sojka and Schunk (1983) in order to account directly for the effects of increased magnetospheric activity. The study "Modeled F-Region Response to Auroral Dynamics Based upon Dynamics Explorer Auroral Observations" (Sojka et al., 1988) has been submitted to JGR for publication and is now in the last stages of review.

V. PUBLICATIONS

The following are cumulative lists of journal publications and meeting presentations supported by this contract.

A. Published Articles

1. Dynamics Explorer-2 Measurements During an Isolated Auroral Substorm," by J. R. Sharber and J. D. Winningham, to be published in *Proceedings of the Third Finnish-American Auroral Workshop*, October 14-18, 1985, Finnish Academy of Science and Letters, Report No. 45, Sodankyla Finland, 1986.
2. E-and F-Region Study of the Evening Sector Auroral Oval: A Chatanika/Dynamics Explorer-2/NOAA-6 Comparison," C. Senior, J. R. Sharber, O. de la Beaujardiere, R. A. Heelis, D. S. Evans, J. D. Winningham, M. Sugiura, and W. R. Hoegy, published in the *Journal of Geophysical Research*, **92**, 2277-2494, 1987.
3. "Ionospheric Convection Signatures Observed by DE-2 During Northward IMF," by R. A. Heelis, P. H. Reiff, J. D. Winningham, and W. B. Hanson, published in the *Journal of Geophysical Research*, **91**, 5817-5830, 1986.
4. "Ionospheric Convection Signatures and Magnetic Field Topology," W. R. Coley, R. A. Heelis, P. H. Reiff, W. B. Hanson, J. D. Winningham, and J. R. Sharber, *Journal of Geophysical Research*, **92**, 12352, 1987.
5. "Coherent Mesoscale Convection Patterns During Northward IMF," H. C. Carlson, R. A. Heelis, E. J. Weber, and J. R. Sharber, *Journal of Geophysical Research*, accepted for publication, 1988.
6. "Simultaneous Density and Electric Field Fluctuation Spectra Associated with Velocity Shears in the Auroral Oval," Sunanda Basu, Santimay Basu, E. MacKenzie, P. F. Fougere, W. R. Coley, R. A. Heelis, N. Maynard, J. D. Winningham, W. B. Hanson, C. S. Lin, W. R. Hoegy, and B. G. Ledley, *Journal of Geophysical Research*, **93**, 115, 1988.
7. "Modeled F-Region Response to Auroral Dynamics Based Upon Dynamics Explorer Auroral Observations," J. J. Sojka, R. W. Schunk, J. Craven, L. A. Frank, J. R. Sharber, and J. D. Winningham, submitted to *Journal of Geophysical Research*, October, 1987.
8. "Theory of Auroral Electron Suprathermal Burst," Y. T. Chin, R. M. Robinson, J. M. Cornwall, R. Heelis, J. R. Sharber, J. D. Winningham, and J. L. Burch, submitted to *Journal of Geophysical Research*, 1987.
9. "Plasma Waves Associated with Electron Beams in the Diffuse Auroral Region," J. D. Menietti, J. R. Sharber, and J. L. Burch, and D. A. Gurnett, *Ionosphere - Magnetosphere - Solar Wind Coupling, SPI Conference Proceedings and Reprint Series*, **7**, 1988.
10. "Further Boundary Conditions on the Low-Energy Electrons in the Plasmopause Region," J. R. Sharber, J. D. Winningham, J. L. Burch, W. R. Hoegy, A. M. Persoon, and J. H. Waite, Jr., *Ionosphere - Magnetosphere - Solar Wind Coupling Processes, SPI Conference Proceedings and Reprint Series*, **7**, 1988.
11. "Plasma Waves Associated with Diffuse Auroral Electrons at Mid-altitudes," J. R. Sharber, J. D. Menietti, H. K. Wong, J. L. Burch, D. A. Gurnett, J. D. Winningham, and P. J. Tanskanen, submitted for publication to *Advances in Space Research*, 1988.

B. Meeting Presentations

1. "E and F-Region Study of the Evening Sector Auroral Oval: A Chatanika/Dynamics Explorer-B Data Comparison" by C. Senior, O. de la Beaujardiere, and J. R. Sharber, presented at the 6th IAGA Scientific Assembly, Prague, Czechoslovakia, August, 1985, abstract published in *Programme and Abstracts, IAGA Bulletin*, IUGG Publications Office, Paris, 1985.
2. "Study of the Evening Sector Auroral Oval with the Chatanika Radar, DE-2, and NOAA-6: I. E-Region Ionization Sources," by J. R. Sharber, J. D. Winningham, C. Senior, D. S. Evans, O. de la Beaujardiere, R. A. Heelis, and M. Sugitara, presented at the 1985 Fall Meeting of the A.G.U., abstract published in *E.O.S.*, **66**, 991, 1985.
3. "Study of the Evening Sector Auroral Oval with the Chatanika Radar, DE-2, and NOAA-6: II. F-Region Ionization Sources," by C. Senior, R. A. Heelis, J. R. Sharber, J. D. Winningham, W. R. Hoegy, presented at the 1985 Fall Meeting of the A.G.U., abstract published in *E.O.S.*, **66**, 991, 1985.
4. "A Study of Auroral Particle Fluxes at Three Altitudes," by R. M. Robinson, Y. T. Chiu, J. R. Sharber, J. D. Winningham, J. L. Burch, J. D. Craven, and L. A. Frank, presented at the A.G.U. *Chapman Conference on Ionospheric Plasmas in the Magnetosphere: Sources, Mechanisms, Consequences*, abstract published in conference program and proceedings, February 3-7, 1986.
5. "Dynamics Explorer Contributions to the 1981 Cooperative Auroral Investigations," J. R. Sharber, J. D. Winningham, J. L. Burch, paper presented in poster session at the Finnish-American Auroral Workshop at Sodankyla, Finland, October 14-18, 1985.
6. "Coordinated High and Low Altitude Observations of the Equatorward Edge of the Central Plasma Sheet and Its Relation to the Plasmaspheric Outer Boundary and the Low Altitude Plasma Trough," J. D. Winningham, J. R. Sharber, and R. A. Heelis, presented at the COSPAR Meeting, Toulouse, France, Abstract: *Abstracts of the Twenty-sixth Plenary Meeting of COSPAR*, paper c.1.3.6, **267**, 1986.
7. "Dynamics Explorer Observations of the Diffuse Auroral Equatorward Boundary, Midlatitude Trough, and the Plasmopause," presented at the Fall Meeting of the A.G.U., abstract published in *E.O.S.*, **67**, 1139, 1986.
8. "Ionospheric Convection Associated with Polar Cap Arcs," H. C. Carlson, R. A. Heelis, E. J. Weber, and J. R. Sharber, presented at the Fall Meeting of the A.G.U., abstract published in *E.O.S.*, **67**, 1162, 1986.
9. "Dynamics Explorer Observations of low Energy Electrons at the Plasmopause," J. R. Sharber, J. D. Winningham, and W. R. Hoegy, presented at the Cambridge Workshop on Ionosphere-Magnetosphere-Solar Wind Coupling Processes, July, 1987.

10. "Plasma Waves Associated with Diffuse Auroral Electron Beams in the Mid-Altitude Range," J. D. Menietti, J. R. Sharber, J. L. Burch, and D. A. Gurnett, presented at the Cambridge Workshop on Ionosphere-Magnetosphere-Solar Wind Coupling Processes, July, 1987.

11. "Plasma Waves Associated with Diffuse Auroral Electrons at Mid-Altitudes", J. R. Sharber, J. D. Menietti, H. K. Wong, J. L. Burch, D. A. Gurnett, J. D. Winningham, and P. J. Tanskanen, presented at the Twenty-seventh Planetary Meeting of COSPAR Symposium 8, Helsinki, Finland, July, 1988.

VI. PROFESSIONAL PERSONNEL

Key professional personnel associated with the research effort at SwRI have been Dr. J. R. Sharber, Staff Scientist, and Dr. J. D. Winningham, Institute Scientist. Both are scientists in the Department of Space Sciences, Instrumentation and Space Research Division.

VII. INTERACTIONS (COUPLING ACTIVITIES)

In the past year we have continued our associations with other research laboratories and programs. As in previous years, the chief among these has been the Air Force Geophysics Laboratory and the Dynamics Explorer Science Working Group.

In our interaction with AFGL we have worked most closely in the past year with Drs. E. J. Weber, H. E. Carlson, J. R. Jasperse, and B. Basu, all of the Ionospheric Effects Branch (LIS). We have worked with these personnel in the study of polar cap phenomena (Sec. IV.B.) and in the study of ionization associated with the evening sector auroral oval (Sec. III.A.).

Drs. Winningham and Sharber continue to be associated with the DE program. Dr. Winningham is a member of the Science Team and Dr. Sharber attends team meetings. They both interact with team members on common research interests. The primary institutions involved have been NASA-GSFC (R. A. Hoffman, W. R. Hoegy, L. Brace), U. T. Dallas (R. Heelis, W. B. Hanson), and the University of Iowa (A. Persoon, D. Gurnett).

Our interactions with members of the DE-Science Team have overlapped to some extent with AFGL interactions particularly in the areas of the diffuse auroral particle and wave studies and in the polar cap phenomena research. This has followed naturally from early planning (in CY1981) in coordinating the AFGL aircraft flights of Jan. 1982 and Jan. 1983 with coincident passes of DE-2. The planning of that polar cap study campaign and the research publications that have followed and will continue stand as an excellent example of the benefits of our joint interaction with both AFGL and the DE Science Team. As a result, the Air Force, as well as the science community at large, has gained a far more complete understanding of physical processes affecting the auroral and polar ionosphere. This has been a very productive collaboration.

Our collaboration with incoherent scatter radar investigators over the past two years has been very productive and will continue. These radar facilities offer a powerful means of determining ionospheric parameters such as ionospheric temperature, ionospheric electric field components, ionization profiles with latitude and altitude, and Hall and Pederson conductances. Depending on the particular radar mode of operation, measurements can be

made with a variety of objectives, focusing on restricted ionospheric regions for localized studies or over volumes on the global scale (in the course of several hours). For our own studies the radars provide added information to be used as boundary conditions in input-output experiments or additional parameters for providing complete descriptions of the auroral ionosphere.

The investigations under this contract have made use of the last months of operation of the Chatanika facility at Fairbanks, the winter months of 1981, and the first months of operation of EISCAT at Tromso, Norway. In the collaboration involving this data, we interact routinely on a scientific level with Dr. O. de la Beaujardiere of SRI, Drs. R. R. Vondrak and R. M. Robinson of Lockheed, Palo Alto, and Dr. C. Senior of the Center for Research on the Physics of Terrestrial and Planetary Environments, St. Maur, France. An additional benefit comes from our association with Dr. Senior. All EISCAT data is archived at the laboratory at St. Maur and is therefore easily obtainable in studies involving that data.

VIII. INVENTIONS OR PATENT DISCLOSURES

No inventions or patent disclosures have resulted from the research effort of this contract.

IX. ACCOMPLISHMENTS

The most significant accomplishments are listed as follows:

- Coordinated study of the evening sector aurora and associated ionization (see Sec. III.B. and Appendix A to this report). This was a comprehensive study involving DE-2, NOAA-6, and Chatanika Radar observations that enabled a very thorough description of a moderately active diffuse aurora from the standpoint of particle (electron and ion) precipitation and E and F layer ionization and electrodynamics.
- Observation of the electrostatic and electromagnetic waves associated with the diffuse aurora. This resulted from a survey of mid-latitude (DE-1) simultaneously measured particle and wave data. The study is described in Sec. III.C. and Appendix B of this report. Implications to the diffuse auroral electron precipitation mechanism are discussed in Sec. III.E.
- The determination of coherent mesoscale convection patterns in the polar cap. This has provided a clear picture of the relationship between particle precipitation, polar cap arcs, and convection at high latitudes. The DE-2 data played an important part in this study which is described in Sec. IV.A. of this report.
- The determination of further boundary conditions on the low-energy (SAR arc-like) electrons at the magnetopause. One of the conditions associated with these <10 eV electrons is the presence of high energy dumping events seen in the precipitating (>15keV) LAPI and Geiger counter (>35 keV) fluxes. The work is described in Sec. III.D. and in Appendix C of this report.

- These and other accomplishments of the research have been reported to the scientific community in the form of 11 presentations at scientific meetings and 11 journal publications.
- In the years of performance of this contract we have built a strong polar research program emphasizing close cooperative investigation and interaction with AFGL, the DE Science Team, and incoherent scatter investigators. This approach has proven beneficial to the U.S. Air Force as well as the scientific community. We will follow this successful program with a proposal to continue the research that has been started and expand the scope of the work.

X. REFERENCES

- Ashour-Abdalla, M., and C. F. Kennel, Diffuse auroral precipitation, *J. Geomag. Geoelectr.*, **30**, 239, 1978.
- Carlson, H. C., R. A. Heelis, E. J. Weber, J. R. Sharber, and J. D. Winningham, Coherent mesoscale convection patterns during northward IMF, accepted for publication in *J. Geophys. Res.*, 1988.
- Coley, W. R., R. A. Heelis, P. H. Reiff, W. B. Hanson, J. D. Winningham, and J. R. Sharber, Ionospheric convection signatures and magnetic field topology, submitted to *J. Geophys. Res.*, 92, 12352, 1987.
- Fairfield, D. H. and A. F. Viñas, The inner edge of the plasma sheet and the diffuse aurora, *J. Geophys. Res.*, **89**, 841, 1984.
- Fontaine, D., and M. Blanc, A theoretical approach to the morphology and the dynamics of diffuse auroral zones, *J. Geophys. Res.*, **88**, 7171-7184, 1983.
- Fontaine, D., S. Perrant, N. Cornilliau-Wehrlin, B. A. Paricio, J. M. Bosqued, D. Rodgers, Coordinated observations of electron energy spectra and electrostatic cyclotron waves during diffuse auroras, *Annales Geophysicae*, 86005A, 405-412, 1986.
- Frank, L. A., J. D. Craven, D. A. Gurnett, D. Shawhan, D. R. Weimer, J. L. Burch, J. D. Winningham, C. R. Chappell, J. H. Waite, R. A. Heelis, N. C. Maynard, M. Sugiura, W.K. Petersen, and E. G. Shelley, The theta aurora, *J. Geophys. Res.*, **91**, 1377-3224, 1986.
- Green, J. L., J. H. Waite, Jr., C. R. Chappell, M. O. Chandler, J. R. Douppnik, P. G. Richards, R. Heelis, S. D. Shawhan, and L. H. Brace, Observations of ionospheric/magnetospheric coupling: DE and Chatanika coincidences, *J. Geophys. Res.*, **91**, 5803, 1986.
- Gurgiolo, C., D. W. Slater, J. D. Winningham, and J. L. Burch, Observation of a heated electron population with 6300Å SAR arc emission, *Geophys. Res. Lett.*, **9**, 965, 1982.
- Hardy, David A., M. S. Gussenhoven, and D. Brautigam, A statistical model of auroral ion precipitation, submitted to *J. Geophys. Res.*, 1988.

- Jasperse, J. R. and B. Basu, Transport theoretic solutions for auroral proton and H atom fluxes and related quantities, *J. Geophys. Res.*, **87**, 811, 1982.
- Kennel, C. F., F. L. Scarf, R. W. Fredricks, J. G. McGehee, and F. V. Coroniti, VLF electric field observations in the magnetosphere, *J. Geophys. Res.*, **75**, 6136-6152, 1970.
- Kozyra, J. U., E.G. Shelley, R. H. Comfort, L. H. Brace, T. E. Cravens, and A. F. Nagy, The role of ring current O^+ in the formation of stable auroral red arcs, *J. Geophys. Res.*, **92**, 7487-7502.
- Lyons, Lawrence R., Electron diffusion driven by magnetospheric electrostatic waves, *J. Geophys. Res.*, **79**, 575, 1974.
- Lyons, L. R., and T. W. Spelser, Evidence for current sheet acceleration in the geomagnetic tail, *J. Geophys. Res.*, **87**, 2276-2286, 1982.
- Robinson, R. M. and R. R. Vondrak, Characteristics and sources of ionization in the continuous aurora, *Radio Science*, **20**, 447-455, 1985.
- Robinson, R. M., S. B. Mende, R. R. Vondrak, J. U. Kozyra, and A. F. Nagy, Radar and photometric measurements of an intense Type A red aurora, *J. Geophys. Res.*, **90**, 457-466, 1985.
- Rodger, A. S., L. H. Brace, W. R. Hoegy, and J. D. Winningham, The poleward edge of the mid-latitude trough--its formation, orientation and dynamics, *J. Atmos. Terr. Phys.*, **45**, 715-728, 1986.
- Roeder, J. L., and H. C. Koons, A survey of electron cyclotron waves in the magnetosphere and the diffuse auroral electron precipitation, submitted for publication in *J. Geophys. Res.*, 1988.
- Senior, C., J. R. Sharber, O. de la Beaujardiere, R. A. Heelis, D. S. Evans, J. D. Winningham, M. Sugiura, and W. R. Hoegy, E- and F-Region Study of the Evening Sector Auroral Oval: A Chatanika/Dynamics Explorer-2/NOAA-6 comparison, *J. Geophys. Res.*, **92**, 1987.
- Sharber, J. R., The continuous (diffuse) aurora and E-region ionization, in *Physics of Space Plasmas (1981)*, 115-139, edited by T. S. Chang, B. Coppi, and J. R. Jasperse, Scientific Publishers, Cambridge, MA, 1981.
- Sharber, J. R., J. D. Winningham, J. L. Burch, W. R. Hoegy, A. M. Persoon, and J. H. Waite, Jr., Further boundary conditions on the low-energy electrons in the plasmopause region, *Ionosphere-Magnetosphere-Solar Wind Coupling Processes, SPI Conference Proceedings and Reprint Series*, **7**, 1988a.
- Sharber, J. R., J. D. Menietti, H. K. Wong, J. L. Burch, D. A. Gurnett, J. D. Winningham, and P. J. Tanskanen, Plasma waves associated with diffuse auroral electrons at mid-altitudes, submitted for publication to *Adv. Space Res.*, 1988b.

- Shumaker, T. L., M. S. Gussenhoven, D. A. Hardy, and R. L. Corovillano, The relationship between diffuse auroral and plasma sheet electron distributions near local midnight, submitted for publication in *J. Geophys. Res.*, 1988.
- Sojka, J. J., R. W. Schunk, J. Craven, L. A. Frank, J. R. Sharber, and J. D. Winningham, Modeled F-Region Response to Auroral Dynamics Based Upon Dynamics Explorer Auroral Observations, submitted to *Journal of Geophysical Research*, October, 1987.
- Swift, Daniel W., Mechanisms for auroral precipitation: A review, *Rev. Geophys. and Space Phys.*, **19**, 185, 1981.
- Toffoletto, F. R. and T. H. Hill, Mapping the solar wind electric field onto the earth's polar caps, accepted for publication, *J. Geophys. Res.*, 1988.
- Wallis, D. D., J. R. Burrows, M. C. Moshupl, C. D. Anger, and J. S. Murphree, Observations of particles precipitating into detached arcs and patches equatorward of the auroral oval, *J. Geophys. Res.*, **84**, 1347-1360, 1979.
- Whalen, J. A., A quantitative description and dynamics of the energy flux in the continuous aurora, *J. Geophys. Res.*, **88**, 7155-7169, 1983.

APPENDIX A

E- and F-Region Study of the Evening Sector Auroral Oval

E and *F* Region Study of the Evening Sector Auroral Oval: A Chatanika/Dynamics Explorer 2/NOAA 6 Comparison

C. SENIOR,¹ J. R. SHARBER,² O. DE LA BEAUJARDIÈRE,³ R. A. HEELIS,⁴
D. S. EVANS,⁵ J. D. WINNINGHAM,² M. SUGIURA,⁶ AND W. R. HOEGY⁷

Simultaneous data obtained with the Chatanika incoherent scatter radar and the Dynamics Explorer 2 (DE 2) and NOAA 6 satellites are used to relate the locations of the precipitating particles, field-aligned currents, and *E* and *F* region ionization structures in the evening-sector auroral oval. The auroral *E* layer observed by the radar extends about 2° equatorward of the electron precipitation region, and its equatorward edge coincides with the equatorward edges of the region 2 field-aligned current and intense convection region ($E \approx 50$ mV/m). It is shown that precipitating protons are responsible for part of the *E* region ionization within the electron precipitation region as well as south of it. *E* region density profiles calculated from ion spectra measured by the DE 2 and NOAA 6 satellites are in fairly good agreement with the Chatanika data. In the *F* region, a channel of enhanced ionization density, elongated along the east-west direction and having a width of about 100 km, marks the poleward edge of the main trough. It is collocated with the equatorward boundary of the electron precipitation from the central plasma sheet. Although enhanced fluxes of soft electrons are observed at this boundary, the energy input to the ionospheric electron gas, calculated from the radar data, shows that this ionization channel is not locally produced by this soft precipitation, but that it is rather a convected feature. In fact, both the trough and the ionization channel are located in a region where the plasma flows sunward at high speed, but the flux tubes associated with these two features have different convective time histories. Keeping in mind that several processes operate together in the *F* region, our data set is consistent with the following trough and ionization channel formation mechanisms. (1) The mid-latitude trough, located equatorward of the electron precipitation region, is mainly the result of transport and enhanced recombination due to large electric fields. Flux tubes on the low-latitude edge of the trough have most probably corotated eastward before flowing sunward at higher latitudes where magnetospheric convection predominates. The trough thus forms by recombination during the long time the flux tubes stagnate in the region where the flow reverses. (2) Flux tubes associated with the ionization channel have drifted antisunward in the polar cap before drifting sunward in the auroral zone. Its formation results from the distortion of polar cap *F* region ionization structures, due to the incompressibility of the flow.

1. INTRODUCTION

The distribution of the plasma in the ionosphere is the result of several processes operating together. These processes include local production by solar radiations and particle precipitation, chemical recombination, and transport.

In the *E* region where recombination processes are very rapid, the ionization is entirely due to local production. In fact, it is well known that the nighttime auroral *E* layer is produced by the precipitation of particles from the central plasma sheet [Lui *et al.*, 1977; Sharber, 1981]. In the following, we will speak of the "particle (or nighttime auroral) *E* layer" to describe the radar observations associated with the continuous/diffuse aurora; the particles which produce this aurora will be described as electrons and protons from the central plasma sheet. Several techniques have been developed to infer the *E* region electron densities from the flux and energy flux of the precipitating electrons [Rees, 1963; Berger *et al.*, 1974; Vondrak and Baron, 1977], and protons [Jasperse and Basu, 1982]. Recent studies have used these techniques to compare densities obtained from satellite particle data and radar observations. Whereas in the morning

sector, *E* region ionization profiles can be accurately reconstructed from precipitating electron data [Vondrak and Robinson, 1985], this is not always the case in the evening sector where protons seem to contribute significantly to the *E* region ionization [Robinson and Vondrak, 1985; B. Basu *et al.*, Linear transport theory of auroral proton precipitation: A comparison with observations, submitted to *Journal of Geophysical Research*, 1986].

The knowledge of *E* region sources is in fact fundamental, since they determine the electrical resistivity of the ionosphere, and therefore influence the way in which magnetospheric and field-aligned currents close into the ionosphere. Some relationships between the different parameters governing this magnetosphere/ionosphere electrical coupling have been explored in the evening sector by Rostoker *et al.* [1975], Kamide and Aka-sofu [1976], Klumpar [1979], Robinson *et al.* [1982], and Sugiura *et al.* [1984].

Because the plasma recombines very slowly in the *F* region, transport mechanisms play an important role in the large-scale plasma distribution, in addition to production by solar radiations and particle precipitation. Furthermore, the *F* region responds very slowly to local production, and a given flux tube must be exposed several tens of minutes to in-situ production for the ionization to build up. Therefore, a correct description of the relation between the ionization sources and the convection pattern is necessary to understand how the *F* region plasma behaves [Schunk *et al.*, 1976; Robinson *et al.*, 1985; Weber *et al.*, 1984, 1985].

Several ionization features have been observed repeatedly in the evening sector high-latitude ionosphere. They include the auroral *E* layer and, in the *F* region, the mid-latitude trough and ionization enhancements. In particular an ionization enhance-

¹Centre de Recherches en Physique de l'Environnement, Saint-Maur-des-Fosses, France.

²Southwest Research Institute, San Antonio, Texas.

³SRI International, Menlo Park, California.

⁴University of Texas at Dallas, Richardson.

⁵National Oceanic and Atmospheric Administration, Boulder, Colorado.

⁶Geophysical Institute, Kyoto University, Kyoto, Japan.

⁷Goddard Space Flight Center, Greenbelt, Maryland.

ment, the boundary blob, often lies at the trough's poleward edge [Rino *et al.*, 1983]. Up to now, a complete description of all the parameters involved in the magnetosphere/ionosphere electrical coupling, and in the dynamics of the *F* region plasma that produce these features—i.e., electron and proton precipitation, *E* and *F* region ionization, conductivities, electric field, ionospheric and field-aligned currents—has not been given. It is the purpose of this paper to give such a description, as well as to evaluate quantitatively the contribution of precipitating electrons and protons to *E* region ionization, and to describe a scheme for the formation of the *F* region trough and density enhancement observed north of it.

For this purpose, we have used Chatanika data from a 24-hour Magnetosphere-Ionosphere-Thermosphere Radar Studies (MITHRAS) campaign on November 11, 1981, together with data from the Dynamics Explorer 2 (DE 2) and NOAA 6 satellites. The MITHRAS 3 experiment provided latitudinal maps of electron density profiles and of electric fields with a very good precision, every 20 minutes. The particle *E* layer, *F* region mid-latitude trough, and a 100-km-wide density enhancement north of the trough were observed for several hours in the evening sector. The steadiness of these features and of the plasma convection for over four hours has enabled a detailed comparison with the satellite observations, providing much insight into the *F* region dynamics of the auroral upper atmosphere.

2. EXPERIMENTAL TECHNIQUE

The Chatanika radar operating mode—the so-called MITHRAS 3 experiment [see *de la Beaujardière et al.*, 1984]—consisted of a set of two scans: one elevation scan in the magnetic meridian, followed by a scan to the west along a path such that, at each invariant latitude, the radar sampled the same magnetic local time that was sampled during the elevation scan. Each cycle took about 20 minutes to complete, and the common region covered by the two scans extended from about 63° to 69° invariant latitude in the *F* region. The transmitted waveform consisted of a 60- μ s (short) pulse used for the density measurement with a 9-km range resolution, followed by a 320- μ s (long) pulse used for the velocity, density and temperature measurements with a 48-km range resolution. As the radar scanned in latitude, the centers of the eight range gates were moved along the line of sight to provide velocity measurements at constant altitudes. The integration time was short (15 s) to minimize the effects of latitudinal smearing while the radar was scanning.

With a single elevation scan operating mode, a model of collision frequencies is needed to infer the north-south component of the electric field from the line-of-sight velocity measurements at two altitudes in the *E* and *F* regions [*de la Beaujardière et al.*, 1980]. The advantage of the MITHRAS 3 experiment is to provide the north-south and east-west components of the electric field by combining at each invariant latitude the line-of-sight velocities in the *F* region from the two scans. The parallel velocity, assumed to be constant over the latitudinal range probed by the radar, is determined when the radar beam is parallel to the magnetic field. Under reasonably steady conditions, the uncertainty in the north-south electric field for the MITHRAS 3 experiment is thus smaller than for an elevation scan mode, and typically on the order of 2–3 mV/m. Moreover, this uncertainty is not enhanced at latitudes near the Chatanika radar—as in the case of the elevation scan operating mode—since at those latitudes, the north-south component of the elec-

tric field (east-west velocity) is given directly by the velocity measured during the scan to the west. The measurement of that component is thus continuous from 63° to 69° invariant latitude, whereas the east-west component, which is known to be quite constant over that latitudinal range, is not determined within a hundred kilometers around the Chatanika radar location at 64.8° invariant latitude.

Altitude profiles of the electron density measurements are used to calculate the height-integrated conductivities. The ionospheric currents are derived by combining the conductivity with the electric field data. The latitudinal structures observed by the radar such as *E* and *F* ionization features and several convection features can be related to simultaneous measurements from the low-altitude polar-orbiting Dynamics Explorer 2 (DE 2) and NOAA 6 satellites.

The DE 2 satellite was in a dawn-dusk orbit during the period of interest and carried instrumentation to measure all the plasma and atmospheric parameters required to complement the radar data. This instrumentation is described in a special issue of *Space Science Instrumentation* [Hoffman, 1981].

In the magnetometer data analysis [Farthing *et al.*, 1981], the Magsat magnetic field model [Langel *et al.*, 1980] is subtracted from the measurements in order to deduce the magnetic field perturbation. If it is assumed that the east-west perturbation of the magnetic field ΔB_x results from the passage of the satellite through an infinite current sheet oriented in the east-west direction, then this is given by

$$\Delta B_x = \mu_0 J_{\parallel} \Delta y \quad (1)$$

where μ_0 is the permeability of free space, and J_{\parallel} is the field-aligned current density flowing within the range $y + \Delta y$ (x is directed in the magnetic east direction, y along magnetic north, and z upward along \mathbf{B}). This assumption is supported by the very small perturbation in the north-south component of \mathbf{B} for the pass considered in this study. A decrease in ΔB_x with increasing latitude corresponds to an upward field-aligned current, and an increase in ΔB_x with latitude corresponds to a downward current.

The NOAA 6 satellite carries instrumentation to measure the populations of both ions and electrons above 0.3 keV [Hill *et al.*, 1985]. Between 0.3 and 20.0 keV, the measurements are made by a set of electrostatic analyzer, particle detector units. This instrument determines the integrated directional energy flux carried by particles, and the energy band within which the differential energy flux maximizes. Every 2 seconds, measurements are made separately for ions and electrons at two pitch angles within the atmospheric loss cone. Above 30 keV, the energetic particle instrument (an array of solid-state detectors) provides the directional intensity, either integral for electrons or differential within certain energy bands for protons, at two pitch angles (one within the loss cone and the other one near local mirroring). It should be pointed out that, whereas the electrostatic analyzers in the total energy detector (TED) (0.3- to 20.0-keV particles) do not differentiate between protons and higher mass positive ions, the solid-state detector system (>30-keV particles) does discriminate in favor of protons.

The satellite tracks for two simultaneous passes of the DE 2 and NOAA 6 satellites over Alaska are shown in Figure 1 together with the latitudinal extent of the Chatanika radar *F* region measurements during the elevation scan on November 11, 1981. The NOAA 6 plotted trajectory corresponds to its location at the foot of the field line obtained by mapping along

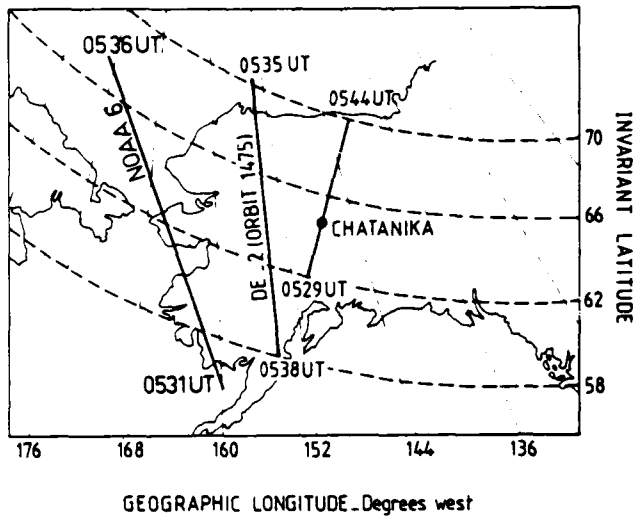


Fig. 1. DE 2 and NOAA 6 ground tracks across Alaska for the passes around 0530 UT on November 11, 1981. The latitudinal extent of the ionospheric F region surveyed by the Chatanika radar during the simultaneous elevation scan is also indicated.

the magnetic field from the satellite altitude at 850 km down to 120 km. The radar meridian scan at 0529 UT to 0552 UT was coincident with the eveningside auroral crossings of DE 2 and NOAA 6, and the spatial separations between the radar and the satellites were about 300 km and 800 km, respectively, at closest approach. This good spatial and temporal coincidence allows a detailed comparison of the three data sets.

In general the calculation of the DE 2 position in geomagnetic coordinates utilizes the Magsat magnetic field model. However, in this paper, we have used the International Geomagnetic Reference Field (IGRF) 1980 model [Trombka and Cain, 1974] for comparisons between the DE 2 and radar data sets. This is necessary because the IGRF model is used routinely to process the Chatanika data. Although the two models give very similar invariant latitudes, the inferred magnetic local times sometimes differ by as much as 30 minutes.

3. DATA

Figure 2 shows the H component of the College magnetogram from 2200 UT on November 10 to 1200 UT on November 11, 1981. The satellite passes over Alaska, shown with the heavy vertical line, occur at the beginning of an afternoon positive bay with a maximum H component of 280 γ at 0700 UT (about 1930

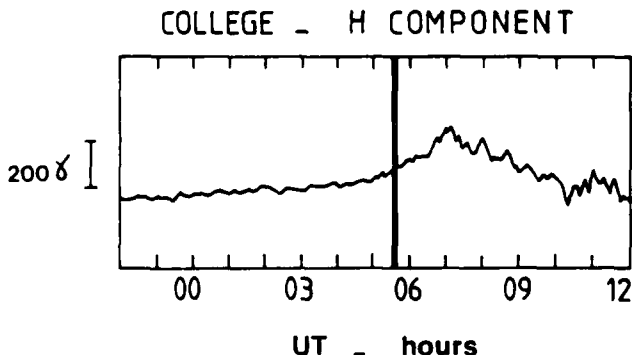


Fig. 2. H component of the College magnetogram. The time of the DE 2 and NOAA 6 passes over Alaska is indicated by a heavy vertical line.

MLT). The magnetic activity at College is moderate and steady during the observation period.

The Chatanika radar data, taken during the meridian scan coincident with the satellite passes, are shown in Figure 3 as a function of invariant latitude. The vertical axis on the contour plot of the first panel denotes altitude measured along a field line. The E region densities together with a neutral atmosphere model were used to compute the height-integrated Hall and Pedersen conductivities in the second panel. These conductivities and the electric field of Figure 3c were combined to give the two components of the current perpendicular to B shown in the last panel.

Several features are seen in Figure 3.

1. The ionization in the E region exhibits a typical auroral eveningside behavior (at Chatanika, LT = UT-10 hours), with densities increasing smoothly from 0.2×10^5 el/cm³ at 63.2° to 2.0×10^5 el/cm³ at 67.5°, with a maximum at about 130 km altitude. Following Robinson et al. [1982], we will refer to this density maximum as the "interface arc." North of it, around 68.4°, there is an abrupt decrease in the electron density to below 1.2×10^5 el/cm³ at 130 km altitude. Poleward of this E region minimum, the electron density increases sharply in an arc structure from the lowest altitude of observation around 150 km up to 300 km. The maximum density of 7.5×10^5 el/cm³ in this arc is observed at 70.4° and 240 km (see next figure). The Hall

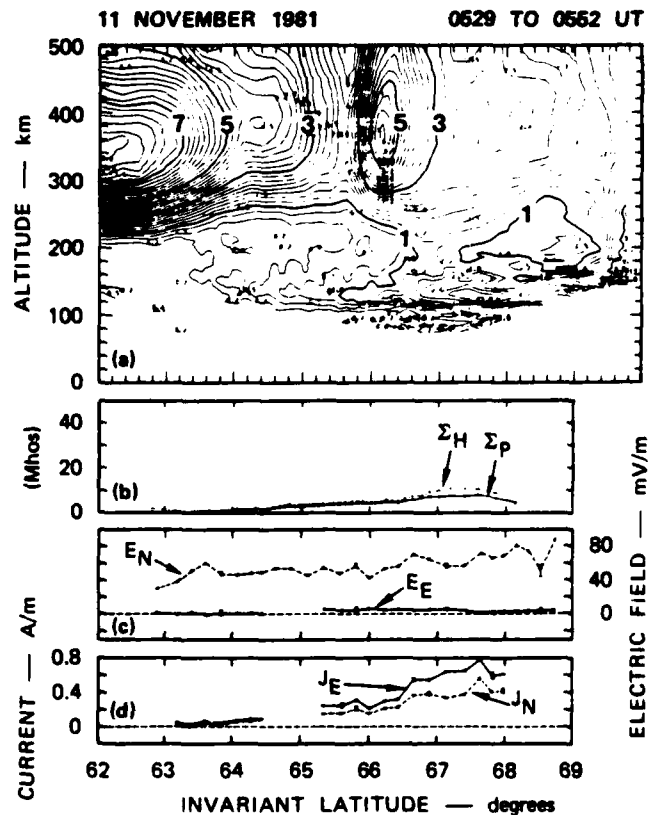


Fig. 3. Physical parameters along the Chatanika magnetic meridian for November 11, 1981 from 0529 UT to 0552 UT. (a) Electron density contours in units of 10^5 el/cm³. (b) Hall (dashed line) and Pedersen (solid line) conductivities. (c) The electric field. (d) The current perpendicular to the magnetic field. The electron density and conductivities are determined from the elevation scan alone from 0529 UT to 0544 UT, while the electric field and current are determined from the combination of the measurements made during the elevation scan and the scan to the west. Local time is about 1930 LT.

and Pedersen height-integrated conductivities increase to the north within the particle E layer associated with the diffuse aurora, reaching values of 8 and 11 mhos, respectively, in the interface arc. The low Σ_H/Σ_P ratio and the relatively high altitude of the E region indicate that the precipitating electrons have average energies of the order of 1 keV.

2. The northward component of the electric field increases with latitude in the southern part of the scan, reaching a value of 50 mV/m, and then remains close to this value from 63.4°, at the equatorward edge of the particle E layer, to the highest latitude of observation. On the average, the two components of the current increase from the lowest to the highest latitudes of observation.

3. Moving from south to north, in the F region, the electron density at 350 km first decreases from 8.2×10^5 el/cm³ at 62° invariant latitude to 1.8×10^5 el/cm³ at 65.6°. Note that the ionosphere at these latitudes is in darkness since, at 350 km and 62° on that day, the sun sets at 0416 UT, about 1 hour and 15 min before the time of this data set. In the latitudinal range north of 63.4° where the E region ionization increases and where large northward electric fields are observed, the F layer rises and the plasma scale height increases. Around 65.6°, an ionization trough is observed with densities of 1.8×10^5 el/cm³, in a region of intense electric field. The density gradient south of the trough is about 2.2×10^3 cm⁻³/km while it is about four times larger north of it, reaching 8.6×10^3 cm⁻³/km. This large density gradient corresponds to the southern wall of a strong ionization enhancement, the so-called "boundary blob" [Rino *et al.*, 1983]. The density at the center of this enhancement at 66.15° reaches 5.8×10^5 el/cm³. North of it, the F region density falls to about 2×10^5 el/cm³.

We present, in Figure 4, electron density contour plots for six consecutive meridian scans before and after the time of the DE 2 and NOAA 6 passes. Note that the latitudinal extent of the data shown on this figure is larger than in Figure 3, and that the interval between two density contours is also different. The interface arc and all the ionization features south of it appear to move to southerly latitudes from scan to scan. This southward shift may be explained in the E region as a result of a displacement of the auroral belt toward the night. In the lower-latitude portion of the F region the density decreases as a result of the recombination of a layer created by solar radiations.

The F region density enhancement, always observed north of the trough and above the diffuse aurora E layer, splits in two parts in the last two panels of Figure 4. This feature, along with the trough, is observed over several hours in local time while the plasma convects westward at high speed. Thus, they both appear to be longitudinally extended structures. We will refer to the density enhancement as the "density channel" to suggest its horizontal extension, rather than the "boundary blob" as used by Rino *et al.* [1983] and Weber *et al.* [1985].

Figure 5 shows 10 consecutive latitudinal profiles of the electric field, from 0308 UT to 0703 UT. The first few panels indicate the presence of a rather sharp boundary in the meridional component of the electric field, E_y . South of this boundary, E_y ranges from 5 to 12 mV/m in the frame of reference of the radar, i.e., on the order of the corotation electric field. Thus, in the inertial frame of reference, the plasma stagnates in this region. North of this boundary, E_y increases to values above 50 mV/m. The boundary between the two electric field regimes coincides with the equatorial boundary of the particle E layer as determined from the radar density contour plots. Drifting southward

from scan to scan, this boundary disappears from the radar field of view after 0550 UT. The locations of the trough minimum and density channel center are shown by the solid and open circles, respectively. These features are consistently located in a region of intense northward electric field and, except for the last two panels, they are associated with a small eastward electric field. Thus, they drift in the northwest direction, and a plasma parcel in these features moves to earlier local time.

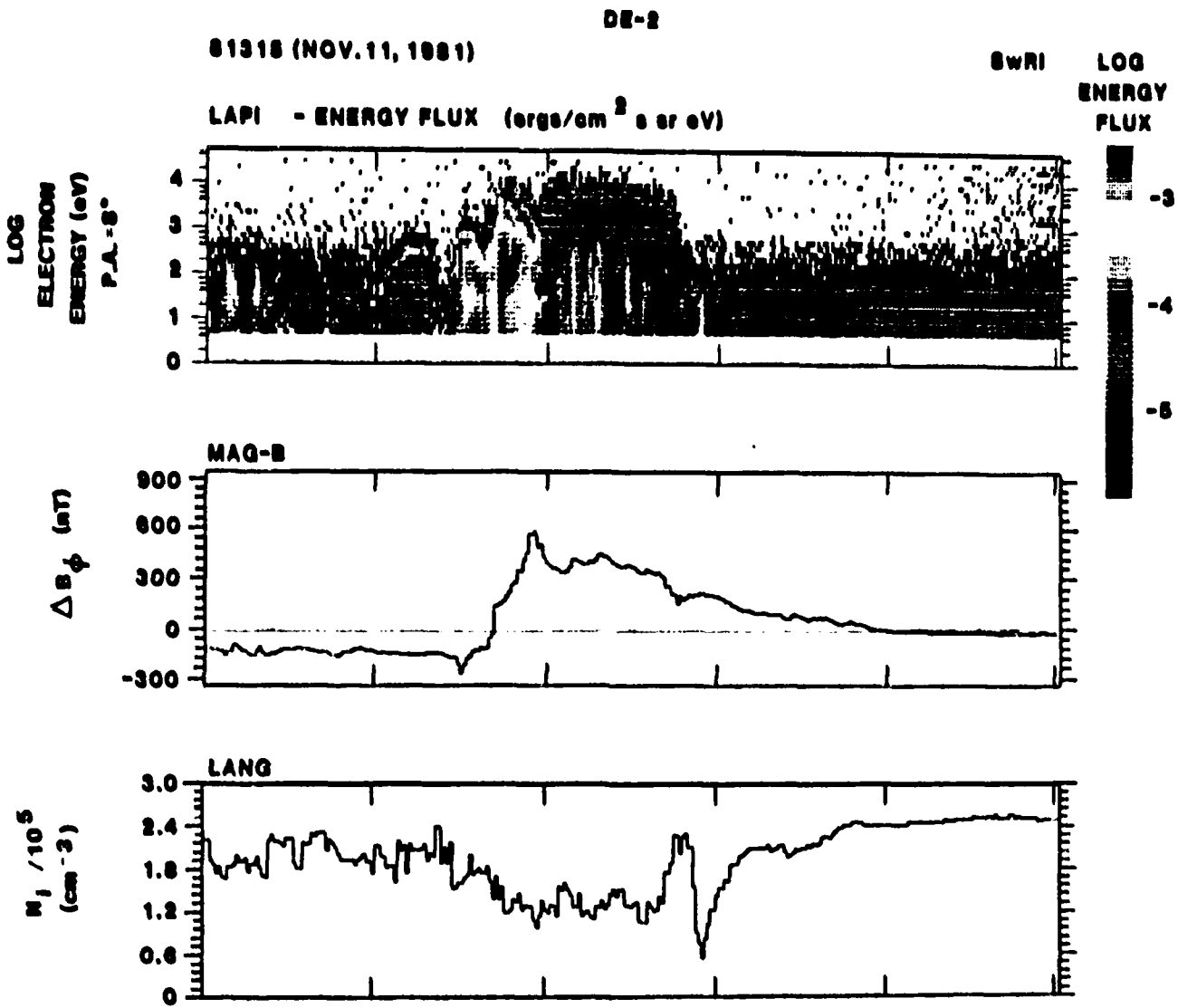
Some DE 2 data are presented in Plate 1 as a function of universal time, invariant latitude, magnetic local time and altitude. They include an electron spectrogram from the 8° pitch angle detector (precipitating electrons) of the low-altitude plasma experiment (LAPI), the magnetic east-west perturbation from the magnetometer, and the ion density from the Langmuir probe.

Plate 1 shows that the region of uniform electron precipitation from the central plasma sheet extends from 0534:55 UT to 0535:45 UT (70.2° to 67.2° invariant latitude). It is embedded in a region of downward field-aligned current that extends south of the equatorward boundary of the electron precipitation, down to 62.8°. The current densities are generally stronger in the region coincident with the electron precipitation region than south of it. The extension of the region 2 field-aligned current sheet equatorward of the electron precipitation region has been shown to be a feature characteristic of the eveningside auroral oval by Klumpar [1979] who used simultaneous particle and magnetic field perturbation measurements from the ISIS 2 satellite. It has been associated by Klumpar [1979] and Senior *et al.* [1982] with the displacement, in the magnetosphere, between the ion Alfvén layer where the region 2 field-aligned current originates [Schield *et al.*, 1969; Pellat and Laval, 1972; Jaggi and Wolf, 1973] and the electron Alfvén layer.

North of the uniform precipitations from the central plasma sheet, the region of discrete aurora with highly structured electron precipitation coincides with intense upward field-aligned currents in the latitudinal range from 71.6° to 70.2° (0534:30 UT to 0534:55 UT). This region, identified previously as the boundary plasma sheet (BPS) [Winningham *et al.*, 1975], is known to be highly structured and dynamic during moderate to disturbed times. The coincidence between the upward field-aligned current sheet and the boundary plasma sheet is a feature commonly observed by DE 2 [e.g., Sugiura *et al.*, 1984; Hoffman *et al.*, 1984].

The electron density from the Langmuir probe in the bottom panel of Plate 1 is almost constant and equal to 2.5×10^5 cm⁻³ in the southern part of the scan. It decreases slightly north of the equatorward boundary of the region 2 field-aligned current, then more rapidly to a minimum value of 6×10^4 cm⁻³ within the mid-latitude trough. North of the trough, the density increases sharply to a local maximum of 2.4×10^5 cm⁻³ at 0535:45 UT which is collocated with the 1-keV electron precipitation boundary. North of it, the density is more irregular. It increases slightly north of 69.9° because the satellite is sunlit prior to 0535:00 UT.

Measurements from the NOAA 6 total energy detector (particles from 0.3 to 20 keV) are shown in Figure 6. The electron energy flux, integrated from 0.3 to 20 keV, increases from 0.04 to 1.0 erg/cm²s between 0536:40 and 0537:40 UT (70.4° to 72.4° invariant latitude). In this region, the maximum detector response, as it swept from 0.3 to 20 keV, was found for electrons of 1–2 keV. For electrons having a Maxwellian energy distribution, this maximum response is twice the characteristic energy,



UT (H:M)	05:34	05:35	05:36	05:37	05:38
IL(DEG)	73.3	69.0	66.4	62.8	59.2
ALT(KM)	672	653	631	612	589
MLT(HR)	17.31	17.69	18.03	18.26	18.47

Plate 1. DE 2 data during orbit 1475 on November 11, 1981. Top panel: electron spectrogram from the LAPI 8° pitch angle detector. A logarithmic color code is used for the differential energy flux (ergs/cm² s sr eV). Middle panel: east-west magnetic field perturbation from the magnetometer. Bottom panel: ion density from the Langmuir probe.

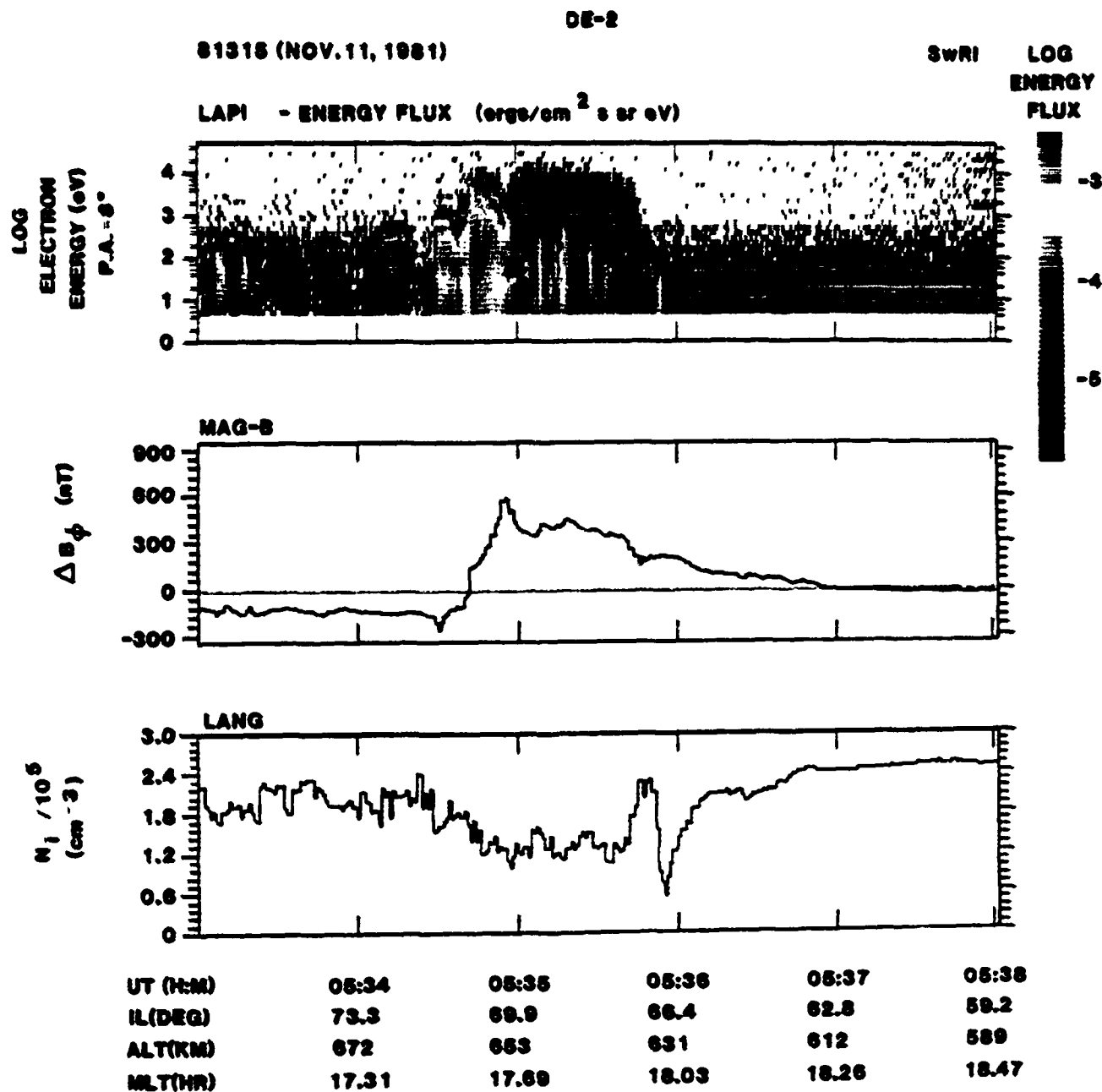


Plate 1 DE 2 data during orbit 1475 on November 11, 1981. Top panel: electron spectrogram from the LAPI 8° pitch angle detector. A logarithmic color code is used for the differential energy flux (ergs: cm² s sr eV). Middle panel: east-west magnetic field perturbation from the magnetometer. Bottom panel: ion density from the Langmuir probe.

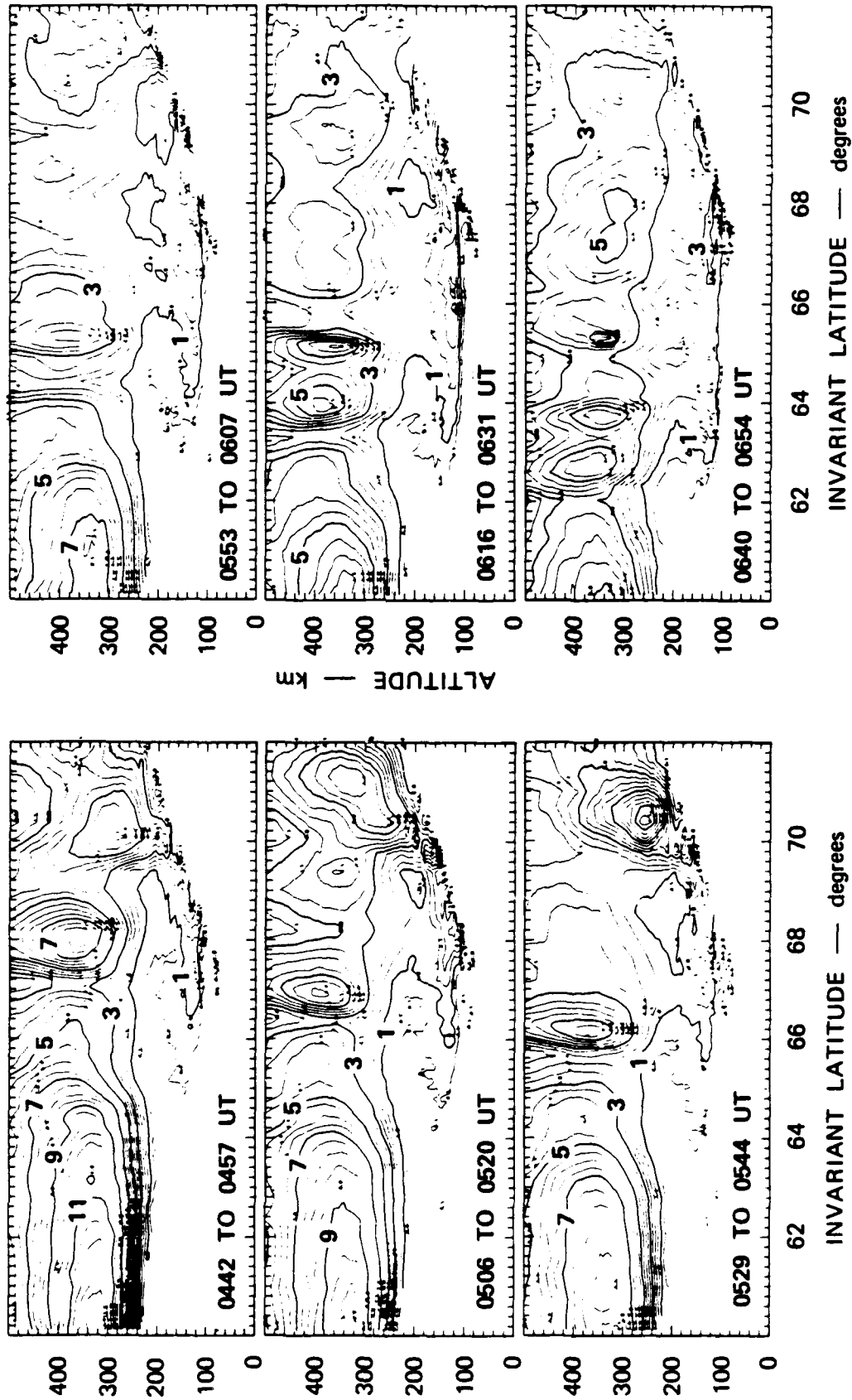


Fig. 4. Electron density (in units of 10^5 el/cm^3) contour plots measured during six consecutive elevation scans between 0442 UT and 0655 UT. The ionization features, except the northern inverted-V structure, are observed to be steady and to move southward.

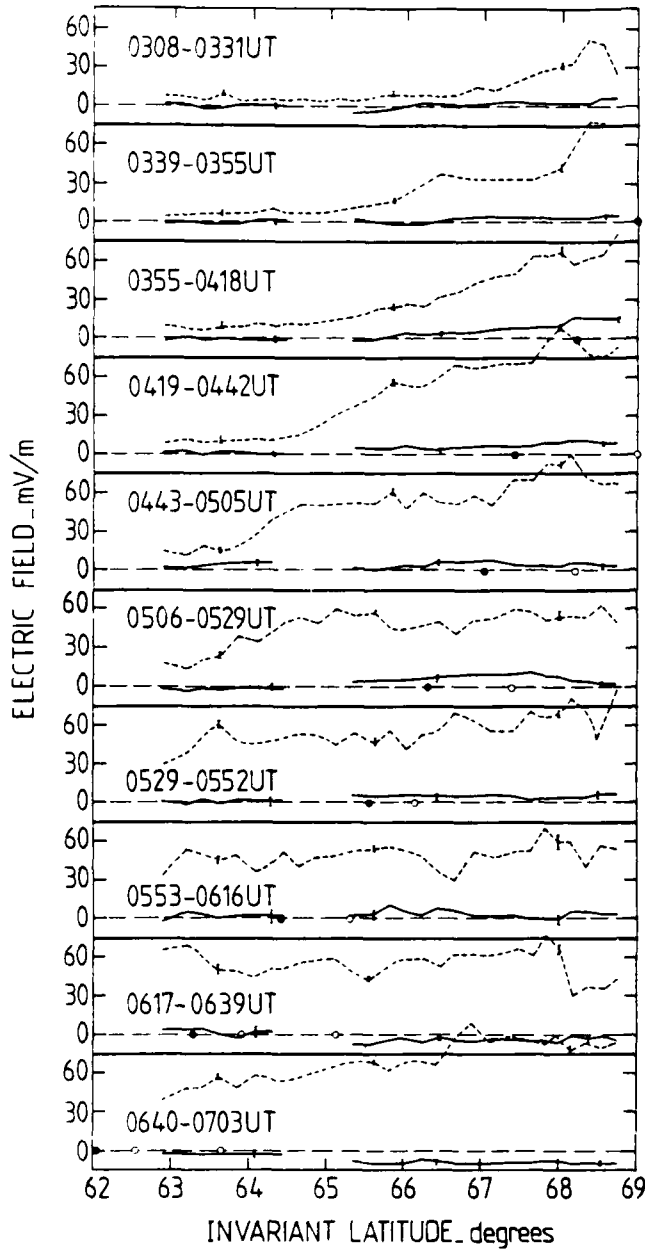


Fig. 5. Latitudinal profiles of the northward (dashed lines) and eastward (solid lines) components of the electric field during 10 consecutive scans from 0308 UT to 0703 UT. The locations of the trough and blobs are indicated by the solid and open circles, respectively.

where the characteristic energy is defined as the energy at the peak of the differential number flux versus energy curve. Thus, electron precipitation in this region is characteristic of precipitation from the central plasma sheet (CPS). North of this region (after 0537.40 UT), the maximum detector response is found for electrons of lower energy on the order of 400 to 600 eV.

It is worth noticing the similarities of the DE 2 and NOAA 6 electron morphology. North of a uniform electron precipitation region, the two spacecraft observe a decrease, followed by a sharp increase of the total energy flux within an arc. The arc was observed at $\Lambda \approx 71^\circ$ on DE 2 and at $\Lambda \approx 72.8^\circ$ on NOAA 6.

Looking again at the NOAA 6 data of Figure 6, ions in the energy range 0.3–20.0 keV precipitate north of 67.7° (0535:27 UT) with very low energy fluxes. From 67.7° to 70.5° , i.e., south

of the electron precipitation region, the ion flux exceeds the electron flux, but never rises above $0.06 \text{ erg/cm}^2 \text{ s}$. *Lui et al.* [1977] and *Sharber* [1981], using data from the ISIS 2 spectrometer, have shown that ions with energy less than 26 keV precipitate equatorward of the electron precipitation region in the evening sector, but that the ion energy flux is typically about 10 percent of the electron energy flux. Because only ions with energy less than about 25 keV are considered here for both satellites, our data set is consistent with observations from the ISIS 2 satellite. However, as will be shown below, most of the ion energy flux is carried by ions with energy greater than 25 keV, whereas the 0.3- to 20.0-keV electron detector sees essentially all of the electron energy flux.

We have stated before that the steadiness of the ionization and convection features observed by the Chatanika radar (see Figures 4 and 5) suggests that these features are longitudinally extended. Therefore, we have plotted in Figure 7 their location in an invariant latitude/magnetic local time frame of reference. These features include the centers of the density enhancements observed on Figure 4, the equatorward boundary of the auroral E layer as determined by the 10^5-e/cm^3 contour, and the latitude where the electric field drops to 15 mV/m. The locations of the region 1 and 2 field-aligned current sheets are also indicated on the figure along the DE 2 track, together with the equatorward edge of the 1-keV electron precipitation from the central plasma sheet as seen by the two spacecraft. The Chatanika measurements taken during the meridian scan simultaneous to the DE 2 and NOAA 6 passes are indicated by an arrow, and the sun terminator at 350 km by a dashed-dotted line. This figure, constructed from the radar measurements from 0158 UT to 0806 UT, may be considered as a snapshot of the boundary locations since the magnetic activity was steady during the experiment. From this figure, it appears that substantial E region ionization in the radar data exists south of the electron diffuse aurora, and that the equatorward edge of the region 2 field-aligned current is closely related to the electric field boundary.

In the F region, the center of the density channel coincides with the equatorward edge of the 1-keV electron precipitation

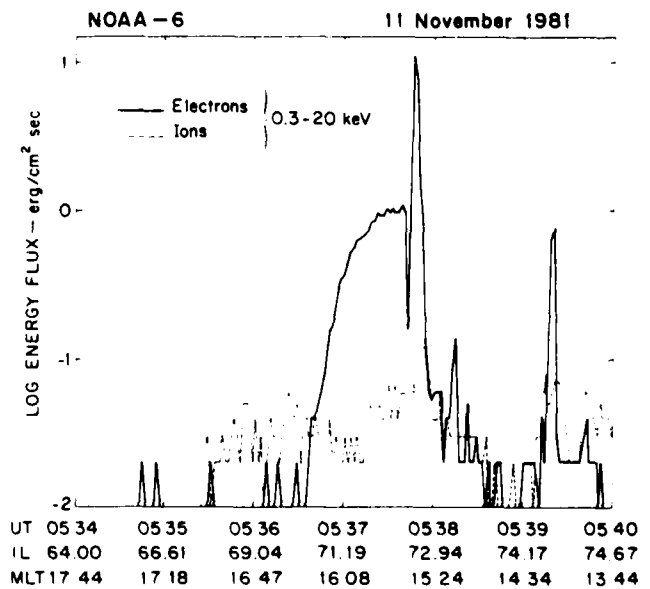


Fig. 6. NOAA 6 particle data from the total energy detector for electrons and ions between 0.3 and 20 keV.

and with the local density enhancement measured by the DE 2 satellite at 1740 MLT. Going back to Figure 3 and Plate 1, it can be shown that the density of $2.4 \times 10^5 \text{ el/cm}^3$ measured by the Langmuir probe within the density enhancement is consistent with the density and scale height derived from the radar measurements. In the MLT sector where the NOAA 6 satellite crosses the radar density channel, the coincidence between the equatorward edge of the electron precipitation and the density channel is also excellent, if one keeps in mind the UT delay of 1.5 hours between the radar and satellite data sets around 1640 MLT. This good spatial coincidence of the two features at two magnetic local times suggests that the density channel is related to the equatorward edge of the keV electron precipitation from the CPS in the evening sector. Nevertheless, the observation of two density channels after 1800 MLT on Figure 7 (see also Figure 4) also suggests that mechanisms other than those purely related to electron precipitation are effective in creating these *F* region ionization channels.

Because the auroral oval position moves south as local time progresses, and because simultaneous measurements by the radar and satellites are made at different local times, we expect

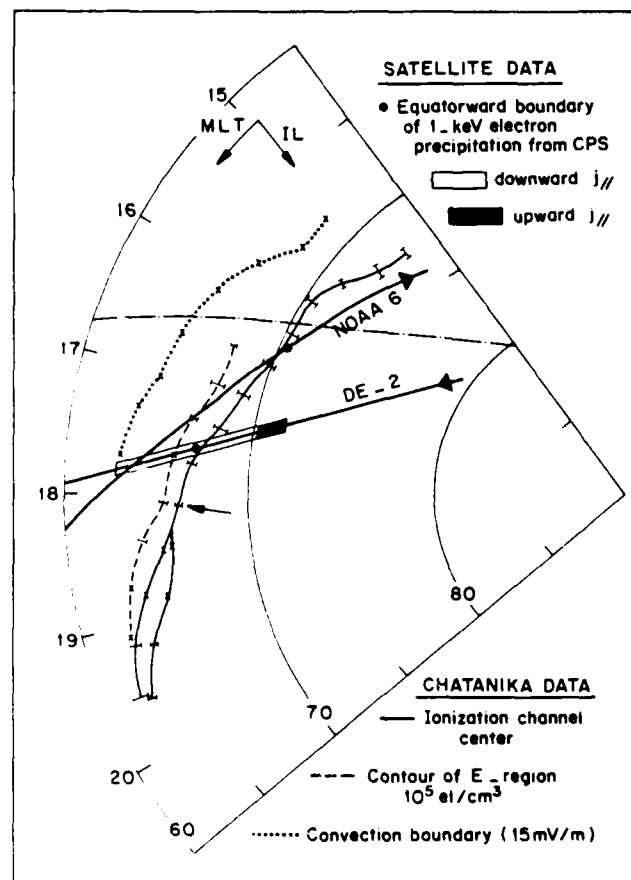


Fig. 7. Invariant latitude/magnetic local time map of the center of the boundary blob (solid line), equatorward boundary of the 10^5-el/cm^3 *E* region density contour (dashed line), and convection boundary as determined by the latitude where the northward electric field drops to 15 mV/m (dotted line). These boundaries are constructed from a succession of the radar meridian scans. Also shown are the DE 2 and NOAA 6 tracks with the locations of the downward and upward field-aligned currents and abrupt equatorward boundary of the 1-keV electron precipitation region. The dashed-dotted line represents the sun terminator at 350 km altitude.

to see a latitudinal displacement of the boundaries related to the auroral oval at the satellites and radar locations. The only common features observed by both the DE 2 satellite and the radar are the density channel and the trough. We have used the density channel, observed at 67.2° and 66.15° , respectively, by the DE 2 satellite and the radar around 0530 UT, to relate all other features that we assumed aligned with the density channel. This is not entirely correct since transport mechanisms are very efficient in the *F* region, whereas the *E* region features are directly mapped from the magnetosphere. Nevertheless, because the longitudinal displacement between the radar and DE 2 satellite is small (300 km at closest approach), this approximation should give a good qualitative insight into the data sets.

Figure 8 shows the result of mapping the various boundaries observed with the DE 2 satellite at the Chatanika local time meridian, using the method described above. These DE 2 boundaries are shown on the radar density contour plot. The entire auroral *E* layer, including the interface arc and the *E* region density minimum poleward of it, is embedded in the large-scale downward current sheet (light-shaded area) while the upward field-aligned current (dark-shaded area) coincides with the discrete arc region located within the boundary plasma sheet. This is in contradiction with *Robinson et al.* [1982] who located the field-aligned current reversal within the interface arc. However, in the data sets presented by *Robinson et al.* there were no inverted V's within the large-scale upward field-aligned current sheet. It is thus likely that the quiet-time field-aligned current behavior described by *Robinson et al.* [1982] and *Senior et al.* [1982] is modified in our data set because of a small-scale field-aligned current pair associated with the inverted V. In fact, the DE 2 magnetic field data in Plate 1 show that the field-aligned currents are weak and upward from 0535:05 to 0535:19 UT, which corresponds to the region delineated by the two dashed vertical lines in Figure 8, i.e., to the poleward portion of the ionospheric *E* layer associated with the diffuse aurora, north of the interface arc. The discrepancy between our data set and the previous authors' observations may well result from the dynamic nature of the CPS/BPS boundary [*Winningham et al.*, 1975].

The solid vertical line labeled *b* at $\sim 66^\circ$ invariant latitude indicates the location of the equatorward edge of the 1-keV electron precipitation from the CPS. As pointed out previously, the particle *E* layer seen by the radar extends well equatorward of it, and the density channel is collocated with it.

Within the region delineated by the two vertical dashed lines of Figure 8, the DE 2 LAPI data show two bursts of low-energy ($E < 400 \text{ eV}$) electron precipitation (see Plate 1). These features produce no significant increases in *F* region density, which is consistent with the fact that they are suprathermal bursts [*Johnstone and Winningham*, 1982], and as such are not spatially stable but are temporal in nature with typical lifetimes of a few seconds. On the contrary, the density channel is coincident with a very weak increase of soft electron precipitation at the equatorward edge of the CPS (see top panel of Plate 1, 0535:45 UT). This increase is not a suprathermal burst, and therefore may be spatially stable.

Finally, it is most interesting to note the structure of the auroral zone north of the auroral *E* layer associated with the diffuse aurora, and to compare it with electron data from the DE 2 and NOAA 6 satellites. The *E* region density minimum and the northern arc correspond to a decrease of the keV electron fluxes, respectively, and to an increase of the lower-energy electron fluxes, respectively, in both satellites' data. Considering

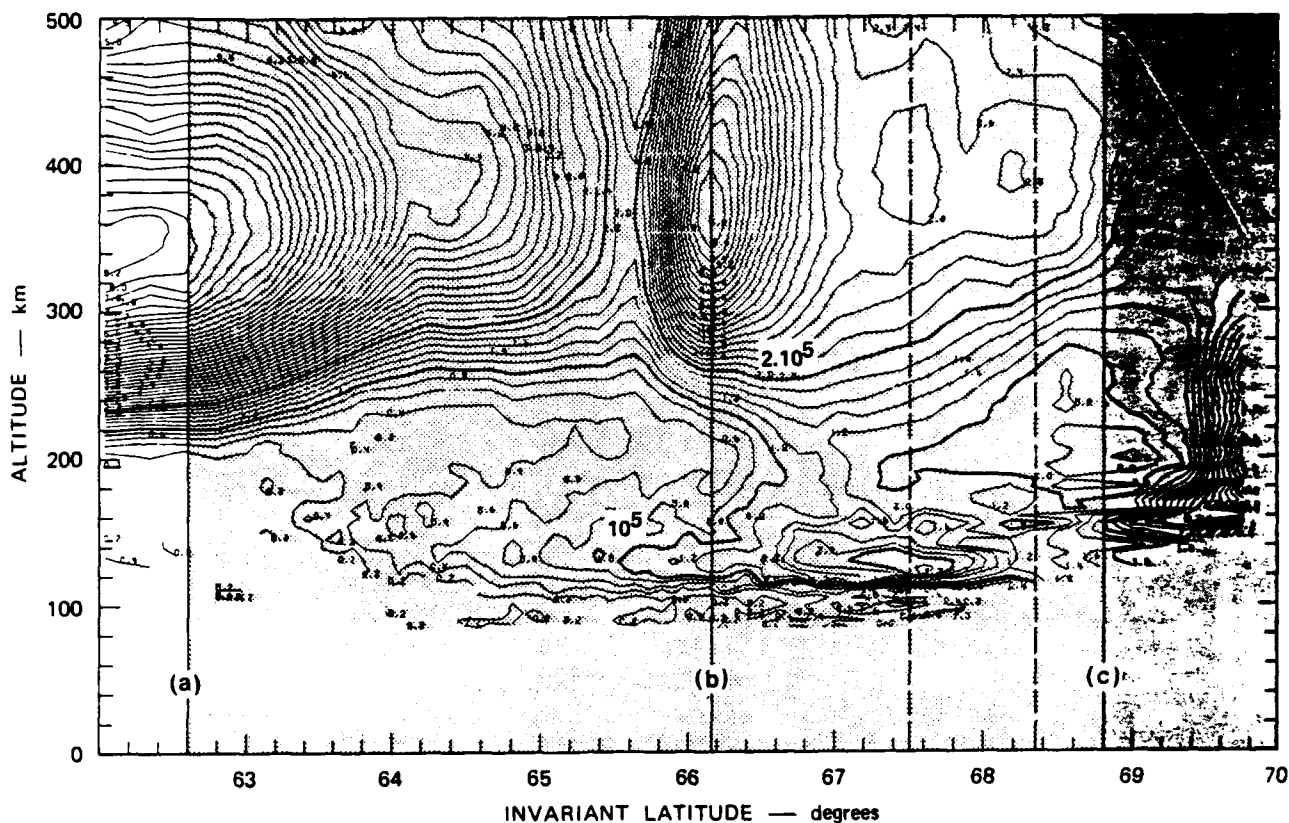


Fig. 8. Locations of the features seen by the DE 2 satellite superimposed on the radar density contour plot. The light-shaded area between the solid lines *a* and *c* represents the region of large-scale downward field-aligned current; the large-scale upward current (dark-shaded area) flows north of line *c*. The solid line labeled *b* marks the equatorward edge of the precipitation from the CPS. The significance of the two dashed lines is given in the text.

the local time difference between the three data sets at the latitudes of these structures (about 3 hours for the most distant observations), we conclude that they are extended over several hours in local time.

4. DISCUSSION

At this point, we raise the following questions related to this data set:

1. In the *E* region, what creates the ionization south of the keV electron precipitation from the central plasma sheet?
2. In the *F* region, how do the trough and ionization channel form?

E Region

It has been shown in the previous section that the particle *E* layer observed by the radar extends well equatorward of the electron precipitation measured on DE 2. In Figure 9 we compare two *E* region density contour plots, one directly measured by the radar (top panel), the other obtained using the LAPI electron spectral measurements as input to the TANGLE code described by Vondrak and Baron [1977] (lower panel). This code uses a library of ionization production profiles for monoenergetic electrons to derive the ionization resulting from incoming electron fluxes. The DE data in Figure 9 have been shifted 1.05° equatorward in order to take into account the orientation of the boundary structures relative to the east-west direction. Contour plots of the LAPI electron data reveal that

incident electrons were isotropic over the downward hemisphere. Therefore, in obtaining the *E* region electron density we have used the 8° pitch angle sensor, multiplying by π to obtain the isotropic angular distribution.

Several differences are apparent between the observed and calculated density distributions. First, the auroral *E* layer as seen by the radar extends 2° equatorward of the ionization created by the LAPI electrons (see for example the 0.6×10^5 el/cm³ contour). Second, the maximum electron density created by the precipitating electrons is calculated to be 1.2×10^5 el/cm³, whereas the radar measurements give 2×10^5 el/cm³. This cannot be attributed to ionization by solar EUV since the entire auroral *E* layer is in darkness at the time of the 0529–0544 UT scan. Finally, the altitude of maximum ionization is ~ 130 km as determined by the radar; the LAPI electrons produce a peak at ~ 120 km. The discrepancy in the shape of the contours at higher altitude (150 km to 200 km) can be attributed to the fact that this region is the transition region between O^+ and molecular ions, so that the recombination coefficient used in the electron degradation code could be inaccurate at these altitudes. It is also due to transport mechanisms which start playing a role above 150 km.

The most striking difference between the radar observations and the LAPI electron data is the first point, that the radar data show ionization extending 2° equatorward of the equatorward boundary of ~ 1 -keV electron precipitation. Having ruled out as possible explanations field model differences (we have used the IGRF 1980 model in reducing the satellite data shown in Figures 7 and 9), spatial variations along the boundary, and temporal

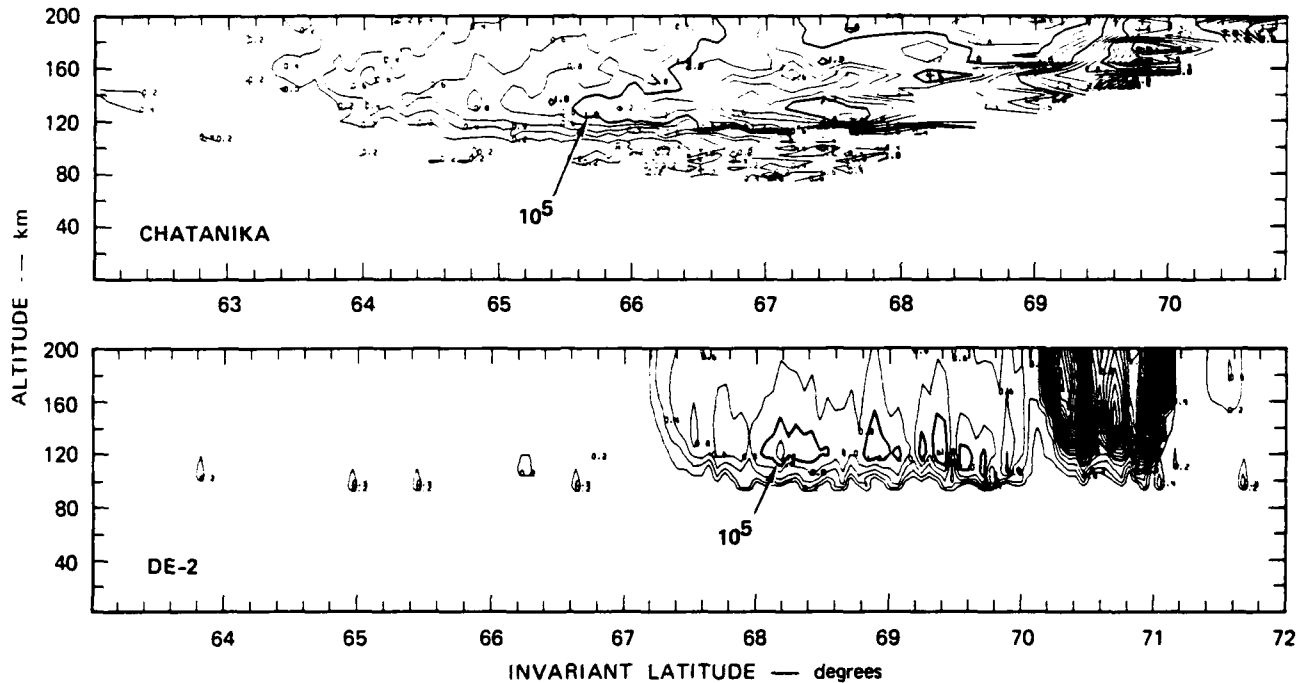


Fig. 9. Comparison of E region electron density measured by the Chatanika radar during the 0529–0544 UT scan (top panel) with that computed from the simultaneous DE 2 measurements of precipitating electron fluxes, using the TANGLE code (bottom panel).

variations, we look first at the precipitating ions as a source of the ionization.

We show in Plate 2 the LAPI ion data measured by the 45° pitch angle sensor (lower panel) along with the electron data from the 8° data pitch angle sensor (upper panel) for easy reference to features already shown in Plate 1. As the spectrogram shows, precipitating ions were observed between ~0534:30 and 0536:12 UT. The first point to notice is that this region extends equatorward to an invariant latitude of $\sim 65.6^\circ$; this is 1.6° equatorward of the equatorward boundary (67.2°) of the > 1 -keV electron precipitation.

A number of studies [Crasnier *et al.*, 1974; Lui *et al.*, 1977; Sharber, 1981; Robinson and Vondrak, 1985] have shown that in the evening sector, ions can precipitate equatorward of the diffuse auroral electron population. The recent studies of Robinson and Vondrak [1985] and of B. Basu *et al.* (Linear transport theory of auroral proton precipitation: A comparison with observations, submitted to *Journal of Geophysical Research*, 1986) have shown that protons can contribute significantly to E region ionization. In order to estimate the E region ionization resulting from ions precipitating into the auroral ionosphere in the region equatorward of the diffuse auroral electrons, we show in Figure 10 a composite spectrum made up of LAPI ion observations providing the data points at 4.18, 7.45, 13.2, and 23.5 keV and proton observations from the NOAA 6 energetic particle experiment providing the data points centered at 55, 165, and 525 keV. The smooth curve drawn through all points is broadly peaked, with a peak value of $48 \text{ ions/cm}^2 \text{ sr eV}$ at an energy between 9 and 10 keV. The high-energy part of the spectrum is approximated by a power law of slope -3.7 .

We will assume now that all the ions being measured are protons, although this is not necessarily true for DE 2 measurements, *i.e.*, for particles below 30 keV. However, it seems to be a good approximation to do so since the bulk of the number flux

is carried by protons above 30 keV that are measured by the NOAA 6 solid-state detectors. Therefore, the spectrum of Figure 10 has been used as an input to the proton-hydrogen ionization production code of Jasperse and Basu [1982], the results of which are shown in Figure 11. The incident proton spectrum produces a peak in ionization of $4.8 \times 10^4 \text{ el/cm}^3$ at a height of 120 km. Also shown in Figure 11 is the ionization profile measured by the radar at an invariant latitude of 65.6° .

In comparing the profiles, we see that the heights and ionization densities of the primary peaks differ; in addition, the radar profile shows a secondary peak at 95 km which does not appear in the calculated results. In addressing these differences several factors must be considered. First, the radar density calibration was very difficult for this particular experiment, due to a problem in the radar receiver chain. Thus, the radar density absolute uncertainty is 20 to 40 percent. Note that the relative density variations, however, are known with a high degree of accuracy. Second, count rates for ions between 1 and 27 keV of both satellite instruments were very low. In obtaining the low-energy part of the spectrum of Figure 10, the LAPI data were averaged over six sweeps and every two adjacent energy samples. The three data points at high energies from NOAA 6 result from integral measurements of ions with $E > 30 \text{ keV}$, $E > 80 \text{ keV}$, and $E > 250 \text{ keV}$. The effective high-energy cutoff for these detectors is $\sim 800 \text{ keV}$. Count rates were typically 3000–5000 in the $E \sim 30 \text{ keV}$ detector, 200–400 in the $E > 80 \text{ keV}$ detector and 10–20 in the $E > 250 \text{ keV}$ channel. Uncertainty bars on the spectral values of Figure 10 reflect count statistics. Similar bars in energy indicate the width of each energy channel. The LAPI calibration for ion detection at high count rates yields an absolute instrumental uncertainty of ~ 5 percent. However, when the detector is operating near its sensitivity level, another source of uncertainty must be considered. The on-board processor does not distinguish between counts of 0, 1, or 2; and because software processing treats these all as zeros, the spectrum of Figure

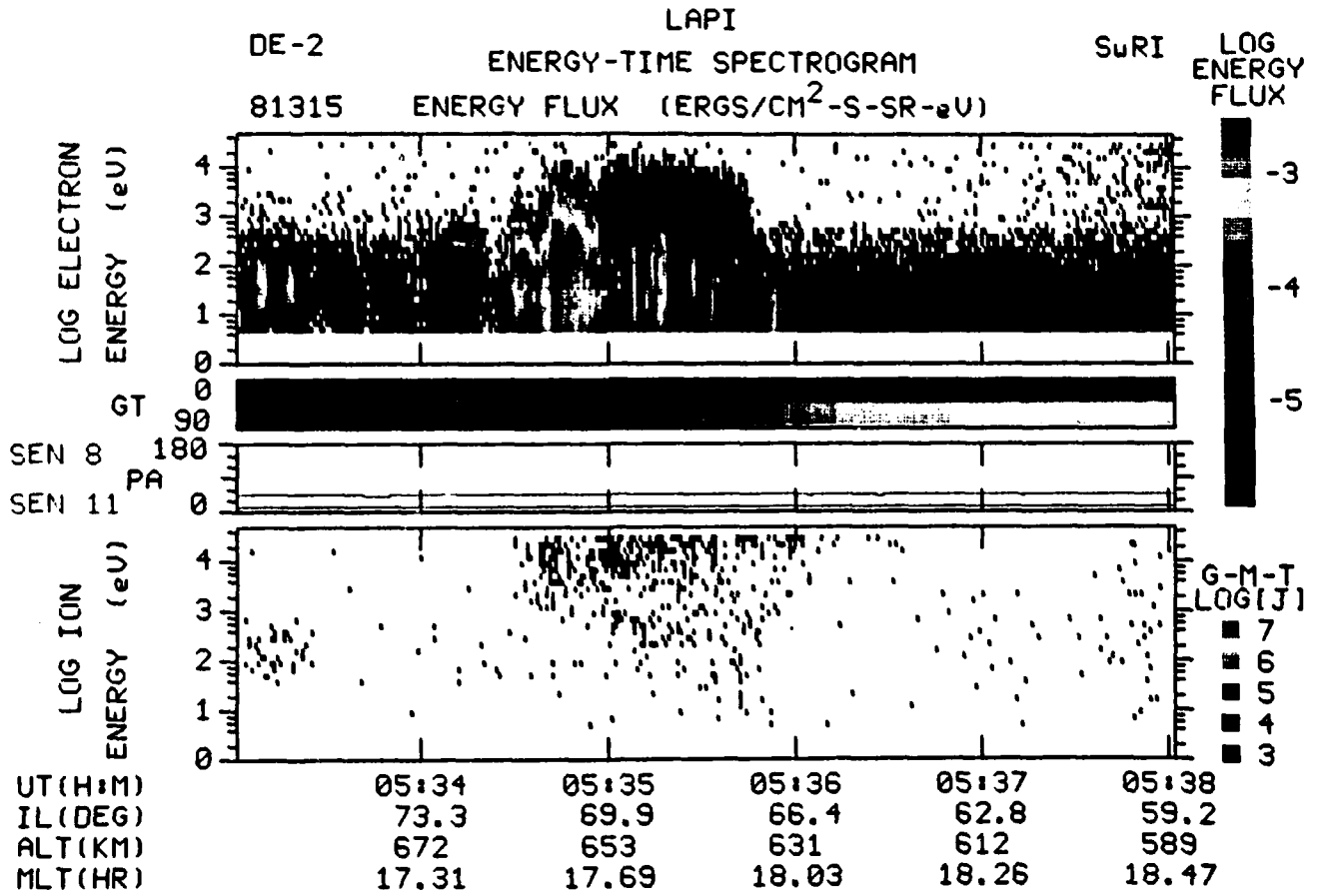


Plate 2. LAPI ion data measured by the 45° pitch angle sensor (lower panel) and electron data measured by the 8° pitch angle sensor (upper panel). Precipitating ions were observed between ~0534:30 and ~0536:12 UT. The ion precipitation region extended 1.6° equatorward of the equatorward boundary of > 1-keV electron precipitation.

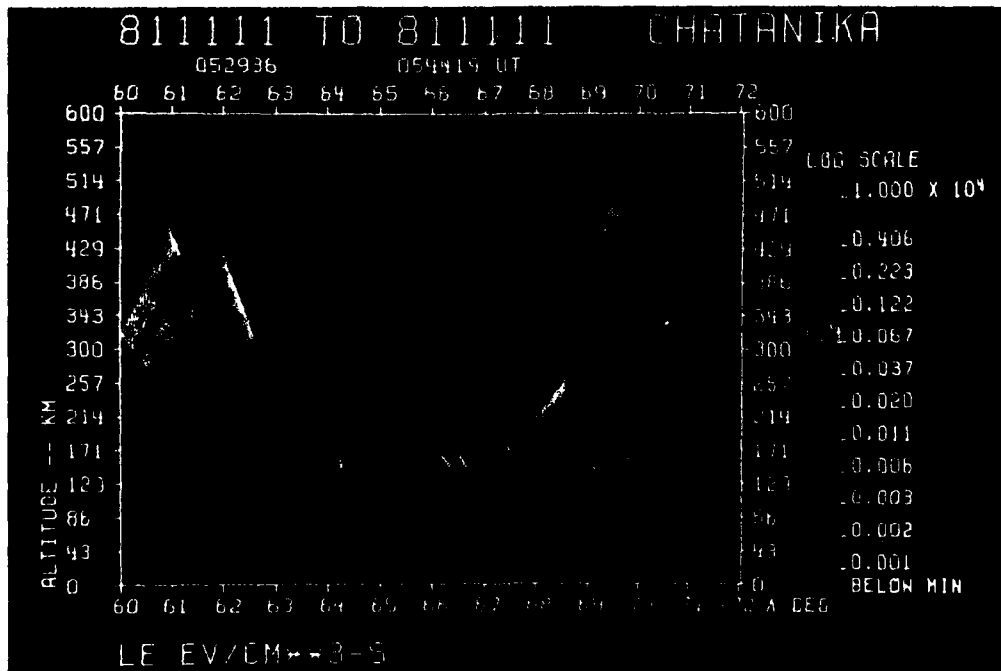


Plate 3. Energy input to the electron gas, I_p , deduced from the radar data for the scan simultaneous to the DE pass. I_p does not increase above the background inside the ionization channel at 66.2°.

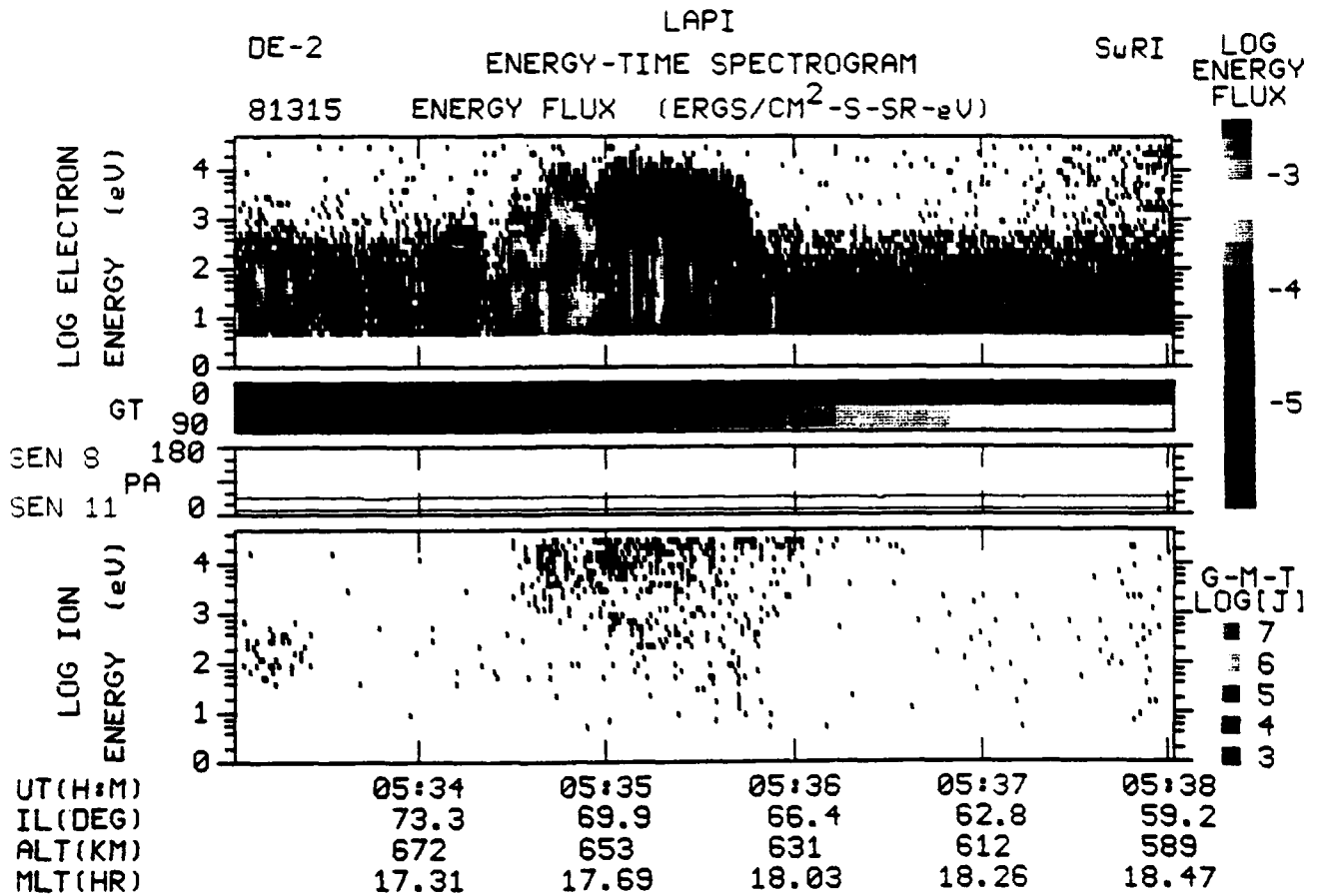


Plate 2. LAPI ion data measured by the 45° pitch angle sensor (lower panel) and electron data measured by the 8° pitch angle sensor (upper panel). Precipitating ions were observed between ~0534:30 and ~0536:12 UT. The ion precipitation region extended 1.6° equatorward of the equatorward boundary of > 1-keV electron precipitation.

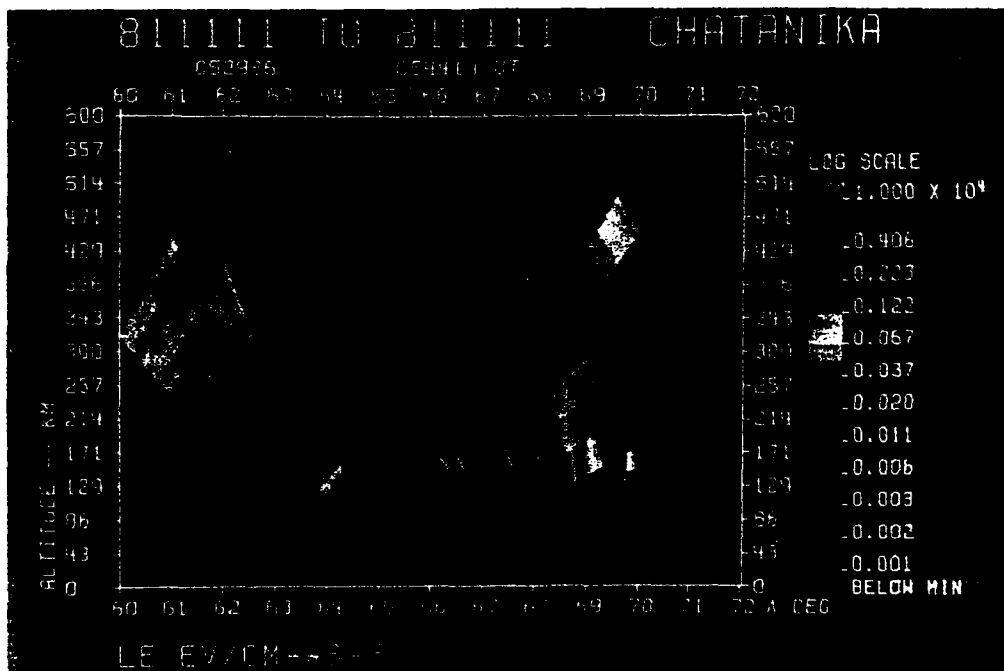


Plate 3. Energy input to the electron gas, L_p , deduced from the radar data for the scan simultaneous to the DE pass. L_p does not increase above the background inside the ionization channel at 66.2°.

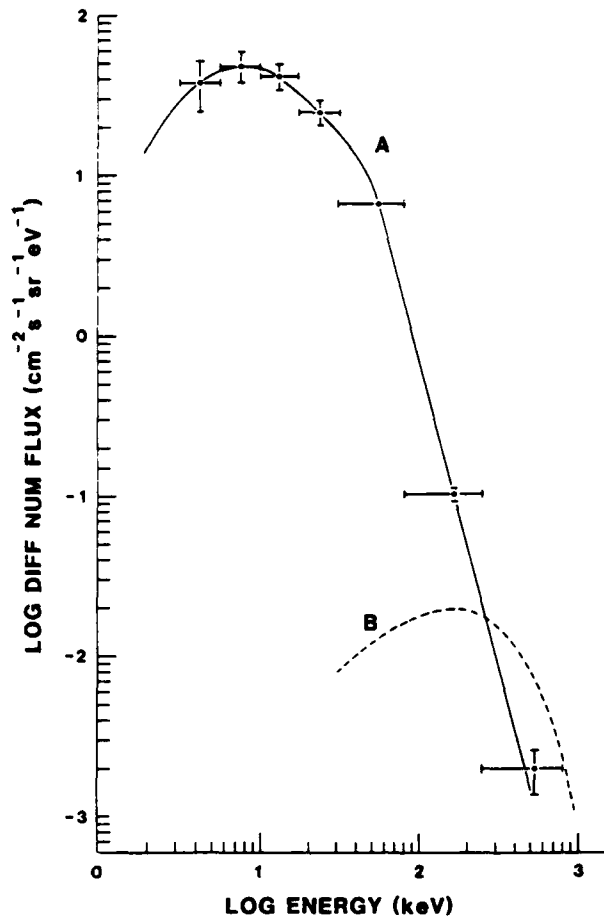


Fig. 10. Ion spectrum (A) equatorward of electron precipitation region. Data points below 30 keV were obtained from LAPI on DE 2 at 0535:(50.5-55.5) UT, which corresponds to an invariant latitude $\Lambda \sim 66.8^\circ$; points at energies > 30 keV were obtained from the NOAA 6 energetic particle experiment at 0535:(43-49) UT, which corresponds to $\Lambda > 68.5^\circ$. These times and latitudes have been chosen by taking into account the latitudinal extent of ions measured at each satellite and the orientation of the boundary structures relative to the east-west direction. They correspond to radar measurements at $\Lambda > 65.6^\circ$ during the 0529-0544 UT elevation scan. The Maxwellian proton spectrum (B) of characteristic energy ~ 170 keV could produce a second peak in ionization 95 km (see Figure 11).

10 actually represents a lower limit of the measurement. Statistics based on this effect indicate that the spectrum could have been more intense by a factor of 2. Similarly, because of uncertainties in the calibration of the NOAA 6 detectors, observed proton intensities tend to be lower limits with uncertainty of up to 50 percent. The number density resulting from a spectrum twice as intense as that of Figure 10 (which remains within the NOAA 6 and DE 2 error bars) would be larger by a factor of $\sqrt{2}$, giving about 7×10^4 el./ cm^3 at the primary peak.

The difference in heights of the ionization peaks may result from the presence of a strong electric field which, according to *Huuskonen et al.* [1984], can change the height and density of the ionization peak. They show that, in particular, a northward field of 50 mV/m can raise the height by ~ 10 km. The addition of an eastward component will increase this difference. We have shown in Figure 3 that at 65.6° , the electric field has a northward component of 48 mV/m and an eastward component of 5 mV/m.

A second possible explanation of the difference in height of

the ionization peak may be uncertainties in the neutral atmosphere model used by the Jasperse and Basu code. This model neutral atmosphere is that of *Banks and Kockaris* [1973] with a 1000° K exospheric temperature. The radar data suggest that the exospheric temperature is on the order of 1350° K on November 11, 1981 (V. B. Wickwar, private communication, 1986). The computed electron density profiles would peak at a higher altitude if a higher neutral atmosphere temperature had been used. Additional discrepancy in the altitude of the maximum ionization most likely results from the effect mentioned above of the low ion count rates.

Some possibilities for producing the secondary ionization peak of 2×10^4 el./ cm^3 at 95 km are a Maxwellian distribution of electrons of characteristic energy ~ 17 keV and peak differential number flux of 88 electrons/ cm^2 sr eV or a Maxwellian distribution of ions of characteristic energy ~ 170 keV and peak differential number flux of 2×10^{-2} ions/ cm^2 sr eV. NOAA 6 electron measurements in the $E > 30$ keV channel indicate a differential flux well below the required level. However, the ion spectrum shown in Figure 10 as a power law is not entirely inconsistent with the required Maxwellian when the energy bandwidth and uncertainty are considered. We show such a population in Figure 10 for illustration. The Maxwellians are of course not the only distributions that would produce a secondary peak at 95 km. Monoenergetic peaks of characteristic energy 3-4 times that of the Maxwellian will deposit their energies at approximately the same altitude. However, in light of the high-energy electron and ion measurements, these possibilities are less likely.

In summary, the protons in the spectrum of Figure 10 account

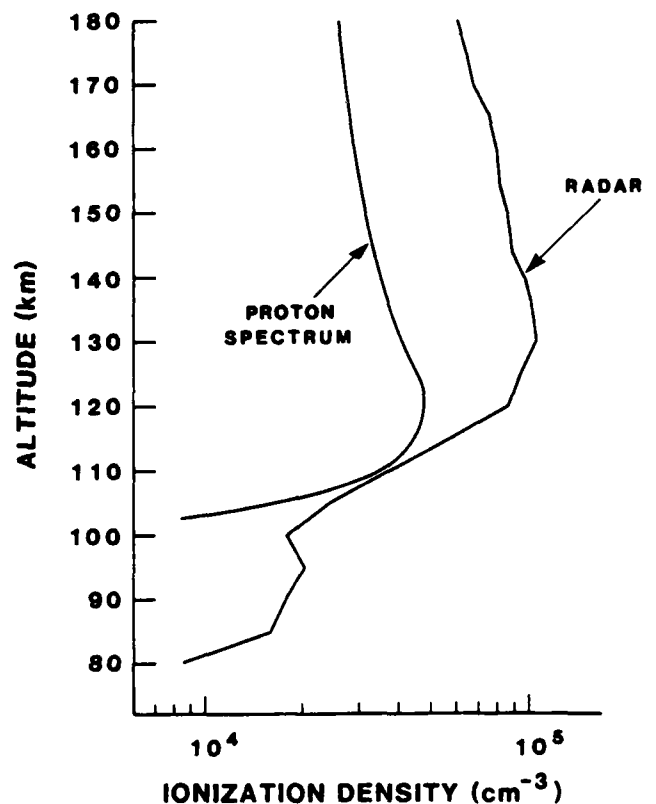


Fig. 11. Ionization profiles determined by the radar observations, and by using the ion (proton) spectrum of Figure 10 as input to the proton-hydrogen ionization production code of *Jasperse and Basu* [1982].

for about half of the ionization measured by the radar. We feel that based on the radar calibration problems, the low count rates and other uncertainties of the measurement, including the fact that data from two satellites ~ 1 hour apart in local time were used to construct the spectrum, the agreement is fair. Although we have not accounted for all observed E region ionization, we have established that the precipitating protons are a major contributor in the region equatorward of the diffuse auroral electron population.

Near the interface arc ($\Lambda \approx 67.5^\circ$ at Chatanika; $\Lambda \approx 68.5^\circ$ at DE 2 (see Figure 9), both electrons and protons contribute significantly to the E layer. A six-sweep-averaged ion spectrum from LAPI centered on time 0535:24 UT shows a Maxwellian component at 17 keV with peak flux of 70 ions/cm² sr eV. Using the *Jasperse and Basu* [1982] code, a Maxwellian distribution of protons having the above characteristics would produce an ionization density of $\sim 1.1 \times 10^5$ el/cm³ at 120 km. The electron density computed at that latitude from the DE 2 electron precipitation data (e.g., lower panel of Figure 9) is $\sim 1.2 \times 10^5$ el/cm³ at 120 km. Thus at this latitude the two populations contribute about equally to the E region ionization. Adding production rates at ~ 120 km to obtain the total electron number density at that altitude gives the value 1.6×10^5 el/cm³. The radar shows that the maximum density of 2×10^5 el/cm³ at this latitude is located at 130 km. Although this represents better agreement in the absolute value of the electron density between the radar and the satellite, there still remains a difference in height of the ionization peaks. Satellite measurements still give a density peak about 10 km lower than the radar measurements. This reinforces our suggestion made earlier that the lack of agreement may be due in part to the presence of a strong northward electric field, and in part to a neutral atmosphere model of exospheric temperature too low for conditions prevailing during this day.

F Region

The F region structure that characterizes our evening sector data set consists of an ionization channel located at the poleward edge of a trough, both features being extended several hundreds of kilometers in local time. This particular structure has been observed quite frequently in the past [*Morse et al.*, 1971; *Bates et al.*, 1973; *Sojka et al.*, 1983; *Weber et al.*, 1985]. Whereas the two features seem to appear in close association, several experimental and theoretical studies have been undertaken to explain separately the formation of the trough [*Moffett and Quegan*, 1983, and references therein; *Schlegel*, 1984] or, more recently, of the ionization channel (or boundary blob) [*Weber et al.*, 1985; *Robinson et al.*, 1985]. Nonetheless, since the two features seem to be linked to each other, a self-consistent explanation should be given to the mid-latitude trough and the ionization channel.

In what follows, we will discuss the relative importance of three mechanisms operating in the F region (production, recombination and transport), and propose a scheme for the formations of the trough and ionization channel that is consistent with our data set.

Production. Data from the DE 2 satellite in Plate 1 have shown that the ionization channel coincides with the equatorward edge of the electron precipitation from the central plasma sheet. South of this boundary, and therefore in the region of the trough, there is no production of ionization by electron precipitation or by solar radiation (since the satellite is in darkness). In

the ionization channel and north of it, there are several instances when enhanced precipitation of electrons with energies of several hundreds of eV is observed. In particular, such an increase (although very small) is observed at 0535:45 UT, at the equatorward edge of the electron precipitation from the CPS. Is it responsible for the density enhancement in the ionization channel?

Because the electron temperature, T_e , responds very quickly to in-situ production [*Roble and Rees*, 1977], a classical method to determine, from radar data, if an F region density enhancement is locally produced, is to examine the electron temperature variations. However, it is also well known that either an in-situ production or a density decrease will result in F region electron temperature enhancements. To overcome the difficulty of distinguishing between several mechanisms responsible for the T_e variations, *Kofman and Wickwar* [1984] calculated the energy loss rate from electron collisions with ions and neutrals, from the radar-measured electron and ion temperatures and from electron density. This energy loss rate, L_e , gives the net energy deposited in the electron gas from all sources, including photoelectrons, soft particle precipitation and heat conduction. It has been shown to be very useful in studying soft precipitation above Chatanika and Sondre Stromfjord. Plate 3 shows L_e as a function of invariant latitude and altitude for the scan at 0529–0544 UT, simultaneous with the DE 2 pass. L_e increases north of 69° to a maximum greater than 10^4 eV/cm³ s at 70.5° , the location of the northern inverted-V structure. Within the region of the ionization channel around 66.2° , L_e does not increase above the background of 200 eV/cm³ s at 350 km. This indicates that the ionization channel is not locally produced by particle precipitation. This result is also consistent with recent studies by *Weber et al.* [1985, 1986].

Ion chemistry. One of the most important mechanisms that has been emphasized in the past to explain the trough formation involves the role of the $O^+ + N_2 \rightarrow NO^+ + N$ reaction. Because the rate coefficient of this reaction strongly depends upon the effective ion temperature, the NO^+ concentration is enhanced in the presence of intense electric fields, and subsequent electron density depletions are created by NO^+ recombination. Recently, *Schlegel* [1984] has reported some experimental evidence that this mechanism operates in the trough region. Using data from the European Incoherent Scatter Radar (EISCAT), he showed that within the mid-latitude trough, the NO^+ concentration increases relative to the O^+ in an intense electric field.

Figure 3 shows that the electric field during the scan at 0529–0544 UT is almost uniform and equal to 50–60 mV/m north of 63.5° . Yet, the trough (i.e., a density depletion) and the ionization channel (i.e., a density enhancement) are both observed in the intense electric field region where rapid charge exchange should occur. We cannot rule out entirely the possibility of a large electric field on the convective path of where the trough is observed. With this caveat in mind, however, it appears that local ion chemistry alone cannot explain the observed F region ionization structure.

Transport. If none of the local production and recombination processes can account for the F region structure, this indicates that transport is a significant mechanism to be considered to interpret the F region observations. In fact the local production time constant is several tens of minutes, and the typical time constant for recombination is 80 minutes (at 350 km and with a 50-mV/m electric field). During these typical characteristic times, the F region plasma can travel long distances, especially if

VELOCITY IN INERTIAL FRAME OF REFERENCE

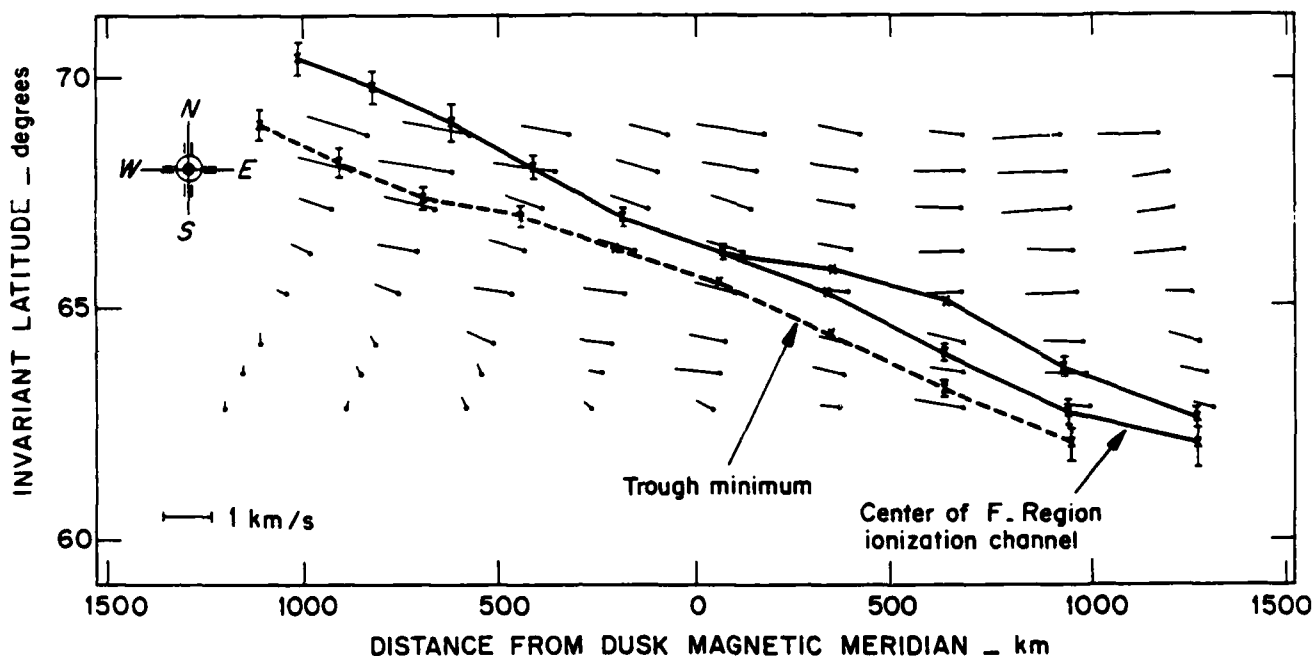


Fig. 12. Drift velocities in the inertial frame of reference, as a function of the distance from the dusk magnetic meridian and invariant latitude. The solid lines show the locations of the center of the ionization channels, and the dashed line, the location of the trough minimum.

the plasma velocity is large as in the present case where it reaches about 1 km/s.

Figure 12 shows the ion velocity in the inertial frame of reference, in a Cartesian projection of the evening sector. The distance scale lengths along the two axes are the same, and the dusk meridian is in the middle of the plot. The velocity vectors are shown for the scans between 0355 and 0726 UT, and the locations of the center of the ionization channel and of the trough minimum are shown with the solid and dashed lines, respectively. The plasma within these two features is transported from the nightside toward the dayside at high speed (~ 1 km/s). However, it seems very unlikely that flux tubes full of plasma, together with empty flux tubes, originate from the same region of the ionosphere. Although they travel side by side in the evening sector, these flux tubes most probably have different convective histories.

Let us therefore first consider the trough. Although several processes operate together in the *F* region, the decay of ionization in flux tubes that spend a long time in darkness can be a significant mechanism responsible for the trough formation. Because our observations are made in winter and at a universal time near the UT when the polar cap is in maximum darkness, there would be ample time for a plasma parcel to recombine along a convective path that goes antisunward from the dayside across the polar cap, then westward in the auroral zone. This was suggested by Watkins [1978]. However, if the westward flow were to transport plasma from the nightside of the auroral zone, one would expect the trough minimum to exist on the most equatorward part of the westward flow, since it represents the longest recombination time. Because this is not what is suggested by our data in Figure 12, it is unlikely that this mechanism is the dominant process by which the trough forms.

The decay of ionization in stagnating flux tubes has also been

proposed to explain the trough formation in the afternoon sector. In this sector, the stagnation of some flux tubes would be the result of the competing influences of convection and corotation. Several years ago, Spiro *et al.* [1978] elaborated a simple theoretical model in which they computed the convection trajectories of plasma flux tubes, in the absence of production sources, using a model electric field, and taking into account the energy dependency of the $N_2 + O^+$ chemical reaction. The results of their model are shown on Figure 13. Figure 13a shows the model convection trajectories in the inertial frame of reference as a function of latitude and local time. The interval between successive dots along a convection trajectory corresponds to the passage of 1 hour. In the southern region, the plasma corotates toward later local times. In the northern region, the plasma drifts sunward as a result of the magnetospheric convection. In between these two regions, the drift reverses along a "stagnation line" where the plasma remains for long periods of time. The stagnation line is located at 58° in their model. Figure 13b shows the latitudinal profiles of the electron density in the *F* region resulting from the convection paths of Figure 13a. A trough forms at latitudes above 59° , i.e., north of the stagnation line. The mean displacement between the stagnation line and the trough minimum is about 2° .

The convection velocity field used as input to the Spiro *et al.* [1978] model in the evening sector is consistent with the radar observations of Figure 12. Therefore, a comparison between the results of this model and our data set is possible. The similarities between the data and model plasma distributions are striking. First, as observed in Figure 12, the trough minimum in our data set is located in a region where the plasma drifts sunward, some 2° or 3° north of the region where the drift velocity is very small, i.e., north of the stagnation region. This is in excellent agreement with the model results. Second, the *F* region electron

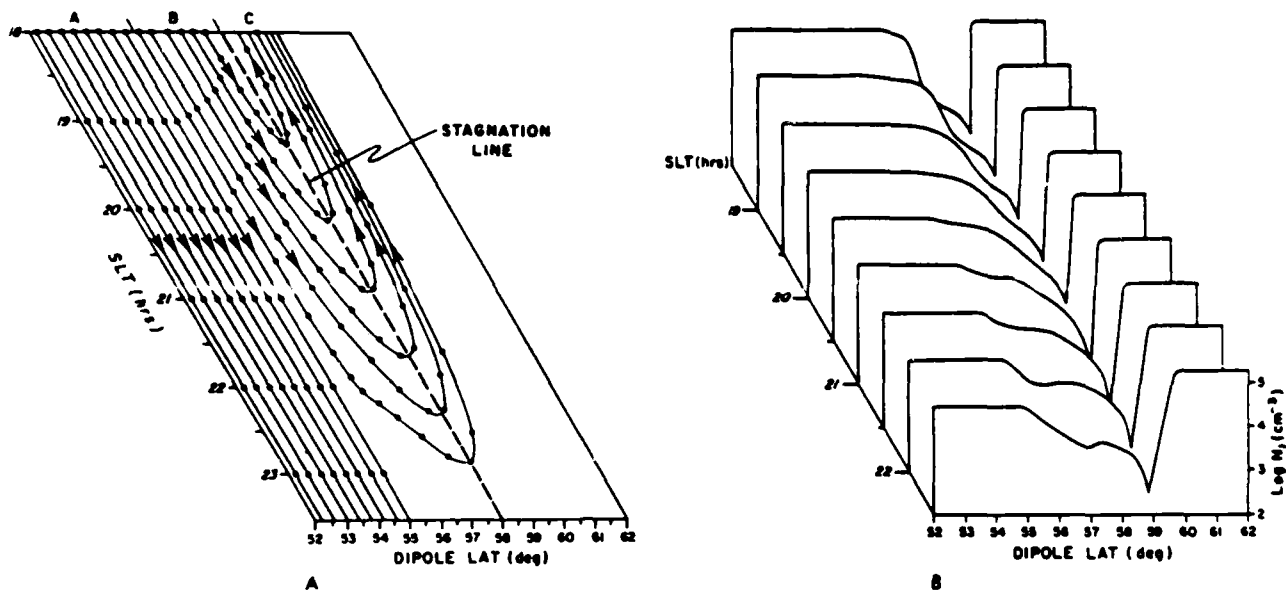


Fig. 13. (a) Convection trajectories, as a function of latitude and local time, used as input to the ionospheric decay computation of Spiro *et al.* [1978]. The interval between successive dots along a convection trajectory corresponds to the passage of one hour. (b) Electron density profiles that result from the convection pattern of Figure 13a. A trough forms north of the stagnation line.

density varies smoothly with latitude south of the trough minimum, whereas the northern edge of the trough is very steep, both in the model calculation and in the data set (see Figure 4 and Plate 1). Although we cannot dismiss possible changes in the convective flow, some constancy in the pattern is suggested by the radar data. Thus, this simple model that only takes into account the plasma convection and the energy dependent ion chemistry can explain most of the observed characteristics of our trough. It should be noticed, however, that the Spiro *et al.* [1978] model does not include production by either sun radiation or particle precipitation, whereas in our case the trough is located above a proton aurora. The importance of *F* region ionization production by proton precipitation should therefore be investigated in the future. Proton precipitation does not, however, fundamentally modify the conclusions of Spiro *et al.*

Neutral winds can also affect the *F* region plasma dynamics and chemistry by raising (or lowering) the layer at altitudes where the recombination is slower (or faster), or by transporting vibrationally excited N_2 molecules into the trough region [Schunk and Banks, 1975]. We have computed the time variations of the meridional component of the neutral wind above Chatanika from the line-of-sight velocity measurements when the radar beam is parallel to the magnetic field, using the method described by Wickwar *et al.* [1984]. The calculation shows that the meridional component of the neutral wind is very small (on the order of 50 m/s) when the ionization channel and the trough are above Chatanika. Thus the neutral wind can have little effect in transporting the plasma up or down the tilted magnetic field lines and in modifying the ion chemistry. During periods when the region north of the ionization channel is above Chatanika, the meridional neutral wind is southward and reaches about 400 m/s around 300 km altitude. This large meridional neutral wind may transport vibrationally excited N_2^* molecules from high latitudes into the trough region and thus enhance the conversion of O^+ to NO^+ . Part of the trough formation could thus be explained by the large meridional neutral winds observed north of the trough.

Other mechanisms have been proposed to explain the trough formation. They include plasma escape, enhancement of the concentration of N_2 by heating of the upper atmosphere, and production of N_2^* by thermal electron impact. The contributions of the two first processes have been shown to be negligible [Knudsen, 1974; Raitt *et al.*, 1975], while the last process requires high electron temperatures [Newton *et al.*, 1974]. The electron temperature measured in our case by the Chatanika radar is about 2100° K in the trough region, which is too low for this mechanism to be important. Finally, the recent fossil theory proposed by Holt *et al.* [1983] and Evans *et al.* [1983] does not appear to apply to our data set, since it concerns those troughs found in regions of small convection electric fields and remaining as fossils of the auroral activity after the auroral oval retracts to higher latitudes. It should be kept in mind, however, that the processes acting on the plasma during its entire UT dependent convection path can affect the observed ion concentrations. Thus, while a simple model serves to conceptually explain the trough in this case, it cannot be representative of many details found in the data.

The second outstanding feature of our data set is the ionization channel located at the poleward edge of the main trough and collocated with the equatorward edge of the electron precipitation from the CPS. Because the *F* region responds slowly to in-situ production [Watkins and Richards, 1979; Sojka *et al.*, 1981a; Sojka and Schunk, 1983], the appearance of an *F* region density enhancement does not necessarily reflect instantaneous production by local auroral precipitation. Indeed, we have shown that the ionization channel is convected westward from the nightside, and that it is not instantaneously produced by a local source of soft electrons. Well-behaved precipitation and electric field patterns may result in electron density increases if the plasma flows along a source region, so that ample time is available for the density to build up. Robinson *et al.* [1985] have shown that this mechanism could account for the ionization channel if the plasma flow lines were parallel to a source located at the equatorward edge of the auroral oval. In that situation,

the east-west extended F region boundary blob and its source would be colocated, and the plasma would drift along these features. In our data set, although the F -region density enhancement is colocated with a small increase of the soft electron flux (see DE 2 data), Figure 12 shows that the plasma flow lines are not, in general, parallel to the center of the ionization channel. Moreover, there is no evidence of enhanced soft-electron fluxes at the equatorward edge of the electron precipitation region in the NOAA 6 data. This suggests that the source region observed at 0535:45 UT by the DE 2 satellite is not extended in local time. Thus, our data set is not consistent with a scenario in which the ionization channel is formed because the F region plasma remains in the source region throughout its convection path. Moreover, the fact that only scarce observations of enhanced soft-electron fluxes at the equatorward edge of the electron precipitation region have been reported in the past [Tanskanen *et al.*, 1981] also supports this conclusion.

Using a model electric field, Robinson *et al.* [1985] have also calculated the ionization distribution resulting from a uniform source in the oval, from a source at the poleward edge of the oval, and from a source in the Harang discontinuity. They have shown that the two latter sources are not efficient in producing the boundary blob, while the first one may produce an east-west extended density enhancement where the velocity is small because the plasma spends a long time within the source region. This mechanism obviously does not apply to our data set, since the ionization channel is observed in a high-velocity region.

Finally, Robinson *et al.* [1985] proposed that the boundary blob forms as a result of the incompressibility of the flow in an electrostatic potential field. They showed that a patch of enhanced F region electron density undergoes a distortion and a reduction of its latitudinal scale size while it convects from the polar cap to the Harang discontinuity and then westward toward dusk in the auroral zone. This arises naturally as a consequence of the difference in the drift velocity between the Harang discontinuity and the eveningside auroral oval. The calculation of Robinson *et al.* clearly showed that a circular blob of ionization located in the dusk sector of the polar cap is distorted by the convection pattern, and eventually shapes as an east-west elongated structure that resembles very much our ionization channel. Furthermore, their calculation shows that the ionization channel that results from this mechanism is not aligned with the flow lines, which is actually supported by our observations in Figure 12. This structuring mechanism seems therefore to be an excellent candidate to explain our ionization channel, wherever the original source of ionization lies. This source could be soft particle precipitation in the polar cap or in the polar cusp, or solar illumination in the dayside polar cap. In fact, it has been often suggested that solar illumination is the most likely candidate [Weber *et al.*, 1984, 1985, 1986; de la Beaujardiere *et al.*, 1985].

Finally, a simple scheme for the F region plasma dynamics emerges from the above discussion. This scheme is consistent with our observations. Although both the trough and the ionization channel are located in a region of rapid sunward flow, the flux tubes associated with these two features have different convective histories. Flux tubes on the low-latitude edge of the trough, where the density varies smoothly, have first corotated eastward toward the night before flowing sunward at higher latitudes where magnetospheric convection predominates. However, flux tubes associated with the ionization channel flow antisunward in the polar cap and then sunward in the auroral zone.

5. SUMMARY

In this paper, we have used simultaneous data from the Chatanika radar and the DE 2 and NOAA 6 satellites to study the typical behavior of the winter evening-sector auroral plasma during moderate and steady magnetic activity. We emphasized the following features:

1. The equatorward edge of the auroral E layer, of the region 2 field-aligned currents, and of the region of intense convection are colocated. The entire auroral E layer observed by the radar and associated with the continuous, diffuse aurora is embedded in the downward field-aligned current sheet, and the precipitation from the BPS is colocated with the upward field-aligned current sheet. An inverted V is observed over several hours of local time in the BPS region. It is associated with intense small-scale field-aligned current sheets that overlap the large-scale quiet-time eveningside field-aligned current pattern.

2. The auroral E layer extends several degrees south of the equatorward edge of the keV electron precipitation from the CPS. This is because proton precipitation contributes significantly to the E region ionization south of the electron precipitation region, and also within it. E region density profiles were calculated, south of the electron precipitation region, from the DE 2 and NOAA 6 measured proton spectra and from the linear transport theory of Jasperse and Basu [1982]. These calculated ionization profiles were found to agree fairly well with the Chatanika data.

3. Although the main trough and ionization channel (or boundary blob) are embedded in a region of intense electric field where the plasma flows sunward at high speed, the flux tubes associated with the two features have different time histories. Our data set suggests that the flux tubes associated with the trough first corotate eastward toward the night and then return sunward in the auroral zone; those associated with the ionization channel drift antisunward in the polar cap and then sunward in the auroral zone.

4. The mid-latitude trough is located south of the region of electron precipitation, above a proton aurora. It is mainly the result of transport and enhanced recombination due to large electric fields. Neutral winds seem to have a minor contribution to its formation. Our data set is consistent with the mechanism described by Spiro *et al.* [1978] according to which the trough would form by recombination during the long time the flux tubes stagnate in the region where corotation and convection compete.

5. The ionization channel, or boundary blob, marks the poleward edge of the main trough and is colocated with the equatorward boundary of the electron precipitation from the central plasma sheet. Although slightly enhanced fluxes of soft-precipitating electrons are observed at this boundary, these particles are not responsible for the ionization channel formation. Rather, the relative orientations of the flow lines and of the channel center support the mechanism proposed by Robinson *et al.* [1985]. This feature could be formed by distortion of polar cap F region structures, due to the incompressibility of the flow.

Magnetospheric simulations only consider electron precipitation [Spiro and Wolf, 1984; Fontaine *et al.*, 1985]. Therefore electrons are the only particles that contribute to the ionospheric conductivity variations, and thus to ionospheric current closure. On the other hand, Schunk *et al.* [1975, 1976], Sojka *et al.* [1981a,b,c], Sojka and Schunk [1983], and Sojka *et al.* [1983] have shown the high degree of sensitivity of the F region plasma densities to the convection and precipitation patterns. There-

fore, the observations described in this paper, because they clarify the relationship between convection, currents, ion and electron precipitation, and F and E region ionization features will provide useful inputs to magnetosphere-ionosphere modeling efforts.

Acknowledgments. We are very grateful to J. R. Jasperse, B. Basu, R. M. Robinson and V. B. Wickwar for useful discussions and to the site crew of the Chatanika radar. This work was supported by AFOSR contracts F49620-83-K-0005 and F49620-85-C-0029, by Air Force Geophysics Laboratory contract FY712184N0006, by NASA grants NAG5-305 and NGR 44-004-120, by NASA contract NAS5-28712, by NSF cooperative agreement ATM 8516436, and by the Centre National de la Recherche Scientifique.

The Editor thanks B. J. Watkins and J. A. Whalen for their assistance in evaluating this paper.

REFERENCES

- Banks, P. M., and G. Kockarts, *Aeronomy*, Part B, p. 314, Academic, Orlando, Fla., 1973.
- Bates, H. F., A. E. Belon, and R. D. Hunsucker, Aurora and the poleward edge of the main ionospheric trough, *J. Geophys. Res.*, **78**, 648, 1973.
- Berger, M. J., S. M. Seltzer, and K. Maeda, Some new results on electron transport in the atmosphere, *J. Atmos. Terr. Phys.*, **36**, 591, 1974.
- Crasnier, J., J. A. Sauvaud, Yu. I. Galperin, R. A. Kovrazhkin, and Yu. N. Ponomarev, Mesures in situ a bord du satellite AUREOLE des protons auroraux durant des periodes magnetiques calmes, *Ann Geophys.*, **30**, 357, 1974.
- de la Beaujardiere, O., V. B. Wickwar, C. Leger, M. McCready, and M. Baron, The software system for the Chatanika incoherent-scatter radar. Technical report, SRI Project 8358, SRI International, Menlo Park, Calif., 1980.
- de la Beaujardiere, O., V. B. Wickwar, M. J. Baron, J. Holt, R. M. Wand, W. L. Oliver, P. Bauer, M. Blanc, C. Senior, D. Alcayde, G. Caudal, J. Foster, E. Nielsen, and R. Heelis, MITHRAS: A brief description, *Radio Sci.*, **19**, 665, 1984.
- de la Beaujardiere, O., V. B. Wickwar, G. Caudal, J. M. Holt, J. D. Craven, L. A. Frank, L. H. Brace, D. S. Evans, J. D. Winningham, and R. A. Heelis, Universal time dependence of nighttime F region densities at high latitude, *J. Geophys. Res.*, **90**, 4319, 1985.
- Evans, J. V., J. M. Holt, W. L. Oliver, and R. H. Wand, The fossil theory of nighttime high-latitude F region troughs, *J. Geophys. Res.*, **88**, 7769, 1983.
- Farthing, W. H., M. Sugiura, B. G. Ledley, and L. J. Cahill, Jr., Magnetic field observations on DE-A and -B, *Space Sci. Instrum.*, **5**, 551, 1981.
- Fontaine, D., M. Blanc, L. Reinhart, and R. Glowinski, Numerical simulations of magnetospheric convection including the effects of electron precipitation, *J. Geophys. Res.*, **90**, 8343, 1985.
- Hill, V. J., D. S. Evans, and H. H. Sauer, TIROS/NOAA satellites space environment monitor archive tape documentation, *NOAA Tech. Memo.*, ERL SEL-71, 1985.
- Hoffman, R. A., (Ed.), Dynamics Explorer, *Space Sci. Instrum.*, **5**, 345, 1981.
- Hoffman, R. A., M. Sugiura, and N. C. Maynard, Current carriers for the field-aligned current system, *NASA Tech. Memo.*, 1984.
- Holt, J. M., J. V. Evans, and R. H. Wand, Millstone Hill study of the trough. Boundary between the plasmopause and magnetosphere or not?, *Radio Sci.*, **18**, 947, 1983.
- Huuskonen, A., T. Nygren, L. Jalonen, and J. Oksman, The effect of electric field-induced vertical convection on the precipitation E layer, *J. Atmos. Terr. Phys.*, **46**, 927, 1984.
- Jaggi, R. K., and R. A. Wolf, Self-consistent calculation of the motion of a sheet of ions in the magnetosphere, *J. Geophys. Res.*, **78**, 2852, 1973.
- Jasperse, J. R., and B. Basu, Transport theoretic solutions for auroral proton and H atom fluxes and related quantities, *J. Geophys. Res.*, **87**, 811, 1982.
- Johnstone, A. D., and J. D. Winningham, Satellite observations of suprathermal electron bursts, *J. Geophys. Res.*, **87**, 2321, 1982.
- Kamide, Y., and S.-I. Akasofu, The locations of field-aligned currents with respect to discrete auroral arcs, *J. Geophys. Res.*, **81**, 3999, 1976.
- Klumpar, D. M., Relationships between auroral particle distributions and magnetic field perturbations associated with field-aligned currents, *J. Geophys. Res.*, **84**, 6524, 1979.
- Knudsen, W. C., Magnetospheric convection and the high-latitude F_2 ionosphere, *J. Geophys. Res.*, **79**, 1046, 1974.
- Kofman, W., and V. B. Wickwar, Very high electron temperatures in the daytime F region at Sondrestrom, *Geophys. Res. Lett.*, **11**, 919, 1984.
- Langel, R. A., R. H. Estes, G. D. Mead, G. B. Fabiano, and E. R. Lancaster, Initial geomagnetic field model from Magsat vector data, *Geophys. Res. Lett.*, **7**, 793, 1980.
- Lui, A. T. Y., D. Venkatesan, C. D. Anger, S.-I. Akasofu, W. J. Heikkila, J. D. Winningham, and J. R. Burrows, Simultaneous observations of particle precipitations and auroral emissions by the ISIS 2 satellite in the 19-24 MLT sector, *J. Geophys. Res.*, **82**, 2210, 1977.
- Moffett, R. J., and S. Quegan, The mid-latitude trough in the electron concentration of the ionospheric F layer: A review of observations and modelling, *J. Atmos. Terr. Phys.*, **45**, 315, 1983.
- Morse, F. A., H. H. Hilton, and P. F. Mizera, Polar ionosphere: Measured ion density enhancements and soft electron precipitation, *J. Geophys. Res.*, **75**, 6099, 1971.
- Newton, G. P., J.-C. G. Walker, and P. H. E. Meijer, Vibrationally excited nitrogen in stable auroral red arcs and its effect on ionospheric recombination, *J. Geophys. Res.*, **79**, 3807, 1974.
- Pellat, R., and G. Laval, Remarks on the steady and time-dependent mathematical convection models, in *Critical Problems of Magnetospheric Physics*, edited by E. R. Dyer, Inter-Union Commission on Solar-Terrestrial Physics, Washington, D. C., 1972.
- Raitt, W. J., U. Von Zahn, and P. Christophersen, A comparison of thermospheric neutral gas heating and related thermal and energetic plasma phenomena at high latitudes during geomagnetic disturbances, *J. Geophys. Res.*, **80**, 2277, 1975.
- Rees, M. H., Auroral ionization and excitation by incident energetic electrons, *Planet. Space Sci.*, **11**, 1209, 1963.
- Rino, C. L., R. C. Livingston, R. T. Tsunoda, R. M. Robinson, J. F. Vickrey, C. Senior, M. D. Cousins, J. Owen, and J. A. Klobuchar, Recent studies of the structure and morphology of auroral zone F region irregularities, *Radio Sci.*, **18**, 1167, 1983.
- Robinson, R. M., and R. R. Vondrak, Characteristics and sources of ionization in the continuous aurora, *Radio Sci.*, **20**, 447, 1985.
- Robinson, R. M., R. R. Vondrak, and T. A. Potemra, Electrodynamic properties of the evening sector ionosphere within the region 2 field-aligned current sheet, *J. Geophys. Res.*, **87**, 731, 1982.
- Robinson, R. M., R. T. Tsunoda, J. F. Vickrey, and L. Guerin, Sources of F region ionization enhancements in the nighttime auroral zone, *J. Geophys. Res.*, **90**, 7533, 1985.
- Roble, R. G., and M. H. Rees, Time-dependent studies of the aurora: Effects of particle precipitation on the dynamic morphology of ionospheric and atmospheric properties, *Planet. Space Sci.*, **25**, 991, 1977.
- Rostoker, G., J. C. Armstrong, and A. J. Zmuda, Field-aligned current flow associated with intrusion of the substorm-intensified westward electrojet in the evening sector, *J. Geophys. Res.*, **80**, 3571, 1975.
- Schild, M. A., J. W. Freeman, and A. J. Dessler, A source for field-aligned currents at auroral latitudes, *J. Geophys. Res.*, **74**, 247, 1969.
- Schlegel, K., A case study of a high-latitude ionospheric density depletion, *J. Atmos. Terr. Phys.*, **46**, 517, 1984.
- Schunk, R. W., and P. M. Banks, Auroral N_2 vibrational excitation and the electron density trough, *Geophys. Res. Lett.*, **2**, 239, 1975.
- Schunk, R. W., W. J. Raitt, and P. M. Banks, Effect of electric fields on the daytime high-latitude E and F regions, *J. Geophys. Res.*, **80**, 3121, 1975.
- Schunk, R. W., P. M. Banks, and W. J. Raitt, Effects of electric fields and other processes upon the nighttime high-latitude F layer, *J. Geophys. Res.*, **81**, 3271, 1976.
- Senior, C., R. M. Robinson, and T. A. Potemra, Relationship between field-aligned currents diffuse auroral precipitation, and the westward electrojet in the early morning sector, *J. Geophys. Res.*, **87**, 10,469, 1982.
- Sharber, J. R., The continuous (diffuse) aurora and auroral E -region ionization, in *Physics of Space Plasma*, edited by T. S. Chang, B. Coppi, and J. R. Jasperse, *SPI Conf. Proc. Reprint Ser.*, vol. 4, Scientific Publishers, Cambridge, Mass., 1981.
- Sojka, J. J., and R. W. Schunk, A theoretical study of the high-latitude F region's response to magnetospheric storm input, *J. Geophys. Res.*, **88**, 2112, 1983.

- Sojka, J. J., W. J. Raitt, and R. W. Schunk, A theoretical study of the high-latitude winter *F* region at solar minimum for low magnetic activity. *J. Geophys. Res.*, *86*, 609, 1981a.
- Sojka, J. J., W. J. Raitt, and R. W. Schunk, Theoretical predictions for ion composition in the high-latitude winter for solar minimum and low magnetic activity. *J. Geophys. Res.*, *86*, 2206, 1981b.
- Sojka, J. J., W. J. Raitt, and R. W. Schunk, Plasma density features associated with strong convection in the winter high-latitude *F* region. *J. Geophys. Res.*, *86*, 6968, 1981c.
- Sojka, J. J., R. W. Schunk, J. V. Evans, J. M. Holt, and R. H. Wand, Comparison of model high-latitude electron densities with Millstone Hill observations. *J. Geophys. Res.*, *88*, 7783, 1983.
- Spiro, R. W., and R. A. Wolf, Electrodynamics of convection in the inner magnetosphere. in *Magnetospheric Currents*. *Geophys. Monogr. Ser.*, vol. 28, edited by T. A. Potemra, p. 247. AGU, Washington D. C., 1984.
- Spiro, R. W., R. A. Heelis, and W. B. Hanson, Ion convection and the formation of the mid-latitude *F* region ionization trough. *J. Geophys. Res.*, *83*, 4255, 1978.
- Sugiura, M., T. Iyemori, R. A. Hoffman, N. C. Maynard, J. L. Burch, and J. D. Winningham, Relationships between field-aligned currents, electric fields and particle precipitation as observed by Dynamics Explorer-2. in *Magnetospheric Currents*. *Geophys. Monogr. Ser.*, vol. 28, edited by T. A. Potemra, pp. 96-103. AGU, Washington, D. C., 1984.
- Tanskanen, P. J., D. A. Hardy, and W. J. Burke, Spectral characteristics of precipitating electrons associated with visible aurora in the premidnight oval during periods of substorm activity. *J. Geophys. Res.*, *86*, 1379, 1981.
- Trombka, B. T., and J. C. Cain, Computation of the IGRF. I. Spherical expansions. *NASA-GSFC Rep. X-922-74-303*, Greenbelt, Md., 1974.
- Vondrak, R. R., and M. J. Baron, A method of obtaining the energy distribution of auroral electrons from incoherent-scatter radar. in *Radar Probing of the Auroral Plasma*, edited by A. Brekke, p. 315. Universitetsforlaget, Tromsø, Norway, 1977.
- Vondrak, R. R., and R. A. Robinson, Inference of high-latitude ionization and conductivity from AE-C measurements of auroral electron fluxes. *J. Geophys. Res.*, *90*, 7505, 1985.
- Watkins, B. J., A numerical computer investigation of the polar *F*-region ionosphere. *Planet. Space Phys.*, *26*, 559, 1978.
- Watkins, B. J., and P. G. Richards, A theoretical investigation of the role of neutral winds and particle precipitation in the formation of the auroral *F* region ionosphere. *J. Atmos. Terr. Phys.*, *41*, 179, 1979.
- Weber, E. J., J. Buchau, J. G. Moore, J. R. Sharber, R. C. Livingston, J. D. Winningham, and B. W. Reinisch, *F* layer ionization patches. *J. Geophys. Res.*, *89*, 1683, 1984.
- Weber, E. J., R. T. Tsunoda, J. Buchau, R. E. Sheehan, D. J. Strickland, W. Whiting, and J. G. Moore, Coordinated measurements of auroral zone plasma enhancements. *J. Geophys. Res.*, *90*, 6497, 1985.
- Weber, E. J., J. A. Klobuchar, J. Buchau, H. C. Carlson, Jr., R. C. Livingston, O. de la Beaujardière, M. McCready, J. G. Moore, and G. J. Bishop, Polar cap *F* layer patches: Structure and dynamics. *J. Geophys. Res.*, *91*, 12,121, 1986.
- Wickwar, V. B., J. W. Meriwether, Jr., P. B. Hays, and A. F. Nagy, The meridional thermospheric wind measured by radar and optical techniques in the auroral region. *J. Geophys. Res.*, *89*, 10,987, 1984.
- Winningham, J. D., F. Yasuhara, S.-I. Akasofu, and W. J. Heikkila, The latitudinal morphology of 10-eV to 10-keV electron fluxes during magnetically quiet and disturbed times in the 2100-0300 MLT sector. *J. Geophys. Res.*, *80*, 3148, 1975.

O. de la Beaujardière, SRI International, 333 Ravenswood Avenue, Menlo Park, CA 94025.

D. S. Evans, NOAA, 325 Broadway, Boulder, CO 80303.

R. A. Heelis, University of Texas at Dallas, Richardson, TX 75080.

W. R. Hoegy, Goddard Space Flight Center, Greenbelt, MD 20771.

C. Senior, Centre de Recherches en Physique de l'Environnement,

4, avenue de Neptune, 94107 Saint-Maur-des-Fosses Cedex, France.

J. R. Sharber and J. D. Winningham, Southwest Research Institute,

6220 Culebra Road, P. O. Drawer 28510, San Antonio, TX 78284.

M. Sugiura, Geophysical Institute, Kyoto University, Kyoto 606,

Japan.

(Received May 20, 1986;
revised September 24,
accepted October 27, 1986.)

APPENDIX B

Plasma Waves Associated with Diffuse Auroral Electrons at Mid-Altitudes

PLASMA WAVES ASSOCIATED WITH DIFFUSE AURORAL ELECTRONS AT MID-ALTITUDES

J. R. Sharber,* J. D. Menietti,* H. K. Wong,* J. L. Burch,*
D. A. Gurnett,** J. D. Winningham,* P. J. Tanskanen***

*Instrumentation and Space Research Division, Southwest Research Institute, San Antonio,
TX 78284; **Department of Physics and Astronomy, University of Iowa, Iowa City,
IA 52242; ***Department of Physics, University of Oulu, SF 90570 Oulu 57, Finland

ABSTRACT

Using simultaneous observations from the High Altitude Plasma Instrument and the Plasma Wave Instrument on board the Dynamics Explorer-1 satellite, we have examined 28 auroral zone crossings equally divided among dayside and nightside cases covering a range of Kp values from 1- to 8. We find that in the diffuse auroral region (CPS) electrostatic emissions of frequencies up to a few kHz are associated with low-energy, field aligned electron beams. Of 15 cases (11 nightside; 7 dayside) examined at high resolution in the particle data, 15 (9 nightside; 7 dayside) exhibited the field aligned beams with the electrostatic waves. In most cases the beams were upward-directed, but occasionally they traveled both up and down the field line. The three cases showing no beams occurred during intervals of Kp < 2. We interpret the electrostatic emissions as electron acoustic mode waves excited by the field aligned beams. A stability analysis based on the plasma parameters of one of the passes supports this interpretation.

INTRODUCTION

The most widely accepted model of the diffuse aurora involves the scattering by waves or turbulence of plasma sheet particles into the loss cone (e. g., see review by Ashour-Abdalla and Kennel /1/, and references therein). The particles undergo little acceleration before reaching the auroral ionosphere. Based on a report on OGO-5 observations /2/ showing strong wave emissions in the 1-10 mV/m range, Lyons /3/ developed a theory of diffuse auroral precipitation resulting from diffusion of electrons into the loss cone by electron cyclotron harmonic (ECH) waves. Using a bounce-averaged diffusion coefficient, he showed that the observed ECH waves would generally cause strong pitch angle diffusion of plasma sheet electrons of energies in the few tenths to few keV range. A later treatment of the problem /4/ that removed the bounce-averaging condition found that wave amplitudes required for strong diffusion of electrons were ~ 2.6 times greater than those computed by Lyons. The same paper showed that ECH waves observed by GEOS-2 were far less intense than the OGO-5 report had presented. Only 9% of the time did the waves exceed 2 mV/m, the amplitude required to put 1 keV electrons on strong diffusion. It thus appeared that the ECH waves, once thought to play a major role in diffuse aurora production, were not observed with sufficient intensity frequently enough to produce the required strong diffusion. More recent satellite studies /5, 6, 7, 8/ have given support to this conclusion. Thus it is clear that key questions regarding diffuse auroral particle precipitation still remain.

The launch of the Dynamics Explorer satellites in August 1981 provided the opportunity to study simultaneous measurements of plasma waves and auroral particles in the intermediate-altitude range. In the study, observations from the High Altitude Plasma Instrument (HAPI) /9/ and the Plasma Wave Instrument (PWI) /10/, both on DE-1, are examined in an effort to determine what relationships, if any, exist between the diffuse auroral particle population and the plasma waves. An earlier report using this data set /11/ showed that field-aligned electron beams are associated with wave emissions in the few hundred Hz to few kHz frequency range suggesting that the electron acoustic mode as the likely source of the emissions. In this paper we carry the analysis further by examining more of the passes at high resolution to confirm the presence of the beams and by including the results of a wave growth calculation using parameters obtained from the particle observations.

The study is based on a subset of DE-1 data consisting of 28 passes that range in altitude from 8000 to 22,000 km. Fourteen crossings were nightside cases; fourteen were dayside cases. They cover a wide range of magnetic activity with Kp varying between 1- and 8.

Submitted for publication to Advances in Space Research,
October, 1988.

OBSERVATIONS

An example of the nightside observations is shown in Fig. 1. It occurred on day 296 (Oct. 23) of 1981 during the recovery phase of a storm. Kp was 4+ for the three-hour interval that included the pass. The spectrogram has three panels, the top of which is the downcoming (0° pitch angle) HAPI electron data. Auroral oval precipitation is seen between ~ 0341:20 UT (~ 67° IL) and 0351:30 UT (~ 60.1° IL). Within these latitudes the diffuse auroral region (or CPS) is seen between about 0349 UT (~ 62.2° IL) and 0351:30 UT (~ 60.1° IL). This lies within a region consisting mostly of downward field aligned current between 0348:40 and 0353:00 UT (J. Slavin, personal communication). The two lower panels are frequency-time spectrograms of the PWI electric and magnetic field amplitude measurements. In the auroral and polar regions are several types of emissions reported previously /12/. Electromagnetic emissions above the electron gyrofrequency (shown as the uppermost black dotted line on the data) are AKR /13, 14/. The emissions seen at latitudes down to 64.5° IL (0346 UT) are auroral hiss and are associated with the intense BPS particle precipitation /12/. Electromagnetic emissions seen at lower latitudes on the right end of the spectrogram are plasmaspheric hiss.

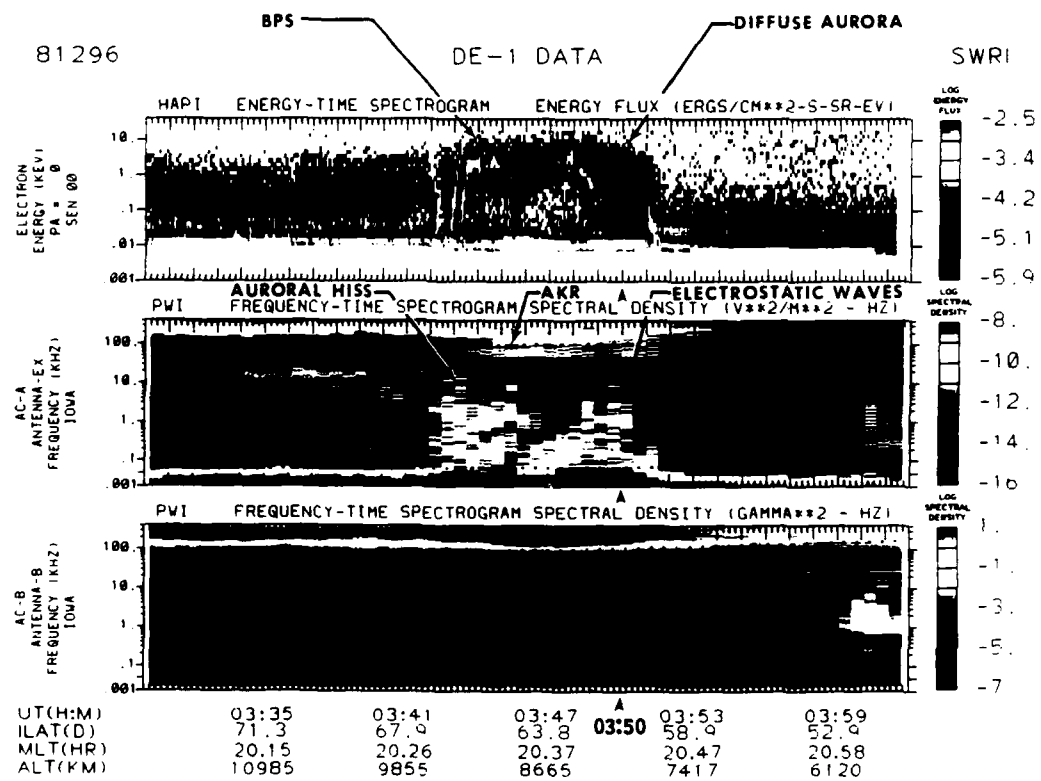


Fig. 1. Nightside example of simultaneous particle and wave measurements from DE-1 on day 296 (Oct. 23) 1981. HAPI measurements for 0° pitch angle electrons are shown in the top panel. The second and third panels are frequency-time spectrograms of the PWI electric and magnetic field amplitude measurements.

As shown in the figure, emissions associated with the diffuse auroral region are electrostatic in nature with frequencies up to a few thousand Hz. The two regions of greatest bandwidth and highest intensity appear to be associated with enhancements in the downcoming electron flux visible in top panel times near the 0349 and 0350 UT minute marks. On the spectrograms these appear as enhancements in the fluxes at low energies (i.e. ~ 20 eV to ~ 100 eV). They are visible immediately above the band of spacecraft-produced photoelectrons which have energies less than ~ 20 eV.

In order to look in detail at one of the regions of intense emission, we examine a high-resolution spectrogram, shown in Fig. 2(a). In this figure the top panel shows all HAPI electron data obtained from a single sensor between ~ 0348:50 and 0351:30 UT. The satellite spin is indicated by the pitch angle plot of the lower portion of the top panel. The second data panel shows PWI electric field data. In the HAPI

spectrogram, highly collimated, field-aligned beams are seen at energies between ~ 20 and ~ 100 eV. In most cases the beams are upward directed, but in some cases they are counterstreaming. Attention is drawn on the figure to several such beams between ~ 0350 and $0350:30$ UT. The contour plot of Fig. 2(b) is produced from a complete spin of DE-1 during the interval $0350:08-0350:14$ UT. It clearly shows both the upward and downward directed beams visible in the spectrogram. A total of 11 passes have been analyzed in high resolution in the HAPI data. Beams of the kind shown in Fig. 2 were seen at diffuse auroral latitudes in 9 of these. It is possible that at times the beam energy is less than 20 eV. In such cases we would not detect it on DE-1 because of the spacecraft photoelectrons.

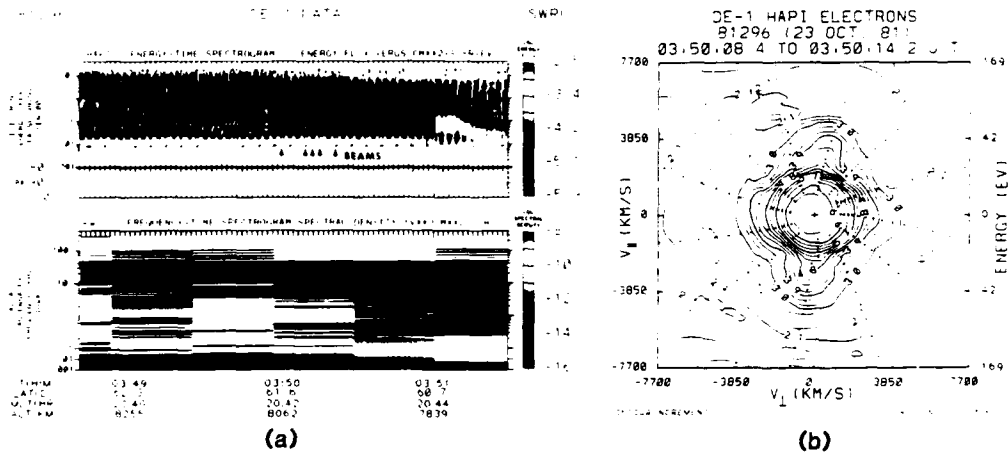


Fig. 2. (a) Expanded HAPI electron and PWI electric field spectrograms showing field aligned, low-energy electron beams. (b) Contour plot made from two spins of DE-1 between $0350:08$ and $0350:14$ UT.

A pass characteristic of the dayside observations is shown in Fig. 3. It occurred on day 274 (Oct. 1) of 1981 during an interval characterized by a K_p of 2-. In this pass the boundary between the dayside diffuse auroral region and the cusp is located at 0741 UT (76.7° IL). The emissions in and poleward of the cusp at frequencies > 1 kHz are auroral hiss, a whistler mode emission investigated previously [12, 14]. Two types of emission are seen in the diffuse auroral region on this pass. One is the same emission present in the nightside observations having a frequency range up to a few kHz. This can be seen on the spectrogram at $0735:30$ UT (75.8° IL). The high-resolution electron spectrogram (see inset above the normal spectrogram) shows the intense low-energy upgoing electron beams associated with these wave emissions. They are seen between ~ 0735 and ~ 0736 UT. For reference, a small pointer appears on each spectrogram panel at $0735:30$ UT. Of seven dayside cases analyzed in high resolution in the particle data, six show electron beams of this kind. Combining the dayside and nightside results, the beams are present in 15 of 15 high-resolution spectrograms. The three cases where they were not observed are characterized by $K_p < 2$.

Another much more extended kind of emission is seen at diffuse auroral latitudes in Fig. 3. It is a relatively narrow band electromagnetic emission shown on the spectrogram between the lowest latitudes $\sim 62.5^\circ$ IL (at 0630 UT) up to at least 76.5° IL (at 0740 UT). It has a peak frequency of about 400 Hz, well below the electron gyrofrequency and a bandwidth of a few hundred Hz. Some of the signature shown in Fig. 3 may be plasmaspheric hiss [12]. However the emissions usually extend through latitudes spanning the entire CPS (diffuse auroral) region. On other passes there is sometimes a break between plasmaspheric hiss (which often peaks equatorward of the diffuse auroral equatorward edge) and a similar but usually lower frequency emission occurring well within diffuse auroral latitudes. We have identified this signature in all 14 of the dayside passes and in 9 of the 14 nightside cases analyzed. Based on these observations we have begun a separate study of this emission to be reported later.

DISCUSSION AND SUMMARY

The presence of the electron beams and their association with the enhancements in the broadband electrostatic emissions suggests that the electron beams might be the source of the electrostatic waves. Since the observed electrostatic waves have a high frequency cutoff at a few kHz, which is less than the electron plasma frequency, the most probable candidates for these electrostatic waves are whistler waves or electron

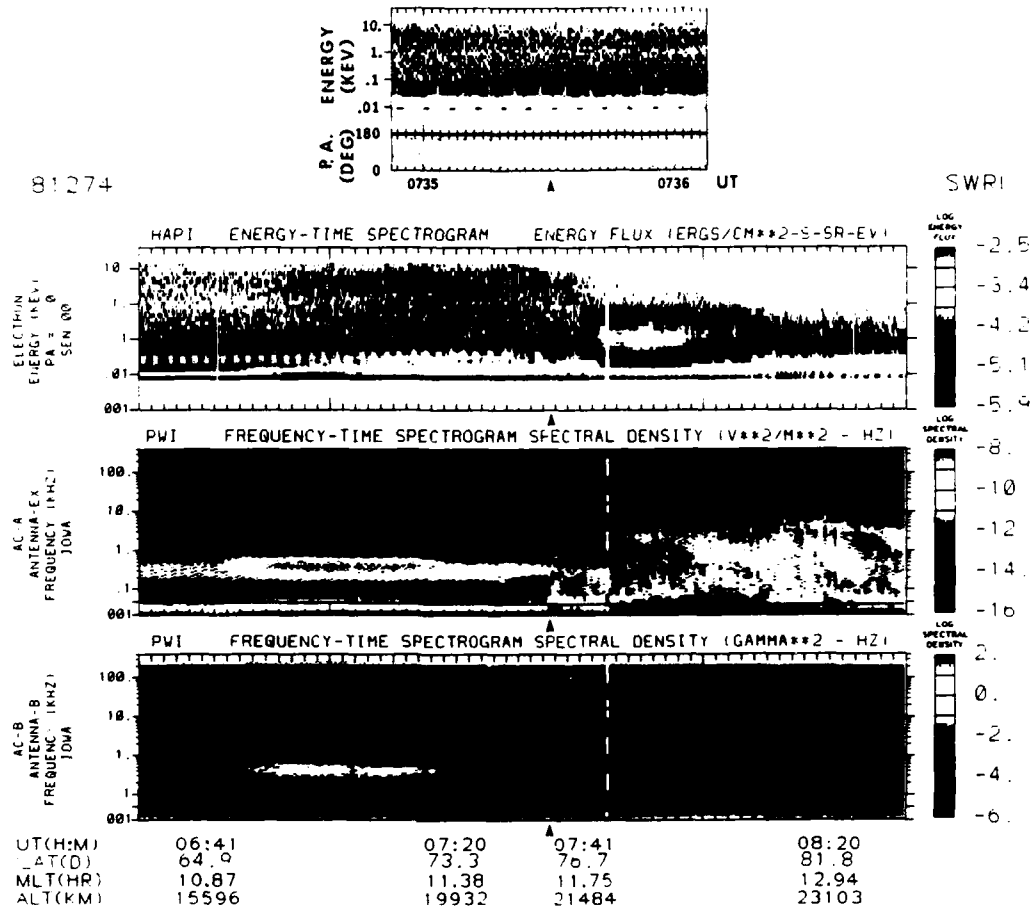


Fig. 3. Dayside example of particle and wave measurements. Beams are indicated in the expanded spectrogram inset at the top. For reference, a pointer on each panel marks the time at 0735:30 UT.

acoustic waves. The excitation of whistler and electron acoustic waves by electron beams in the polar region has been thoroughly studied in the past few years [15, 16, 17, 18, 19]. One distinct feature of the beam-excited whistler waves is the funnel-shaped behavior in the frequency-time spectrogram [12], which is not evident in our observations; thus, we speculate that these electrostatic emissions are generated in the electron acoustic mode.

In order to examine whether the electron beams can excite the electron acoustic waves in the observed frequency range, we have performed a stability analysis of the electron acoustic mode using the electron plasma parameters obtained between 03:50:08.71 and 03:50:08.91 UT of day 296 (see Figs. 1 and 2). During this sweep, the electron pitch angle varied from 171.2° to 173.9° . As determined from analysis of the HAPI electron data, the beam has a peak energy of 32 eV with a temperature of 8.6 eV, and a density of 2.32 cm^{-3} ; the warm Maxwellian background electrons have a temperature of 46.1 eV and density of 0.73 cm^{-3} . Because of the spacecraft-produced photoelectrons, it is not possible to measure the density of the cold background electrons directly. We therefore perform our calculations by choosing three values of n_c (1.3 cm^{-3} , 2 cm^{-3} , and 0 cm^{-3}) and assuming a temperature of the cold electrons of 1 eV. The results are shown in Fig. 4 where the real and imaginary parts of the frequency are plotted as functions of the wavenumber. In the figure, the frequencies are normalized to the electron cyclotron frequency Ω_e , which has a value of 110 kHz at the time of the measurement; the wavenumber k is normalized to α_A/Ω_e (α is the beam thermal speed). As is clear from the figure, both the real frequency and the growth rate (ω_i/Ω_e) increase as the density of the cold electrons increases. This result is consistent with the results obtained by Liu *et al.* [17] and is in agreement with the frequency range and broadband character of the emissions observed.

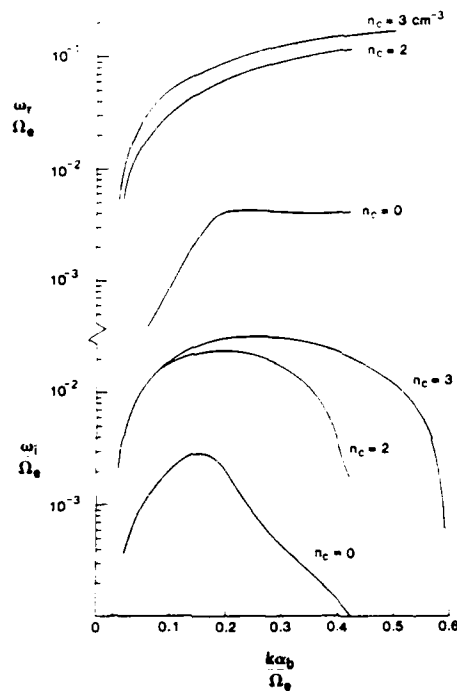


Fig. 4. Results of the stability analysis of the electron acoustic mode based on plasma parameters obtained from HAPI. Real and imaginary parts of the wave frequency are plotted vs. wavenumber for cold electron densities indicated on each curve. Real frequency and wave growth increase as the cold electron density increases.

In summary, we have examined 28 crossings of the auroral regions, equally divided among dayside and nightside cases, in which simultaneous measurements of particle and wave observations were made. We find that, in general, in the diffuse auroral regions, increases in intensity and bandwidth of electrostatic wave emissions are associated with low-energy, field-aligned electron beams. In particular, of 18 (11 nightside, 7 dayside) cases examined at high resolution in the particle data, 15 (9 nightside, 6 dayside) exhibited the field-aligned electron beams associated with electrostatic waves. In most cases the beams were upward directed, but in a few cases they were counterstreaming. The three cases in which no beams were seen took place within $Kp < 2$ intervals. We interpret the electrostatic emissions as electron acoustic mode waves excited by the beams. A growth rate calculation based on plasma parameters of one of the passes supports this interpretation.

ACKNOWLEDGEMENTS

The work was supported at Southwest Research Institute by AFOSR contract F49620-85-C-0029, NASA contracts NAS5-28711 and NAS5-28712, and NSF grant ATM-8713225. Work at the University of Iowa was supported by NASA/GSFC grant NAG5-310. We thank C. Lin for helpful discussions, J. Slavin for providing the magnetic field perturbations from DE-1, and R. Spinks and A. Ramirez for technical assistance.

REFERENCES

1. Ashour-Abdalla, M. and C. F. Kennel, Diffuse auroral precipitation, *J. Geomag. Geoelectr.*, **30**, 239, 1978.
2. Kennel, C. F., F. L. Scarf, R. W. Fredricks, J. G. McGehee and F. V. Coroniti, VLF electric field observations in the magnetosphere, *J. Geophys. Res.*, **75**, 6136, 1970.
3. Lyons, L. R., Electron diffusion driven by magnetospheric electrostatic waves, *J. Geophys. Res.*, **79**, 575, 1974.

4. Belmont, G., D. Fontaine and P. Canu. Are equatorial electron cyclotron waves responsible for diffuse auroral electron precipitation. *J. Geophys. Res.*, 88, 9163, 1983.
5. Fairfield, D. H. and A. F. Viñas. The inner edge of the plasma sheet and the diffuse aurora. *J. Geophys. Res.*, 89, 541, 1984.
6. Fontaine, D., S. Perraut, N. Cornilleau-Wehrlin, B. A. Paricio, J. M. Bosqued, D. Rodgers. Coordinated observations of electron energy spectra and electrostatic cyclotron waves during diffuse auroras. *Annales Geophysicae*, 86005A, 405, 1986.
7. Roeder, J. L. and H. C. Koons. A survey of electron cyclotron waves in the magnetosphere and the diffuse auroral electron precipitation. submitted for publication to *J. Geophys. Res.*, 1988.
8. Shumaker, T. L., M. S. Gussenhoven, D. A. Hardy and R. L. Corovillano. The relationship between diffuse auroral and plasma sheet electron distributions near local midnight. submitted for publication in *J. Geophys. Res.*, 1988.
9. Burch, J. L., J. D. Winningham, V. A. Blevins, N. Eaker and W. C. Gibson. High-altitude plasma instrument for Dynamics Explorer-A. *Space Sci. Instrum.*, 5, 455, 1981.
10. Shawhan, S. D., D. A. Gurnett, D. L. Odem, R. A. Halliwell and C. G. Park. The plasma wave and quasi-static electric field instrument (PWI) for Dynamics Explorer-A. *Space Sci. Instrum.*, 5, 535, 1981.
11. Menietti, J. D., J. R. Sharber, J. L. Burch and D. A. Gurnett. Plasma waves associated with electron beams in the diffuse auroral region. *Ionosphere-Magnetosphere-Solar Wind Coupling Processes. SPI Conference Proceedings and Reprint Series, 7*, Chang, Jasperse, Crew (eds.), Scientific Publishers, Cambridge, MA, 1988.
12. Gurnett, D. A., S. D. Shawhan and R. R. Shaw. Auroral hiss, Z mode radiation, and auroral kilometric radiation in the polar magnetosphere: DE-1 observations. *J. Geophys. Res.*, 88, 329, 1983.
13. Gurnett, D. A., The earth as a radio source: Terrestrial kilometric radiation. *J. Geophys. Res.*, 79, 4227, 1974.
14. Persoon, A. M., D. A. Gurnett and S. D. Shawhan. Polar cap electron densities from DE-1 plasma wave observations. *J. Geophys. Res.*, 88, 10123, 1983.
15. Lin, C. S., J. L. Burch, S. D. Shawhan and D. A. Gurnett. Correlation of auroral hiss and upward electron beams near the polar cusp. *J. Geophys. Res.*, 89, 925, 1984.
16. Tokar, R. L. and S. P. Gary. Electrostatic hiss and the beam driven electron acoustic instability in the dayside polar cusp. *Geophys. Res. Lett.*, 11, 1180, 1984.
17. Lin, C. S., D. Winske and R. L. Tokar. Simulation of the acoustic instability in the polar cap. *J. Geophys. Res.*, 90, 8269, 1985.
18. Roth, I. and M. K. Hudson. Simulations of electron beam excited modes in the high-altitude magnetosphere. *J. Geophys. Res.*, 91, 8001, 1986.
19. Lin, C. S. and D. Winske. Simulation of the electron acoustic instability for a finite size electron beam system. *J. Geophys. Res.*, 92, 7569, 1987.

APPENDIX C

Further Boundary Conditions on the Low-Energy Electrons in the Plasmapause Regions

FURTHER BOUNDARY CONDITIONS ON THE LOW-ENERGY ELECTRONS IN THE PLASMAPAUSE REGION

J. R. Sharber, J. D. Winningham, J. L. Burch
Department of Space Sciences, Southwest Research Institute
San Antonio, TX 78284

W. R. Hoegy
Laboratory for Planetary Atmospheres, Goddard Space Flight Center
Greenbelt, MD 20771

A. M. Persoon
Department of Physics and Astronomy, University of Iowa
Iowa City, IA 52242

J. H. Waite, Jr.
Space Science Laboratory, Marshall Space Flight Center
Huntsville, AL 35812

ABSTRACT

Data from instruments on the Dynamics Explorer satellites are used to describe particle precipitation and plasma properties in the plasmopause region for two cases of plasmopause crossings late in storm recovery phases. A low-energy population of electrons (<10 eV), previously identified with SAR arcs, was observed by the Low Altitude Plasma Instrument on DE-2 on both crossings. The relationship between these electrons and enhancements in the high-energy particle fluxes, the electric field amplitude variations, and the ambient plasma temperature are examined.

INTRODUCTION

The plasmopause has long been recognized as a region characterized by strong magnetosphere-ionosphere coupling. It is the region within which the hot ring current particle population interacts with cold plasma of the plasmasphere. Satellite measurements with Langmuir probes [1] have shown a positive electron temperature gradient of ~ 1 K/km between ~ 800 km and several thousand kilometers. A temperature maximum as a function of latitude in this altitude range has been associated with the plasmopause region [2,3,4]. The SAR arc, observed during the main and early recovery phases of magnetic storms, has been interpreted as evidence of magnetosphere-ionosphere coupling (see review by Roble and Rees [5]). In 1982 Gurgiolo *et al.* [6] using DE-2 particle observations, reported downward flowing, low-energy electrons (~ 5 – 10 eV) at ~ 850 km altitude above a SAR arc. Slater *et al.* [7] later showed that these electrons constitute a major source of energy for production of the 630 nm emissions. Mechanisms proposed for the

magnetosphere-ionosphere coupling resulting in SAR arcs are Coulomb dissipation (Cole, 1965) [8], electromagnetic ion cyclotron turbulence (Cornwall *et al.* 1971) [9], and kinetic Alfvén waves (Hasegawa and Mima, 1978) [10]. Kozyra *et al.* [11] have recently shown that Coulomb scattering of O^+ ions with plasmaspheric electrons can account for the ionospheric heating and 630 nm emissions in some SAR arcs. At this point the determination of which mechanism or combination of mechanisms is operative continues to be investigated.

In this paper we present some additional aspects of the problem by examining two cases in which the Dynamics Explorer satellites passed over the plasmopause region. Even though each observation took place several days after the main phase of a magnetic storm (see Fig. 1), the Low Altitude Plasma Instrument (LAPI) on DE-2 detected a low-energy electron population which appears to be the same population as that previously associated with SAR arcs [6] except for reduced densities and temperatures. Other measurements from both DE-1 and DE-2 made in this region are presented.

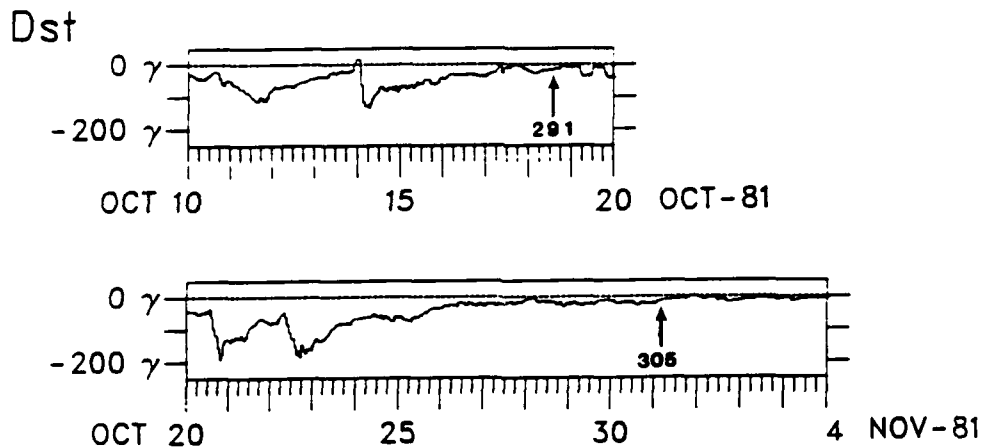


Figure 1. Dst graphs showing approximate times of the satellite passes of this study labeled by day numbers.

All the DE instruments are described in Dynamics Explorer edited by R. A. Hoffman [12] and for brevity will not be referenced separately here.

OBSERVATIONS

October 18, 1981 (Day 291). The first example is a near-conjunction of DE-1 and DE-2 occurring four days after the magnetic storm of October 14, 1981. The day was generally quiet with AE never exceeding 65 nT after 0200 UT until around 1300 UT. Dst averaged -17 nT during this hour and B_z was northward, having been so since 0825 UT.

The panels of Figs. 2 and 3 show DE-1 and DE-2 particles and electric field data from the auroral precipitation region to the plasmasphere. The DE-1 altitude range was 19,000 to 10,000 km. The first panel of the spectrogram of Fig. 2 shows precipitating electrons measured by the High Altitude Plasma Instrument (HAPI). HAPI ions near 90° are shown in the middle panel. The "ram ions" near 1400 UT are a signature of the plasmasphere. The lower panel shows a frequency-time spectrogram of the electric field amplitude measurements (V^2/m^2 Hz) from the Plasma Wave Instrument (PWI). Auroral hiss emissions are observed below ~10 kHz in the auroral region. Intense AKR emissions are seen above ~100 kHz. Plasmaspheric hiss is seen at latitudes below about 70° IL (~1349 UT on the spectrogram) and is most intense in the latitude range ~62° and 66° IL.

The LAPI observations (altitude range ~925 - 950 km) are shown in Fig. 3. The top panel shows precipitating electrons at 7° pitch angle. Of particular relevance are electrons of a very low-energy population seen between invariant latitudes of 68° and 56° (~1350:20 - 1353:30 UT) and a small enhancement in the keV electron fluxes at these latitudes. It is the low-energy population that intensifies during more disturbed times to become the "SAR arc electrons" first reported by Gurgiolo *et al.* (1982)[6]. These electrons occur in LAPI's lowest energy channels (5.1 - 8.8 eV). At their peak intensity (~1352 UT) the population is best represented by a flowing Maxwellian of temperature ~6630 K, density ~4 cm⁻³ and downward bulk flow speed of 260 km/s. (Values are corrected for a spacecraft potential of -1.5 V.) Note that these electrons are not visible in the lowest spectrogram panel of Fig. 3, which shows electrons at 97° pitch angle.

In the top panel a population of keV electrons is seen at all latitudes equatorward of ~68° IL. These electrons are definitely precipitating at LAPI altitude (~950 km). In the latitude range between ~68° and ~62.5° their spectra peak broadly between 1 and 15 keV. Equatorward of ~62.5° the population is masked by the outer belt radiation observed between ~62° IL and ~55° IL. We note that the high-latitude cut-off of these keV electrons is approximately the same as that of the low-energy electrons.

The middle panel shows observations of the LAPI 0° and 90° Geiger counters. Two features to be noted are the increase associated with components of the ring current and outer radiation belt, and the structure, particularly in the 0° counter, occurring at latitudes corresponding to the poleward half of the low-energy electron population. The Geiger counters respond to electrons of $E > 35$ keV and protons of energy > 500 keV.

The panels of Figure 4 show additional data from experiments on DE-1 and DE-2. The first panel obtained from PWI on DE-1 shows the plasma density derived from the electron plasma frequency cutoff of the auroral hiss emissions at auroral latitudes [13] and from the upper hybrid resonance at lower latitudes. The next two panels show the Retarding Ion Mass Spectrometer (RIMS, also on DE-1) measurements of the H⁺ ion density and ion temperature. From these plots and the RIMS spectrograms (not shown) cold, isotropic plasma was observed as far

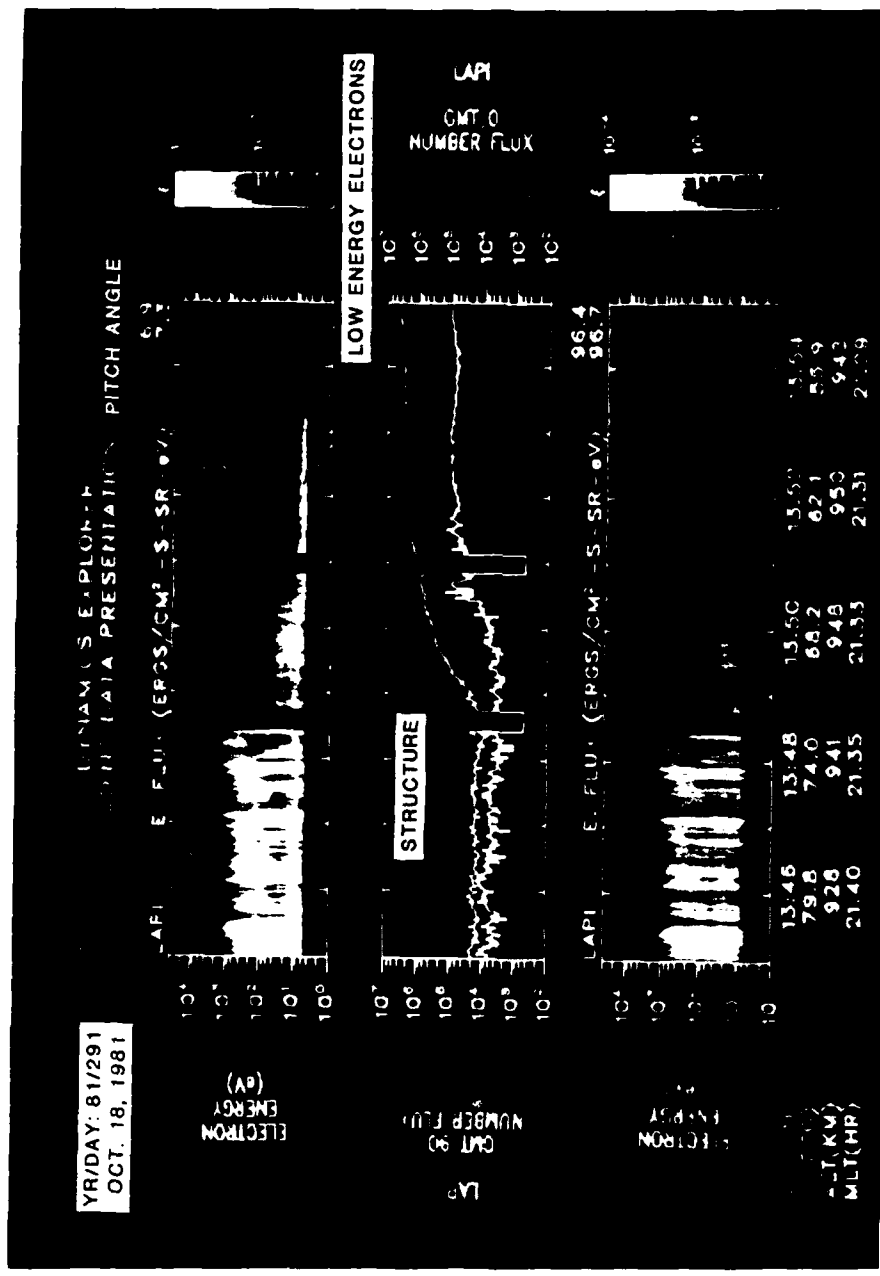


Figure 3. Day 291 LAPI data from DE-2 showing precipitating electrons at 7° pitch angle (top panel), fluxes measured by the Geiger tubes at 0° (GMT 0) and 90° (GMT 90) (middle panel), and electrons at 97° pitch angle (lower panel).

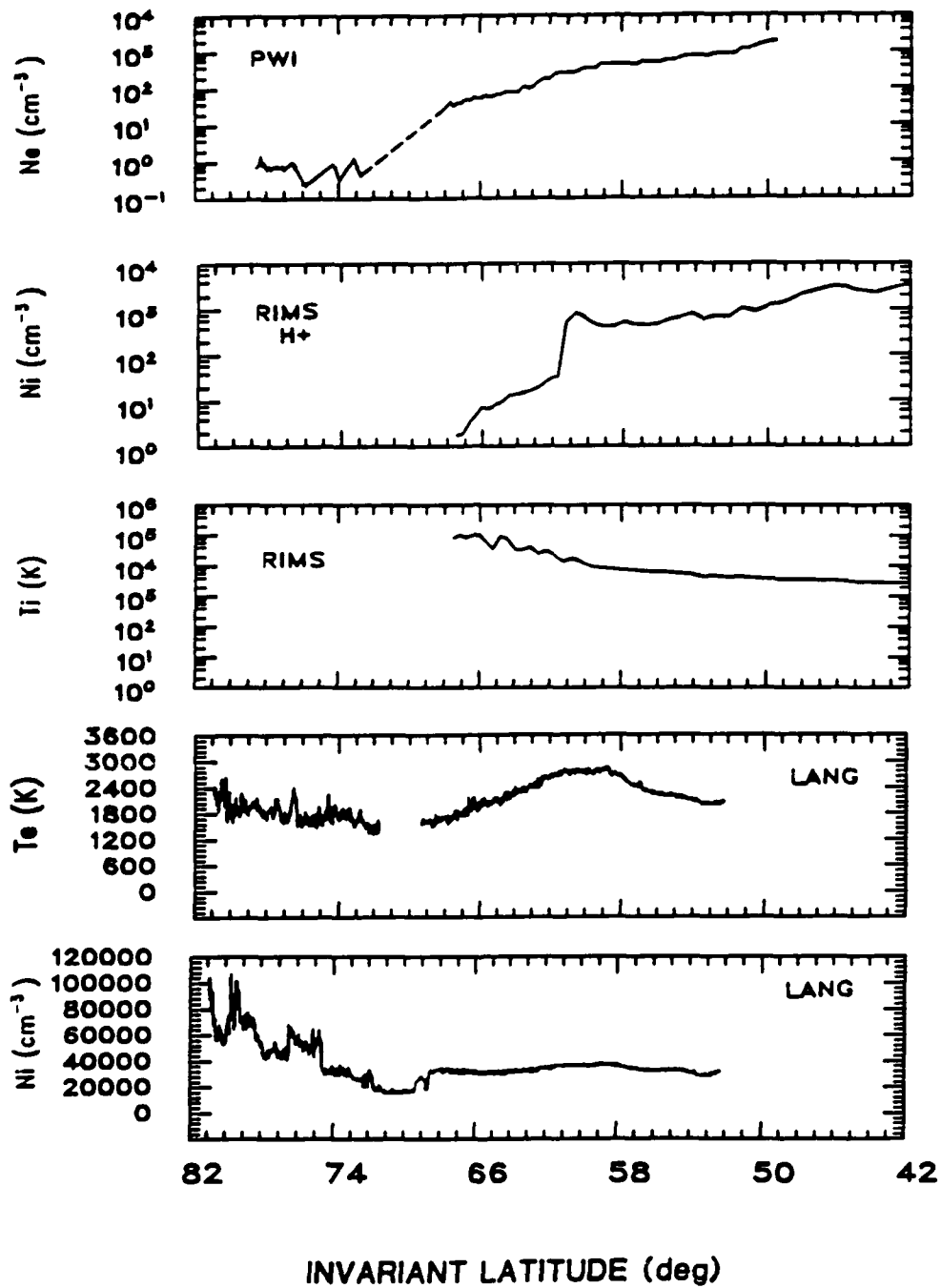


Figure 4. Measurements of plasma density from PWI and H^+ density and ion temperature from RIMS, both instruments on DE-1, are shown in the top three panels. Ion density and ionospheric temperature at DE-2 from the Langmuir probe (LANG) are shown in the lowest two panels.

poleward as $\sim 68^\circ$ IL. Thus the plasmopause region is identified as the region between $\sim 61^\circ$ and 68° IL. The two lowest panels show ion density and electron temperature measurements from the Langmuir probe (LANG) on DE-2. The broad peak in T_e is associated with the plasmopause region. (The break in the T_e data occurs when $N_i < 2 \times 10^4 \text{ cm}^{-3}$, in which case the inflight T_e measurement is no longer accurate; however, T_e is available from the volt-ampere curves at these densities.) We note that the low-energy electrons detected by LAPI occur at the same latitudes as the broad peak in T_e and the plasmopause region as seen at the high altitude DE-1. In this case ion density measurements at low altitudes show almost no evidence of the plasmopause at 925 km, although a trough remnant is seen between 69° and 73° IL.

November 1, 1981 (Day 305). The DE-2 pass occurred nine days after the magnetic storm of October 22, 1981 (Fig. 1). During the previous eight hours AE was below 60 nT and Dst was never more negative than -2 nT. B_z had been negative since ~ 0230 UT. As the pass occurred (between 0307 and 0317 UT), a substorm was developing. Its expansive phase began at ~ 0320 UT, minutes after the satellite pass.

The DE-2 observations are shown in Fig. 5. A clear enhancement in the low-energy electrons is seen between 0312:20 and 0312:43 UT. At the peak (0312:36) their temperature was 11,600 K and their density was $\sim 3 \text{ cm}^{-3}$. Associated with these electrons are a reduction in the conjugate photoelectron flux, an enhancement in keV electron fluxes, peaks in the 0° and 90° fluxes measured by the Geiger tubes, and emissions in the frequency range $\sim 100 - 1000$ Hz as shown in the Vector Electric Field Instrument (VEFI) data of the third spectrogram panel. LANG data in the panels below the spectrogram show a local T_e peak at 0312:36 UT and only slight structure in the ion density of $\sim 9 \times 10^4 \text{ cm}^{-3}$.

The greatest enhancements in the low-energy electrons, the keV electrons, the high-energy (Geiger) fluxes, and the emissions measured by VEFI occur at $\sim 0312:36$ UT (64.6° IL). However, we note that a less intense population of keV electrons is seen extending from $\sim 66.6^\circ$ IL down to $\sim 54^\circ$. Along this same range of latitudes one also sees a population of low-energy electrons, most of which is probably below the 5.1 eV cut-off, and emissions in the 512-1024 Hz band. On this pass, these features correspond roughly to the presence of high-energy radiation as detected by the Geiger tubes. The lowest panel of the spectrogram photo shows the average flux of precipitating ions between pitch angles of 7° and 46° . Auroral ions are seen down to $\sim 66^\circ$ IL ($\sim 0312:12$ UT). Equatorward of that latitude the only ions observed are a low level of precipitation associated with the radiation belt and the ring current. At the position of the enhancements in the low-energy electrons and the Geiger fluxes (i.e. 0312:36 UT), the ion number (energy) flux in the 20-30,000 eV range is $< 2 \times 10^5 \text{ cm}^{-2} \text{ s}^{-1}$ ($< 3 \times 10^{-6} \text{ erg cm}^{-2} \text{ s}^{-1}$).

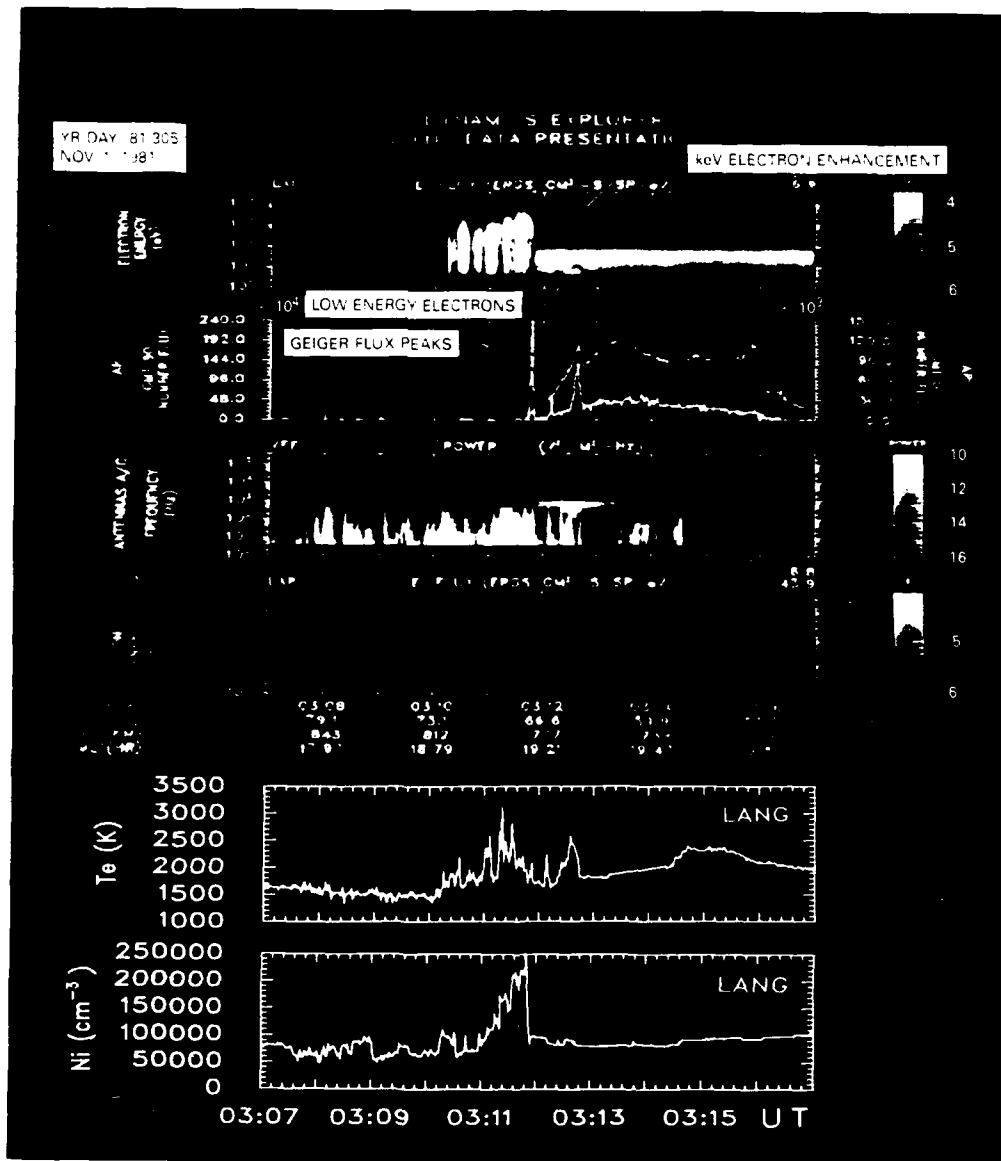


Figure 5. LAPI and LANG measurements from DE-2 on Day 305 between 0307 and 0317 UT. At 0336:12 UT the data show collocation of low-energy electrons, conjugate photoelectron flux reduction, peaks in the Geiger tube fluxes, waves in the 100-1000 Hz range, very low ion fluxes below 30 keV, and a peak in the ionospheric electron temperature.

DISCUSSION

As reported by Slater, *et al.* (1987) [7], the SAR arc electrons measured above the SAR arc of Oct. 23, 1981, had a typical temperature of 13,000 K and a density of 150 cm^{-3} , whereas those reported here are $\sim 7000 \text{ K}$ and 4 cm^{-3} for Day 291 and $11,600 \text{ K}$ and 3 cm^{-3} for Day 305. Therefore the energy available from this population for heating ionospheric electrons and exciting 630 nm emissions on Day 305 was 1/80 that of the SAR arc of Oct. 23, 1981; on the Day 291 pass it was 1/120 that of the Oct. 23 SAR arc. The emissions from such weak fluxes, particularly the Day 291 case, would probably be difficult to detect against the night sky background. In [7] a few cases in which the low-energy electron signature of LAPI was not accompanied by a SAR arc observed from the ground were attributed to the exponential dependence on temperature of the excitation of the $\text{O}(^1\text{D})$ state. The low-energy electrons thus become a sensitive means of determining when the "SAR arc process" is operative. It is clear from these and many other cases that the process occurs far more often than has been documented from ground observations and operates at times when the ring current intensity is much lower than during storm main and early recovery phases. It is appropriate at this point to stress that the low-energy electrons are not always present. The geophysical conditions associated with their occurrence are a subject of another study.

Of particular interest in determining the physical processes occurring in the plasmopause region is the collocation of the low-energy electrons with the enhancements in the 0° and 90° Geiger fluxes, the enhancement in the keV electron fluxes, and the reduction in the conjugate photoelectron fluxes, shown best in the Day 305 example.

The most plausible explanation of the enhancements in the Geiger fluxes is that the Geiger tubes are responding to the high energy component ($> 35 \text{ keV}$) of the same population that produces the increased $\sim\text{keV}$ electron fluxes in LAPI. For example, if a Maxwellian spectrum having a characteristic energy of 6000 eV and a peak flux of $540 \text{ cm}^{-2} \text{ s}^{-1} \text{ sr}^{-1} \text{ eV}^{-1}$ is fitted to the electron spectrum measured at 0312: (36-40) UT, the integral flux of electrons exceeding 35 keV is $1.76 \times 10^5 \text{ cm}^{-2} \text{ s}^{-1} \text{ sr}^{-1}$ (see Fig. 6). The second panel of Fig. 5 shows a value of $\sim 9 \times 10^4 \text{ cm}^{-2} \text{ s}^{-1} \text{ sr}^{-1}$. Thus the electrons alone can account completely for the Geiger tube responses. This observation, taken with the measurement of very low ion flux levels at the same latitude in this example, argues against the general applicability of the ion cyclotron wave hypothesis [9,14,15]. This is reasonable since both examples presented here occur late in the storm sequence.

The emissions detected by the VEFI experiment in the Day 305 example show a clear enhancement at latitudes where the low-energy electrons are most intense (i.e. $\sim 64^\circ - 66^\circ \text{ IL}$). At these latitudes the frequency range is $\sim 100 - 1000 \text{ Hz}$. Poleward of these latitudes, up to 67° IL , and equatorward, down to $\sim 54^\circ \text{ IL}$, the emissions are less intense and are seen primarily in the 512 - 1024 Hz channel. This narrowing of the range of detected frequencies may be a sensitivity ef-

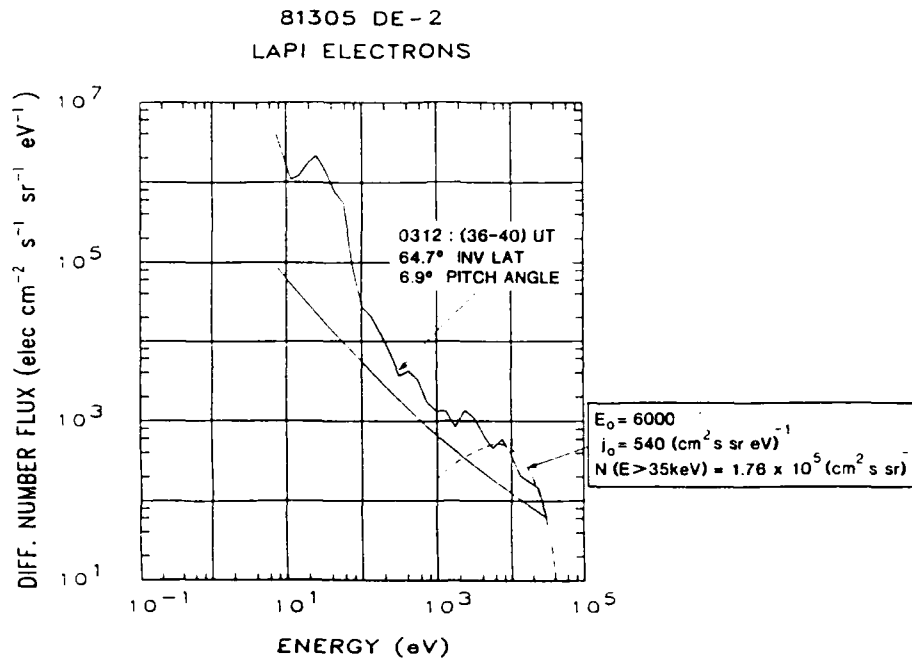


Figure 6. LAPI electron differential number spectrum measured at 0312:(36-40) UT. The Maxwellian (dashed) curve fitted to the measured spectrum contains an integral flux of $1.76 \times 10^5 \text{ cm}^{-2} \text{ s}^{-1} \text{ sr}^{-1}$ at energies exceeding 35 keV. This more than accounts for the flux of $\sim 9 \times 10^4 \text{ cm}^{-2} \text{ s}^{-1} \text{ sr}^{-1}$ measured by the 0° Geiger tube (see Fig. 5).

fect only. The frequency range and enhancement in intensity of these emissions in the plasmapause region suggest that they may be plasmaspheric hiss ducted down to DE-2 heights (770 km) [16,17], although it is possible that some of the wave intensity results from the generation of electrostatic ion cyclotron waves at these altitudes. The importance of enhanced regions of plasmaspheric hiss in the plasmapause region has been suggested by Kozyra *et al.* [17] and is the subject of another study.

The recent work of Kozyra *et al.* [11] gives strong support to Coulomb interactions as the primary mechanism of energy transfer from the magnetosphere to the ionosphere in the plasmapause region. The key element of that paper is the demonstration that ring current O^+ ions at energies $> 6 \text{ keV}$ provide the major source of energy to heat the plasmaspheric electrons and thus "drive" the SAR arc. While other mechanisms may not be ruled out, our observations of the relatively low densities of the low-energy electrons and very low fluxes of precipitating ions are consistent with this finding, in that in both cases the passes occurred several days after the storm main phase when the ring current was known to be low (Fig. 1) and its O^+ content is expected to be low [18].

OBSERVATIONAL SUMMARY

Our observations made late in storm recovery phases may be summarized as follows:

1. The low-energy electrons are observed in the plasmopause region as determined by either direct measurement by RIMS and PWI on DE-1 or by the ionospheric electron temperature increase seen in the LANG data on DE-2.
2. The electrons were detected in LAPI's lowest three energy channels (5.1 - 8.8 eV) and were observed most intensely over a latitude range of $\sim 12^\circ$ in one case (Day 291) and $\sim 1.5^\circ$ in the other (Day 305).
3. The low-energy electrons observed in these cases differ from "SAR arc electrons" only in that their densities and temperatures are lower. Densities for both these cases are a few electrons cm^{-3} ; temperatures were low on the Day 291 case (6630 K) and higher for the Day 305 case (11,600 K).
4. When conjugate photoelectrons were observed with sufficient intensity (Day 305), their fluxes were diminished where the low-energy electrons were observed. This decrease has been reported for SAR arcs as well [6] and suggests scattering of the population on plasmopause field lines.
5. In both examples, enhancements in electron fluxes between 1 and 15 keV are seen at latitudes where the low-energy electrons are observed.
6. The low-energy electrons are associated with enhancements in the Geiger fluxes (Day 305) or structure in these fluxes (Day 291). Both situations occur on the poleward gradient of the outer belt trapped fluxes; although in the Day 291 case, the low-energy electrons extended equatorward to latitudes where very little gradient and structure were present. The Geiger tubes respond primarily to electrons of $E > 35$ keV and protons of $E > 500$ keV, but extension of the electron spectrum to high energies can account for the Geiger tube responses.
7. In the Day 305 example, emissions in the frequency range ~ 100 -1000 Hz are observed at the same latitudes as the precipitating low-energy electrons, enhancements in the LAPI keV electron fluxes and Geiger counters, and the reduction in conjugate photoelectron flux. These emissions are probably plasmaspheric hiss; their part in the energy transfer process is currently the subject of further investigation.

ACKNOWLEDGEMENTS

We wish to thank DE Principal Investigators C. R. Chappell, D. A. Gurnett, and N. C. Maynard for making their data available; C. Gurgiolo, H. K. Wong, J. U. Kozyra, and N. C. Maynard for very helpful discussions; and R. A. Frahm, P. J. Gryting, A. O. Sawka, L. P. Post, and D. W. Moore for technical assistance.

The work was supported at SwRI by AFOSR contract F49620-85-C-0029, NASA contracts NAS5-28711 and NAS5-28712, and AFGL contract F19628-084-N-0006; at the University of Iowa by NASA/GSFC grant NAG5-310; and at the Goddard and Marshall Space Flight Centers by the Dynamics Explorer program.

REFERENCES

- [1] L. H. Brace and R. F. Theis, *J. Atmos. Terr. Phys.* **43**, 1317 (1981).
- [2] L. H. Brace, R. F. Theis, and W. R. Hoegy, *Geophys. Res. Lett.* **9**, 989 (1982).
- [3] J. L. Horwitz, L. H. Brace, R. H. Comfort, and C. R. Chappell, *J. Geophys. Res.* **91**, 11203 (1986).
- [4] J. U. Kozyra, A. F. Nagy, T. E. Cravens, and L. H. Brace, *J. Geophys. Res.* **91**, 11,270 (1980).
- [5] M. H. Rees and R. G. Roble, *Reviews of Geophys. and Space Phys.* **13**, 201 (1975).
- [6] C. Gurgiolo, D. W. Slater, J. D. Winningham, and J. L. Burch, *Geophys. Res. Lett.* **9**, 965 (1982).
- [7] D. W. Slater, C. Gurgiolo, J. U. Kozyra, E. W. Kleckner, and J. D. Winningham, *J. Geophys. Res.* **92**, 4543 (1987).
- [8] K. D. Cole, *J. Geophys. Res.* **70**, 1968 (1965).
- [9] John M. Cornwall, F. V. Coroniti, and R. M. Thorne, *J. Geophys. Res.* **76**, 4428 (1971).
- [10] A. Hasegawa and K. Mima, *J. Geophys. Res.* **83**, 1117 (1978).
- [11] J. U. Kozyra, E. G. Shelley, R. H. Comfort, L. H. Brace, T. E. Cravens, and A. F. Nagy, *J. Geophys. Res.* **92**, 7487 (1987).
- [12] R. A. Hoffman, ed. *Dynamics Explorer, Space Science Instrumentation 5* (D. Reidel Publishing Co., Dordrecht, 1981).
- [13] A. M. Persoon, D. A. Gurnett, and S. D. Shawhan, *J. Geophys. Res.* **88**, 10,123 (1983).
- [14] D. J. Williams and L. R. Lyons, *J. Geophys. Res.* **79**, 4195 (1974).
- [15] J. A. Lundblad and F. Corraas, *Planet. Space Sci.* **26**, 245 (1978).
- [16] C. Y. Huang, C. K. Goertz, and R. R. Anderson, *J. Geophys. Res.* **88**, 7927 (1983).

- [17] J. U. Kozyra, T. C. Cravens, A. F. Nagy, D. A. Gurnett, R. L. Huff, R. H. Comfort, J. H. Waite, Jr., L. H. Brace, J. D. Winningham, J. L. Burch, and W. K. Peterson, 26th Plenary Meeting of COSPAR, in Toulouse, June 30-July 11, Abstracts of the General Assembly, **263** (1986).
- [18] E. G. Shelley, R. G. Johnson, and R. D. Sharp, *J. Geophys. Res.* **77**, 6104 (1972).